Soil Physical and Hydrological Evaluation of Aluminum Recycling By-Product as an Infiltration Barrier for Potash Mine Tailings

---

Bodenphysikalisch-hydrologische Bewertung von Rückständen der Aluminium-Kreislaufführung als Infiltrationsbarriere für eine Halde des Kalibergbaus

Vom Fachbereich Geowissenschaften und Geografie der Universität Hannover

zur Erlangung des Grades

Doktor der Naturwissenschaften

Dr. rer. nat.

genehmigte Dissertation

von

Dipl.-Geogr. Dirk Hermsmeyer

geboren am 25.12.1964 in Bünde / Westfalen

Hannover, im Juli 2001

Danksagung

Vorderer Einband: Orthofoto der Rückstandshalde Sigmundshall, Bildflug 14.08.2000.

viii

Inhalt

Zusammenfassung

Von Rückstandshalden des Kalibergbaus gehen beträchtliche Abfluss-mengen mit NaCl-Konzentrationen nahe der Sättigung aus. Diese verunreinigen Oberflächengewässer und das Grundwasser. Die Abdeckung solcher Halden mit natürlichem Bodenmaterial oder Bodenersatzstoffen und die Begrünung der Ab-deckung verringert das Abflussvolumen aufgrund der Speicherung von Nieder-schlagswasser in der Deckschicht und aufgrund der Pflanzenverdunstung. Eine direkte Begrünung von Kali-Rückstandshalden ist wegen der hohen Salzgehalte in der Regel nicht möglich.

Im Fall der Rückstandshalde des Kalibergwerks Sigmundshall in Bokeloh bei Wunstorf wird für den Aufbau einer Deckschicht ein feinkörniger Rückstand der Aluminium-Kreislaufführung (Aluminum Recycling By-Product, ALRP) verwendet. Zur mechanischen Stabilisierung werden zementierende Rückstände der Rauchgasreinigung aus einem Kohlekraftwerk (Flue Gas Desulfurization By-Product, FGDP) beigemischt. Über die Eignung der bei Aufbringung eben-falls salzhaltigen ALRP-FGDP Mischung als Deckschichtmaterial ist jedoch wenig bekannt. Unter humiden Klimabedingungen wird leicht lösliches NaCl mit dem abwärts gerichteten Sickerwasserstrom aus der Deckschicht ausge-waschen. Der zurückbleibende salzfreie Anteil soll begrünt werden, um die in den Haldenkörper eindringende Sickerwassermenge und die an den Fluss Leine abgegebene Abflussspende deutlich zu verringern.

Ziel der vorliegenden Arbeit ist die bodenphysikalisch-hydrologische Bewertung der Eignung von ALRP sowie von ALRP-FGDP als Deckschicht-material zur Reduzierung des Sickerwasserstroms. Es wurde untersucht, nach welcher Zeit eine salzfreie, zur Begrünung ausreichend mächtige Schicht vor-liegt, welche bodenphysikalischen Voraussetzungen der zurückbleibende salz-freie Anteil dem Wachstum von Pflanzenwurzeln bietet, welche Verdunstung und Sickerung aus einer bewachsenen Deckschicht zu erwarten sind, und welchen Einfluss die Exposition der Haldenflanken auf die Verdunstung hat.

Die Materialeigenschaften Wassergehalt, Salzgehalt, Dichte der Fest-substanz, Lagerungsdichte, Porosität, Textur, Durchlässigkeit für Luft, Wasser und Salzlösung, Wasserspannung, Plastizität sowie Erodibilität wurden im Labor untersucht. Lysimeter wurden mit ALRP und ALRP-FGDP gefüllt und über drei Jahre unter Feldbedingungen beobachtet. Mittels der Ergebnisse der Labor- und Feldversuche wurde ein numerisches Wasserhaushaltsmodell für die ungesättigte Zone (HYDRUS-1D) kalibriert. Unter Nutzung langjähriger

Wetterdaten werden mit dem kalibrierten Modell mittlere Sickerraten über 31 Jahre im Rahmen einer kontinuierlichen Langzeitsimulation vorhergesagt. Unter Verwendung eines geografischen Informationssystems (GIS) wurde ein komplexes Modell der Globalstrahlung und der potenziellen Evaporation von der Haldenoberfläche entwickelt, mit dem diese Größen für die Rasterzellen eines digitalen Höhenmodells (Digital Elevation Model, DEM) berechnet werden.

Die Textur sowohl von ALRP als auch von FGDP entspricht einem schluffigen Lehm. Der anfängliche Salzgehalt der ALRP-FGDP Mischung betrug 36 Gew.-%, der Wassergehalt 13 Vol.-%. Die Lagerungsdichten von ALRP und ALRP-FGDP Mischung betrugen 0,93 und 0,88 g cm^{-3}. Die Durchlässigkeitsbeiwerte bei Sättigung variierten zwischen 7 und 284 cm d^{-1}. Die nutzbare Feldkapazität betrug 36% für gewaschenes ALRP und 45% für gewaschenes ALRP-FGDP. Die Erodibilität von ALRP wurde durch den zementierenden Effekt von FGDP in der Mischung deutlich reduziert. Der Plastizitätsindex wurde von 2% auf 9% erhöht.

Im Lysimeterversuch über drei Jahre betrug die Sickerwassermenge aus ALRP 39% und aus ALRP-FGDP 24% des Niederschlags. Der Salzgehalt beider Materialien war 28 Monate nach Versuchsbeginn in einer Schicht von etwa 0,3 m ausreichend gering, um das Wachstum von Raygras (*Lolium perenne*, L.) zu ermöglichen. Das Wasserhaushaltsmodell beschreibt die gemessenen Sickerwassermengen und den zeitlichen Verlauf der Sickerung aus den Lysimetern hinreichend genau. Der prognostizierte 31-jährige Mittelwert der Sickerung beträgt 237 mm für ALRP und 186 mm für ALRP-FGDP, oder 31% bzw. 24% des (korrigierten) Niederschlags. Die berechnete mittlere tatsächliche Verdunstung einer horizontalen Oberfläche beträgt für bewachsenes ALRP-FGDP 577 mm und ist nur um 11 mm geringer als die potenzielle Verdunstung. Im dreijährigen Mittel ist die potenzielle Verdunstung bei 35° Neigung vom Südhang der Halde um bis zu 12% höher als in der Ebene, vom Nordhang dagegen um bis zu 37% geringer. Durch eine optimal begrünte Deckschicht aus ALRP-FGDP kann die an die Leine abgegebene Abflussspende sowie die Salzfracht um etwa 60% reduziert werden.

Mit Blick auf die physikalischen Eigenschaften ist im Anschluss an die Entsalzung insbesondere ALRP-FGDP für den Aufbau einer begrünbaren Deckschicht geeignet. Durch die zementierenden Eigenschaften von FGDP scheint dies auch für steile Hangpositionen gegeben. Durch eine begrünte Deckschicht lässt sich die Sickerung deutlich reduzieren. Die ALRP-FGDP Mischung ist wegen ihrer günstigeren physikalischen Eigenschaften reinem ALRP vorzuzie-

hen. Die metallurgische Herkunft von ALRP läßt erwarten, dass chemische Eigenschaften eher als bodenphysikalische Eigenschaften die Verwendbarkeit des Materials zum Aufbau einer Deckschicht für die Halde Sigmundshall einschränken. Durch eine Vergrößerung der südexponierten Hänge der Haldenoberfläche gegenüber den nordexponierten Hängen bei der zukünftigen Haldenerweiterung kann die Gesamtverdunstung von der Haldenoberfläche ebenfalls erhöht werden.

Abstract

In Germany, mounds of solid wastes from potash mining (rock salt, NaCl) produce annually large amounts of briny runoff which are conveyed into streams and rivers, or may pollute the groundwater. Covering mine wastes with natural soil material, or soil substitutes, and planting the cover with grass will reduce the amount of discharge from mine waste. Precipitation will be stored in the cover and will be transpired by plants. Because of high salt content direct planting of potash mine waste is commonly impossible.

At the potash mine 'Sigmundshall' near Hannover, Germany, fine grained aluminum recycling by-product (ALRP) is used as soil substitute in a surface barrier over mine waste. To stabilize this material mechanically, it is blended with cementing flue gas desulfurization by-product (FGDP) from a coal combustion plant. Little is known about the feasibility and effectiveness of the initially saline ALRP-FGDP mixture as cover material. It is expected that under humid conditions seepage will leach easily soluble components (predominantly NaCl) from the material. Remaining salt-free components shall subsequently be planted with grass. This is expected to reduce the amount of seepage into the mine waste and hence the amount of discharge conveyed from the waste mound into the River Leine.

This study was conducted to evaluate, from a soil physical and hydrological perspective, the feasibility of ALRP and ALRP-FGDP as cover material to reduce discharge. The amount of seepage necessary to leach the material to plant-tolerable salinity needed to be estimated. Soil physical properties of the salt free components relevant to plant root growth were studied, expected amounts of evapotranspiration and seepage from a planted surface barrier are estimated and the effect of slope aspect on evaporation around the mine waste mound is described.

Water content, salt content, particle density, bulk density, porosity, texture, permeability to air, water, and salt solution, moisture retention, consistency and erodibility were studied in the laboratory. Four free-drainage lysimeters were filled with ALRP and ALRP-FGDP mixture and were monitored for three years under humid field conditions. Results of laboratory and field experiments were used to calibrate a numerical water flow model for the vadose zone (HYDRUS-1D). In combination with 31-yr-long weather records, the calibrated model was used to predict longterm seepage rates from the tested materials. Commercially available geographic information system (GIS) computer software was extended to compute global radiation and potential evaporation from every cell of a grid digital elevation model (DEM) of the mine waste mound.

The texture of both ALRP and ALRP-FGDP resembled a silt loam. The initial salt content of ALRP-FGDP was 36 wt.%, its volumetric water content was 13%. Bulk densities of ALRP and ALRP-FGDP mix were 0.93 and 0.88 Mg m^{-3}, respectively. Saturated hydraulic conductivity of salt-washed and unwashed materials varied between 7 and 284 cm d^{-1}. Plant available water holding capacity was 36% for washed ALRP and 45% for washed mix. Erodibility of ALRP was high but was reduced considerably in the mix because of the cementing effect of FGDP. Addition of FGDP increased the plasticity index of 2% moisture of ALRP to 9% for the washed ALRP-FGDP.

In the lysimeter study, mean annual discharge from ALRP and from ALRP-FGDP over a three year period was 39% and 24% of rainfall, respectively. After 28 months, materials were sufficiently leached to a depth of about 0.3 m to support the growth of rye-grass (*Lolium perenne*, L.). The calibrated water flow model adequately describes seepage flow from the materials. Predicted longterm average discharge is 237 mm from the aluminum waste and 186 mm from the mix, or 31% and 24% of the longterm mean annual precipitation (764 mm). Longterm mean annual actual evaporation is 577 mm for planted ALRP-FGDP and is only 11 mm short of mean annual potential evaporation for the area of the mine. The three-year average of potential evaporation from the south slope of the waste mound at 35° steepness is about 12% higher than from a horizontal surface. From the north slope, potential evaporation is about 37% less than from a horizontal surface. It is expected that discharge and NaCl-load conveyed into the River Leine can be reduced by about 60% when a densly planted ALRP-FGDP surface barrier is installed.

In view of its soil physical properties, ALRP-FGDP seems to be suitable as cover material, even on steep slopes. Seepage from a planted engineered

surface barrier into the mine waste below will be reduced considerably. Because of its more favorable soil physical properties with respect to plant root growth, ALRP-FGDP is more suitable as cover material than ALRP. Because of its metallurgical origin, it is expected that chemical rather than soil physical properties of ALRP may limit its feasibility as cover material. Shaping future enlargements of the waste mound with larger south facing slopes and smaller north facing slopes is another possibility to enhance total evaporation from the mound surface.

1. Einführung

Kali-Dünger, Auftausalze und Salze für die chemische Industrie werden in Deutschland unter Tage abgebaut. Das gilt auch für Salze, die bei der Rückgewinnung von metallischem Aluminium aus Schrott eingesetzt werden. Feste Rückstände sind im Salzbergbau unvermeidlich. Im Fall des Kalibergwerks Sigmundshall in Bokeloh bei Wunstorf bestehen diese Rückstände überwiegend aus NaCl. Hiervon werden etwa 60% zurück nach unter Tage verbracht, der Rest wird in Schachtnähe aufgehaldet. Der aufgehaldete Rückstand besteht zu etwa 96% aus NaCl und zu etwa 4% aus Verunreinigungen in der Tonfraktion (Kali und Salz GmbH, mündliche Mitteilung). Um eine Kontamination des Grundwassers zu vermeiden, wird als Basisabdichtung vor der Aufhaldung eine Schicht Kreideton ausgebracht und durch Walzen verdichtet. Der salzhaltige Abfluss von der Basisabdichtung wird in einem mit Ton gedichteten Ringgraben aufgefangen und über eine Pipeline in den Fluss Leine abgeführt. Auf diese Weise werden lokale Fließgewässer entlastet.

Derzeit beträgt die Fläche der Basisabdichtung 311 157 m^2 und das aufgehaldete Volumen etwa 13,4 Millionen m^3. Pro Jahr werden etwa 150 000 m^3 „Haldenlauge" an die Leine abgegeben. Die NaCl-Konzentration der „Haldenlauge" liegt nahe der Sättigung: außer nach starken Niederschlägen können zu jeder Zeit Salzkristalle im Ringgraben beobachtet werden (Kali und Salz GmbH, mündliche Mitteilung). Ausgehend von einer gesättigten NaCl-Lösung mit einer Konzentration von 357 g L^{-1} (Weast, 1987) ergibt sich überschlägig eine Fracht von 53 550 Tonnen NaCl pro Jahr. Unter Berücksichtigung der maximalen Lagerungsdichte von NaCl (2,165 g cm^{-3}, Weast, 1987) entspricht dies einer im Mittel etwa 8 cm mächtigen Schicht über die Fläche der Basisabdichtung. Dieser Wert stimmt gut mit Beobachtungen an der Haldenoberfläche überein, wonach pro Jahr eine etwa 8 bis 15 cm mächtige Salzschicht durch Lösung verloren geht (Kali und Salz GmbH, mündliche Mitteilung).

Ausgehend von einer gesättigten Lösung im Ringgraben wird mit der Reduktion der Abflussspende an die Leine auch die Salzfracht reduziert. Es wird erwartet, dass durch Abdeckung der Halde mit Bodenmaterial oder einem Bodenersatzstoff und Begrünung die Abflussspende verringert wird, da infiltrierendes Niederschlagswasser in der Deckschicht gespeichert und über die Verdunstung zumindest zum Teil zurück an die Atmosphäre geführt wird. Besonders hoch ist die Verdunstung einer dicht bewachsenen Deckschicht.

Als mögliches Bodenersatzmaterial für den Aufbau einer Deckschicht für die Halde Sigmundshall wurde vom Bergwerksbetreiber ein feinkörniger Rückstand der Wiedergewinnung von Aluminium aus Schrott (Aluminum Recycling By-Product, ALRP) vorgeschlagen. Die Al-Rückgewinnung ist zu einem bedeutenden Segment der Kreislaufführung von Stoffen geworden. In 1996 wurden in Deutschland 324 kt (oder 46%) des gesamten produzierten Aluminiums aus Schrott gewonnen (Statistisches Bundesamt, 1997). Zur Rückgewinnung wird Aluminiumschrott häufig in Drehtrommelöfen geschmolzen. Der Schrott wird im Ofen durch eine Schicht bereits geschmolzener Flussmittelsalze (etwa 70% NaCl und 30% KCl) gesenkt. Das Flussmittel nimmt Oxide und andere Verunreinigungen (z.B. Carbide, Nitride und Sulfide) aus dem Schrott auf und hält Oxidationsverluste an die Atmosphäre gering (Karvelas et al., 1991).

Das flüssige Aluminium wird aus dem Ofen abgegossen. Die oberste Schicht, die aus festem Al_2O_3, verunreinigtem Flussmittel und eingeschlossenen Metallen besteht, wird abgezogen. Diese Schicht, Krätze genannt, beinhaltet häufig 10-20% metallisches Al und wird daher oft zusammen mit minderwertigem Schrott unter erneutem Einsatz von Flussmittel weiter verarbeitet. Bei der Weiterverarbeitung fällt als Rückstand sogenannter „Salzkuchen" an, eine Krätze mit erhöhtem Salzgehalt. „Salzkuchen" besteht häufig aus 3-5 Gew.-% Al, 15-30 Gew.-% Al_2O_3, 30-55 Gew.-% NaCl und 15-30 Gew.-% KCl. Insgesamt fallen pro Tonne wiedergewonnenen Aluminiums etwa 0,4 bis 0,7 Tonnen Rückstand an (Hryn et al., 1995).

In der Vergangenheit sind Verfahren zur Rückgewinnung sowohl des Restaluminiums als auch der Salze aus Rückständen der Al-Kreislaufführung entwickelt worden. Die Rückgewinnung der Salze geschieht durch Auswaschung mit Wasser und anschließender Filtration und Eindampfung der Salzlösung. Auf diese Weise kann praktisch das gesamte Salz zurückgewonnen und erneut in der Aufbereitung von Al-Schrott eingesetzt werden. Von 1987 bis 1991 wurden in Deutschland etwa 120 kt Flussmittel zurückgewonnen und wiederverwendet (Jody et al., 1992).

Die Verdampfung des Wassers zur Rückgewinnung der Flussmittelsalze ist ein energieintensiver Vorgang. Jody et al. (1992) schätzen, dass die Energiekosten einen großen Anteil der Gesamtkosten der Aufbereitung von Krätze und „Salzkuchen" ausmachen. Die Kreislaufführung der Salze sowie des Restaluminiums ist nur dann wirtschaftlich, wenn der Al-Gehalt von Krätze und „Salzkuchen" und die Kosten für deren Entsorgung hoch sind.

Auf Sigmundshall wurde 1996 eine Fabrik zur Aufbereitung von etwa 90 kt Al-Krätze und „Salzkuchen" pro Jahr in Betrieb genommen. In einer trockenen Verarbeitungsstufe wird metallisches Al vom einkommenden Rohmaterial durch Brechen und Sieben abgetrennt. Nachfolgend wird in einer nassen Verarbeitungsstufe KCl bei einer Temperatur von 104°C ausgewaschen. Die hierbei entstehenden Gase werden gereinigt und zur Produktion von festem $(NH_4)_2SO_4$ verwendet, dass als Düngemittel vermarktet wird. Ebenfalls anfallendes Methan und Wasserstoff werden zur Dampf- und Elektrizitätserzeugung genutzt. Die anfallende Salzlösung wird in einer Vakuumatmosphäre auf 35°C abgekühlt, wobei KCl kristallisiert. Die Kristalle werden getrocknet und als Düngemittel mit einem K_2O-Äquivalentanteil von etwa 50% vermarktet. Natriumchlorid verbleibt in der Lösung. Diese wird nicht eingedampft, sondern erneut zur Wäsche von Al-Krätze und „Salzkuchen" eingesetzt.

Die Hauptbestandteile des zurückbleibenden festen Rückstands (ALRP) sind Al_2O_3 (27-33 Gew.-%), SiO_4 (4-10 Gew.-%), und NaCl (45-55 Gew.-%). Weitere Bestandteile sind $MgAl_2O_4$, Fe_2O_3, CaO, CaF_2 sowie KCl. Der Rückstand wird durch Zentrifugieren auf etwa 16-18 Gew.-% Wasseranteil entwässert. Der wirtschaftliche Vorteil gegenüber herkömmlichen Verfahren liegt in der Energieeinsparung, da das Wasser aus der Salzlösung nicht verdampft wird.

Als Verwendungsmöglichkeit für ALRP wurde von der Kali und Salz GmbH der Aufbau einer Deckschicht für die Halde aus dem Salzbergbau vorgeschlagen. Es wurde argumentiert, dass unter den gegebenen humiden Klimaverhältnissen anfänglich mit einer Auswaschung insbesondere von NaCl aus der Deckschicht mit dem Sickerwasser zu rechnen ist, was keine Verschlechterung gegenüber dem gegenwärtigen Zustand der nicht abgedeckten Halde bedeute. Jedoch sei zu erwarten, dass leicht lösliche Salze einige Jahre nach der Aufbringung aus einer ausreichend mächtigen Schicht ausgewaschen sein werden. Die Deckschicht könne dann begrünt und der weitere Sickerwasserfluss in den Haldenkörper verringert werden.

Frühe Versuche zeigten, dass ALRP auf steile Haldenflanken nicht standsicher aufgebracht werden kann. Deshalb wurde dazu übergegangen, vor der Aufbringung zur mechanischen Stabilisierung etwa 30 Vol.-% eines Rückstands der Rauchgasreinigung aus einem Kohlekraftwerk (Flue Gas Desulfurization By-Product, FGDP) mit zementierenden Eigenschaften beizumischen. Die bodenhydrologischen Eigenschaften von ALRP-FGDP waren jedoch weitgehend unbekannt. Es war ungewiss, (i) ob dieses Material dauerhaft und standsicher aufgebracht werden kann, (ii) wann eine Begrünung möglich ist und

(iii) ob sich mit einer Deckschicht aus ALRP-FGDP die gewünschte deutliche Reduzierung der Sickerung erreichen läßt.

Ziel der vorliegenden Arbeit ist die bodenphysikalisch-hydrologische Bewertung der Eignung von ALRP und ALRP-FGDP als Deckschichtmaterial für die Halde Sigmundshall zur Reduzierung der Sickerung. Bodenphysikalische Eigenschaften wurden im Labor ermittelt. Mit Blick auf die Wachstumsbedingungen von Pflanzenwurzeln wurde dabei jeweils auch gewaschenes ALRP und ALRP-FGDP, d.h. die nach der Entsalzung zurückbleibenden Bestandteile untersucht. Im Lysimeterversuch unter Feldbedingungen wurde beobachtet, in welcher Zeit die leicht löslichen Salze aus einer zur Begrünung ausreichend mächtigen Schicht ausgewaschen wurden. Mithilfe der ebenfalls am Lysimeter erhobenen Sickerwassermengen sowie einem numerischen Wasserhaushalts-modell (HYDRUS-1D, Šimunek et al., 1998) wird die langjährige mittlere Sickerung aus einer bewachsenen Deckschicht prognostiziert. Schließlich wird ein Modell zur Beschreibung der Globalstrahlung entwickelt, mit dessen Hilfe der Einfluss der Exposition der Haldenflanken auf die Verdunstung beschrieben wird.

Aufbau der Arbeit

Der kumulative Aufbau der vorliegenden Arbeit spiegelt die unterschied-lichen verwendeten methodischen Ansätze wider. Die einzelnen Kapitel bauen inhaltlich aufeinander auf; Ergebnisse vorhergehender Kapitel werden in nach-folgenden Kapiteln genutzt:

In Kapitel 2 werden die Herkunft von ALRP sowie die bodenphysikalisch relevanten Eigenschaften von ALRP und ALRP-FGDP Mischung beschrieben. Untersucht wurden die Materialeigenschaften Wassergehalt, Salzgehalt, Dichte der Festsubstanz, Lagerungsdichte, Porosität, Textur, Durchlässigkeit für Luft, Wasser und Salzlösung, Wasserspannung, Plastizität sowie Erodibilität. Die Zusammenschau ergibt ein Bild über die physikalischen Wachstumsbedingun-gen für Pflanzenwurzeln (Wasserhaushalt, Lufthaushalt). Die ermittelten Wass-erspannungskurven und die zugehörigen sog. „van Genuchten Parameter" (van Genuchten, 1980) sind wichtige Voraussetzungen für die Anwendung des nu-merischen Wasserhaushaltsmodells (Kapitel 4).

In Kapitel 3 werden der Aufbau, die Messgeräteausstattung, der Verlauf und die Ergebnisse des Lysimeterversuchs behandelt. Vier frei dränende Lysimeter wurden über drei Jahre unter Feldbedingungen beobachtet. Zwei Lysimeter waren mit ALRP gefüllt, die beiden übrigen mit ALRP-FGDP. Die

Größen Niederschlag, Verdunstung und Sickerwasserfluss sowie die Wasserspannung in drei Tiefen wurden quasi-kontinuierlich gemessen. Zur Erfassung der Entsalzung wurde die elektrische Leitfähigkeit von Sauglösungen aus vier Tiefen beobachtet. Aus den Ergebnissen werden vergleichende Aussagen zur Begrünbarkeit und zur Sickerwasserbildung von ALRP und ALRP-FGDP abgeleitet.

In Kapitel 4 wird die Kalibrierung des numerischen Wasserhaushaltsmodells für die ungesättigte Zone (HYDRUS-1D) sowie dessen Anwendung zur Prognose der langjährigen mittleren Sickerwasserbildung aus ALRP und ALRP-FGDP beschrieben. Als Eingangsdaten werden zunächst aus Labordaten ermittelte „van Genuchten Parameter" zur Beschreibung von Wasserspannungskurven verwendet. Werte der kumulativen Sickerwasserbildung und deren zeitlicher Verlauf aus dem dritten Jahr der Lysimeterversuche (Kapitel 3) werden zur Kalibrierung von HYDRUS-1D durch inverse Neuberechnung der „van Genuchten Parameter" genutzt. Für die Beschreibung der Bedingungen am oberen Rand des Modells (Niederschlag und Verdunstung) während der Langzeitsimulation wird eine 31-jährige Wetterreihe der Station Flughafen Hannover (etwa 25 km Luftlinie von der Halde Sigmundshall) verwendet.

In Kapitel 5 wird neben der zeitlichen die räumliche Variabilität der Verdunstung von der Haldenoberfläche behandelt. Über die Verdunstung ist der Wasserhaushalt an den Strahlungs- und Energiehaushalt gekoppelt. Die Flussdichte der eingehenden Solarstrahlung wird entscheidend durch die Topografie (Hangneigung und Exposition) beeinflusst. Ein umfangreiches Modell zur Ermittlung von Werten der Globalstrahlung aus Hangneigung, Exposition, Bewölkung und Sichtweite (VDI, 1994) wurde als Erweiterung des geografischen Informationssystems (GIS) ArcView (ESRI, 1998) umgesetzt. Zur Schätzung der potenziellen Verdunstung aus der Globalstrahlung wird die Gleichung von Priestley und Taylor (1972) sowie Messwerte der Lufttemperatur verwendet. Mithilfe des Modells werden für die Rasterflächen eines digitalen Höhenmodells (Digital Elevation Model, DEM) der Halde Tageswerte der potenziellen Verdunstung berechnet. Die Ergebnisse werden zu einer Karte der mittleren jährlichen Verdunstung von der Haldenoberfläche über drei Jahre aggregiert. Berechnete Werte der Globalstrahlung und Verdunstung für drei Punkte an Hängen unterschiedlicher Neigung und Exposition (Südhang, Nordhang, Ebene) werden mit Messwerten verglichen. Abschließend werden in Kapitel 6 die Schlussfolgerungen diskutiert.

2. Physical Properties of a Soil Substitute Derived from an Aluminum Recycling By-Product

2.1 Abstract

Recycling of aluminum has become a significant industrial process. In this process, large amounts of fine-granular, so-called aluminum recycling by-product (ALRP) are generated. It has been suggested to use ALRP, possibly mixed with other industrial by-products, as a soil substitute, especially as cover material for mine tailings. To judge the feasibility of ALRP as a soil substitute, its properties must be known. In this study, physical characteristics of an industrially produced ALRP, mixed with the flue gas desulfurization by-product (FGDP) of a coal combustion plant, were determined. The texture of both ALRP and the ALRP-FGDP mix resembled a silt loam. The volumetric water content of the produced mix was 13%, and the salt content (NaCl) averaged 35.5 wt.%. Bulk densities of ALRP and ALRP-FGDP mix were 0.93 and 0.88 Mg m^{-3}, respectively. Saturated hydraulic conductivity of the salt-washed and unwashed materials varied between 6.7 and 293.8 cm d^{-1}. Plant-available water-holding capacity was 36.3% for washed ALRP and 45% for the corresponding mix. The erodibility factor K of ALRP was estimated as 0.62 Mg ha^{-1} h N^{-1}. Because of the cementing effect of FGDP, the erodibility of ALRP-FGDP was reduced considerably. Addition of FGDP increased the plasticity index of 2.2% moisture of ALRP to 8.9% for washed ALRP-FGDP. In view of its physical properties, ALRP-FGDP seems to be suitable as cover material for mine tailings, even on steep slopes. The collected data may serve future users of similar products.

2.2 Introduction

Aluminum Recycling

Aluminum for industrial use is provided by two distinct suppliers: primary aluminum (Al) producers and secondary Al smelters. In recent years, production of primary Al, predominantly from mined bauxite ore, has increased considerably. In 1986, 16,396 kt of primary Al was produced worldwide. By 1998, Al production had increased to 22,100 kt (USGS, 1999a). Recycled Al performs equally well as primary Al in most applications. Because secondary Al is produced with as much as 90% energy, capital, and labor savings, an increase in Al recycling has also been observed. In the United States, for example, the

production of recycled Al rose from 850 kt in 1986 to 1,500 kt in 1998 (USGS, 1999b). Other countries with a high secondary Al production are Germany, Italy, Japan, Great Britain, France, and the Netherlands. In Germany, for example, 324 kt (or 46%) of the total 709 kt of Al produced in 1996 was recovered from scrap (Federal Statistical Office Germany, 1997).

During the recycling process, Al scrap is melted in reverberatory or rotary furnaces. At the charging well of the furnace, the scrap is lowered through a layer of molten salt, called flux. Flux is a product sold by the salt-mining industry. The salt flux layer in the furnace serves multiple purposes. It enhances heat transfer to the scrap, strips oxides and other impurities such as carbides, nitrides, and sulphides from the molten metal, and keeps inclusions in suspension. By acting as a physical barrier between the air and Al, the salt flux minimizes Al losses by oxidation. Fluxes of various chemical compositions have been developed. Besides reducing losses, it is believed that selected fluxes are effective in refining the metal for different types of scrap. Most commonly, the salt flux is a mixture of NaCl (about 70 wt.%) and KCl (about 30 wt.%). The mixture also can contain small amounts of CaF_2 (Rao and Dawson, 1980).

The amount of salt used depends on the amount of impurities contained in the scrap. For each kg of impurities, approximately 1 kg of flux is used. When liquified, the metal is tapped from the furnace, and the top layer (which consists of solid Al_2O_3, spent flux, entrapped metal, and other contaminants) must be skimmed. This top layer of dark-gray material is generally called black dross. Typically, black dross contains metallic Al (10-20 wt.%), a salt flux mixture (40-55 wt.%), and 20-50 wt.% of Al_2O_3 (Karvelas et al., 1991). Depending on the market price of Al and the cost of landfill, black dross can be processed further to recover as much as 20% of the remaining metal by means of salt bath rotary furnaces or hammer mills, which separate Al physically from the dross. When the recovery of Al is economically not feasible, and if environmental regulations permit dumping of the dross, it is usually disposed of in conventional landfills.

During black dross processing, low-grade scrap that includes black dross is melted in rotary furnaces. Because of the high content of impurities, considerably more flux is used during black dross processing as compared with recovering Al from scrap. The residues that are generated during black dross processing are referred to as salt cake. The composition of salt cake depends on that of the black dross; often it contains 3-5 wt.% Al, 15-30 wt.% Al_2O_3, 30-55 wt.% NaCl, and 15-30 wt.% KCl. The amount of Al recycling by-products (ALRP), including black dross and salt cake, produced per ton of recovered Al,

ranges from 400 to 700 kg. Worldwide, considerable amounts of ALRP are produced yearly; for example, 510 kt of salt cake were generated in the United States in 1993 (Hryn et al., 1995).

In Germany and Italy, the disposal of ALRP in landfills is not permitted. In these countries, ALRP recycling systems have been developed to recover both the aluminum and salt components from the salt cake. The German and Italian systems employ essentially the same dry and wet processing steps: crushing (generally to less than 1 mm size) and screening for Al recovery, salt leaching, off-gas treatment, and evaporation/crystallization for salt recovery. During the wet processing stage, ALRP is leached with water to produce a saturated brine slurry. This slurry is vacuum-filtered, yielding a clear brine solution and an Al_2O_3 cake. Water is evaporated from the brine at about 115°C, and essentially all the fluxing salts crystallize and can be recovered. The salts from this process meet the user specifications of the secondary Al industry. From 1987 to 1991, approximately 120 kt of salts were recovered in Germany and reused by Al smelters (Jody et al., 1992).

Current Research and Developments in ALRP Processing

The evaporation of water to recover salt during ALRP processing is an energy-intensive process. Using a single-stage evaporator, it requires about 0.64 kWh per kg of water. Multi-effect evaporators use vapor compression to recycle the latent heat. They operate at a reduced pressure to lower the brine's boiling temperature. In this way, the required amount of energy is reduced by 50%. Jody et al. (1992) stated that a considerable portion of the operating expenses of the recycling process is the cost of energy. These authors concluded that recycling technology is economical only when either the Al content of the salt cake or the cost of landfill, or both, are high. Research has been conducted to review and evaluate energy-reducing salt-recovering concepts for ALRP. These include freeze-crystallization, solvent/antisolvent extraction, common-ion effect, high-temperature/high-pressure processes, capillary effect systems, and electrodialysis (see Karvelas et al., 1991, or Graziano et al., 1996). A new dross treatment process utilizes a plasma torch to remelt Al scrap and dross. The plasma torch, unlike conventional oil or gas burners, does not require large amounts of air being blown into the furnace. The oxidation of Al is therefore inhibited without the use of flux salts (Lavoie et al., 1990).

In Germany, the use of processed ALRP as a cover material for salt-mine residue mounds has been suggested. Potash fertilizer, road salt, and salts for

application in the chemical industry are produced there mostly in underground mines. In this process, especially in potash mining, solid residues of mainly rock salt (NaCl) are unavoidable. Although this material is partly sold, and as much as 60% of the residue is returned to abandoned mine caverns, the remaining salt wastes are piled up in mounds. Briny discharge from such mounds during and after rainfall is conveyed through pipelines into rivers of low stream order and high runoff to relieve smaller local streams and to accomplish maximum dilution ratios. Under Germany's humid climate, salt mine tailings annually produce large amounts of highly contaminated runoff. Because the number of such mine tailings in Germany is large, these bare salt mounds pose a serious environmental problem. Covering such tailings with soil or soil-like material and establishing a plant cover is one possibility to reduce the amount of discharge. Additional advantages of this practice are the establishment of a low-cost method of ALRP disposal and the conservation of natural soil that would have to be used alternatively to cover such mine tailings.

In 1996, an Al recycling plant opened at the site of a potash mine near Hannover in northern Germany. The mine, operated by the K+S Company (Kali und Salz GmbH), generates among other products salt flux for the secondary Al industry. The new facility has a yearly processing capacity of 90 kt black dross and salt cake. About 3.6 kt of metallic Al is separated annually from raw material in a dry processing stage that involves both crushing and screening. In the wet processing stage, KCl is leached at a temperature of 104°C. During the leaching process, gases also are produced. These gases are cleaned to yield solid $(NH_4)_2SO_4$, which is sold as fertilizer. Also, CH_4 and H are produced in this process, and are used for onsite steam and electricity production. In the process, 8.7 kt of KCl are recrystallized yearly by cooling the hot brine in a vacuum atmosphere to 35°C. The crystallized potash is dried and sold as a fertilizer containing an equivalent of about 50% of K_2O. Sodium chloride remains in the solution, which is not evaporated but reused for the leaching process.

Main components of the remaining, granular ALRP are Al_2O_3 (27-33 wt.%), SiO_2 (4-10 wt.%), and soluble NaCl (45-55 wt.%). Magnesium aluminate ($MgAl_2O_4$), Fe_2O_3, CaO, CaF_2, and KCl (1-3 wt.%) are additional minerals known to occur in the material. By centrifugation, this material is dewatered to a water content of 16 to 18 wt.%. Subsequently it is used as a main substance in a cover material for the nearby salt-mine residue mound. The main advantage of this process over systems recovering the flux salts entirely lies in the energy saved by not evaporating the water from the brine. Table 2.1 shows the chemical composition of air-dry ALRP, indicating that Al and Si are main

constituents, but also that the amounts of Na and Cl in the recycling by-product are high. The table indicates further that ALRP contains a number of trace elements, some of them (e.g., Cu and Cr) occurring in concentrations that trigger environmental concerns when ALRP is proposed as a soil substitute.

Table 2.1   *Principal components and trace elements in the aluminum recycling by-product (ALRP) used in the present study.* †

Element	Wt.%	Element	Wt.%	Element	mg kg^{-1}
Al	18.78	Na	13.65	Cu	2314
Si	2.40	Cl	18.19	Cr	417
Ca	1.58	P	0.02	Ni	169
Fe	0.77	S	0.18	Pb	116
K	2.53	F	0.33	Zn	708
Mn	3.66	Ti	0.29	As	4

† Ignition loss was 13.79%; Mg was not determined

Other Possible Uses of ALRP

Besides use as a cover material for mine tailings, alternative applications of ALRP have been considered. Hryn et al. (1995), for example, mentioned the use of ALRP oxide residues in manufacturing ceramics, refractory, and cement. However, before any application of ALRP can be recommended, its properties and the possible environmental impacts of its use must be assessed. Numerous studies have been conducted to assess the properties and environmental impacts of different solid industrial and municipal wastes. Examples of such wastes are alkaline-stabilized sewage sludge (Logan and Harrison, 1995), jarosite waste from copper mining (Kanabo and Gilkes, 1992), and coal combustion residues (Carlson and Adriano, 1993).

Some research on the chemical, in particular fertilizing, properties of ALRP has been conducted. The use of ALRP as a soil amendment, for example, has been considered. Rader et al. (1945) conducted greenhouse experiments to study the N-fertilizing value of 21 ALRPs from 14 U.S. melting and refining plants. In an experiment with millet (*Pennisetum*, L.) and tomatoes (*Lycopersicon lycopersicum*, L.), Rader et al. (1945) found that ALRP was only

1 to 33% as effective in increasing dry-weight yield as the same N quantity given as $(NH_4)_2SO_4$. There were indications that some samples of the dross contained substances with depressive effects on plant growth. Rader et al. (1945) concluded that the fertilizer value of dross depended on the transformation rate of dross N into NH_4 and NO_3.

Lindo (1997) studied the fertilizing effect of K from ALRP on corn (*Zea mays*, L.) and pearl millet (*Pennisetum americanum*, L.), grown under field conditions. Lindo (1997) found that ALRP was just as effective as KCl in maintaining crop yield and soil fertility. No serious deleterious effects were detected on either the soil or the crop. For our present study, however, the work of Lindo (1997) hardly applies, because from our final product (ALRP) almost all K has been removed.

Little work in the field of metallurgy has been published on physical ALRP properties, (see, for example, Manfredi et al., 1997). To our knowledge, no study has been published about the soil physical properties of ALRP. The objective of our study was to determine the physical properties of the ALRP that is produced by the dross processing plant near Hannover. Physical data are essential if ALRP is to be used as a substitute for soil to reclaim disturbed land or to cover mine tailings. For example, hydraulic properties are needed to estimate the material's capability of storing infiltrated water and enhancing evaporation when applied as a cover layer. Besides studying ALRP, physical properties of a coal combustion by-product and a 7:3 mixture of ALRP and this coal combustion flue gas desulfurization by-product (FGDP) will be determined.

The ALRP-FGDP mixture was established at the Hannover dross-processing plant after it was observed that pure ALRP as a cover material on the steep slopes of the mine's residue mound was susceptible to erosion. FGDP are known for their stabilizing properties. Flue gas desulfurization at coal combustion power plants involves the removal of SO_x from the smokestack, usually by adding a limestone slurry to the flue gas stream. As a result, FGDP is a combination of fly ash, Ca-S salts (CaS and/or $CaSO_4$), and $CaCO_3$. Actual composition of FGDP may vary considerably, depending on the parent coal, the conditions of combustion, and the type of emission control devices, including the desulfurization system used (Carlson and Adriano, 1993; Henzel et al., 1982). In construction engineering it is well known that FGDP has cementing properties. For example, the FGDP described by Laperche and Traina (1999), which was similar to the one we applied, was used recently for construction of embankments and livestock waste lagoons.

2.3 Materials and Methods

Sample Preparation of ALRP and ALRP-FGDP

The dross-processing plant near Hannover has been producing ALRP since 1996. On one of the slopes of the nearby mine-residue mound an area has been assigned for experiments with ALRP as a cover material. Initially, pure ALRP was transported with a conveyor belt up the 120-m-high mound and dumped on the test site below. Later, after considerable erosion had been observed, a 7:3 ALRP-FGDP mix was applied as cover material.

For the present study, 7 parts of ALRP at the plant were mixed with 3 parts of FGDP on a volumetric basis in a device resembling a concrete mixer. Shovels of ALRP, FGDP, and ALRP-FGDP mixture were taken at equal time intervals from the material flow as the materials entered or left the blending device. Samples of several kg were transported from the recycling plant to the laboratory in sealed containers and were stored at 10°C. Properties determined included moisture and salt content, particle and bulk density, total porosity, particle size distribution, air permeability, saturated conductivity for water and salt solution, moisture retention at approximate suctions of 0.1, 0.3, 0.6, 1.0, 3.0, and 158 m, consistency limits, and erodibility. Unless specified otherwise, standard methods of analysis were used.

Some analyses involved saturation or intensive mixing of samples with water. With high-salt content materials, this led to a partial sample loss, because of leaching. Therefore, some methods were only applied to salt-free samples. To produce such samples, the material was washed with deionized water in an overhead shaker at room temperature. Solution and solids were separated in a centrifuge, and electrical conductivity (Ec) was measured in the solution. The solution was replaced by fresh water, and washing was repeated until Ec was lower than $0.6 \, \text{mS cm}^{-1}$ ($\approx$ tap water). Besides water, brine from the first washing cycle, in equilibrium with the corresponding material, was used for measurements of saturated hydraulic conductivity.

Moisture Content

Moisture content of the studied materials was determined as follows. Samples were weighed in metal cups and oven-dried at 105°C to constant weight. Moisture content was calculated as a percentage of total sample weight and is reported on a dry solid basis including salts. No significant weight loss of

ALRP was observed during drying, i.e., the material did not seem to contain volatile solids.

Stainless steel cylinders ($\approx$ 56 mm in diameter and 40 mm in height) were used to determine volumetric moisture content, bulk density, moisture retention, and saturated hydraulic conductivity. A thin dish-washing cloth was placed at one end of each cylinder and held in place with a rubber band. Each cylinder was filled one-third and compacted with a steel cylinder; this procedure was repeated until a cylinder was completely filled. Samples were weighed and oven-dried at 105°C to constant weight. Moisture content was calculated as a percentage of sample volume. The density of water was assumed to be unity.

Salt Content

The salt content of the test materials was determined with the use of the Ec of aqueous solutions. Small samples of oven-dry material ($\approx$ 10 g) were mixed with de-ionized water and shaken thoroughly. Suspensions were left standing for 0.5 h in order to let undissolved particles settle. Subsequently, Ec was measured in the solution over the solids. Assuming that a rise in Ec of 1 mS cm^{-1} corresponded to a rise in salt concentration of 0.64 g L^{-1} (Richards, 1954), we calculated the salt content S (in wt.%) as

$$S = \frac{0.064 \, w \cdot Ec}{m} 100 \qquad\qquad [2.1]$$

where w (in g) is the amount of water added, and m (also in g) is the weight of the oven-dry sample. Initial measurements showed that the ratio of oven-dry material to water had to be at least 1:7 in order to dissolve all solid-soluble components. In view of this experience, a ratio of 1:10 was chosen for all determinations of salt content.

Particle Density, Bulk Density, and Total Porosity

Particle density (PD) of washed samples was determined with the pycnometer method, described by Blake and Hartge (1986b). PD of samples including salt was calculated from PD of both salt and nonsalt components. Percentages of nonsalt and salt components were used as weighting factors. Because ALRP salts consisted primarily of NaCl, the PD of salt components was assumed to be 2.165 Mg m^{-3} (Weast, 1987). Following Blake and Hartge

(1986a), packed cylinder samples as described earlier were oven-dried, weighed, and bulk density (BD) was calculated as weight divided by cylinder volume.

Total porosity was calculated from PD and BD according to Danielson and Sutherland (1986) as

$$\text{Porosity (\% by volume)} = \left(1 - \frac{\text{BD}}{\text{PD}}\right)100 \qquad [2.2]$$

Particle Size Analysis

Particle size analysis was carried out according to Gee and Bauder (1986). Samples were crushed to pass a 2-mm sieve. Weighed samples ($\approx$ 10 g) were sieved into the following classes (mm): 0.63 to 2, 0.2 to 0.63, and 0.063 to 0.2. Stokes' sedimentation procedure was used to partition the fraction < 0.063 mm into the following classes: 0.02 to 0.063, 0.0063 to 0.02, 0.002 to 0.0063, and < 0.002 mm (clay). Fractions were oven-dried and weighed, and the difference between initial sample weight and the sum of all fractions was assumed to be the initial salt content of the sample.

Particle size distribution data for the FGDP were provided by the GfR Company (Gesellschaft für die Aufbereitung und Verwertung von Reststoffen, mbH), Würzburg, Germany. A laser-light scattering method as described by Allen (1981) or Cooper et al. (1984) was applied, using a Malver Diffraction Particle Sizer, Type Mastersize S. No pretreatment of samples was conducted.

Particle-size distribution for the salt-free ALRP-FGDP mix was computed, using results from pure ALRP and pure FGDP, with the fractions of the mixing ratio as weighting factors. Fractions were 7:3 on a volumetric basis for saline ALRP and FGDP, which corresponds to 5.2:3 for the leached mix, when an initial salt content of ALRP of 50 wt.% is assumed.

Permeability to Air, Water, and Salt Solutions, and Saturated Hydraulic Conductivity

Packed cores of air-dried material were used to determine the air permeability k_a (Evans, 1965; Corey, 1986). The flux q, defined as the air volume Q, passing through a sample of length l and cross-section A during a time increment Δt under a constant pressure gradient $\Delta P/l$, was measured with an air permeameter from the Eijkelkamp Company (Giesbeek, the Netherlands). Permeability k_a was calculated from the equation:

$$q = \frac{Q}{A \, \Delta t} = \frac{k_a}{\eta} \frac{\Delta P}{l} \qquad [2.3]$$

where η is the dynamic viscosity of the air (1.82×10^{-4} P at 20°C, see Weast, 1987).

Saturated hydraulic conductivity Ks was measured using the constant-head method (Klute and Dirksen, 1986). Water was used as flow medium for both washed and unwashed samples. Additionally, salt solutions in equilibrium concentration with the investigated material were used to determine Ks of unwashed samples in order to reduce leaching losses during the measurement. Each Ks measurement was repeated six times. In addition to Ks, the intrinsic permeability $k_{w \, (or \, s)}$ was determined as

$$k_{w \, (or \, s)} = Ks_{w \, (or \, s)} \frac{\eta_{w \, (or \, s)}}{\rho_{w \, (or \, s)} \, g} \qquad [2.4]$$

where η is the dynamic viscosity, ρ is the fluid density, and g is the acceleration due to gravity.

The subscript w (or s) in Eq.[2.4] denotes that either water or brine solution was used as fluid. The density $\rho_{w \, (or \, s)}$ of the fluids was measured with pycnometer flasks and the viscosity $\eta_{w \, (or \, s)}$ with a capillary flow viscosimeter, submerged in a water tank kept at a constant temperature of 20°C. Intrinsic permeability is a property of the medium, supposedly independent of the fluid, and has the dimension of length squared (L^2). For comparison with older soil literature, we express permeability in units μ^2 (= 10^{-8} cm^2).

Moisture Retention

The drying branch of the water retention relation was measured on packed core samples of unwashed and washed ALRP, washed FGDP, and washed ALRP-FGDP mix. Samples, carefully saturated from the bottom with de-aerated tap water, were placed on a porous ceramic plate and dewatered with a hanging water column in steps of 0.1, 0.3, 0.6, and 1.0 m, and a kaolin box for 3.0 m. A pressure plate apparatus was used at 158 m (conventionally called permanent wilting point) to drain washed samples of 1 cm height. Plant-available water

holding capacity was defined as the difference in water content between 1.0 and 158 m of suction, and was calculated accordingly.

Because of salt loss during saturation and dewatering, unwashed ALRP samples settled during the measurement, thus influencing the results. Settling was recorded, and changes in sample volume and weight, salt content, bulk density, and volumetric water content were estimated after each dewatering step, using average particle densities for soluble and non-soluble sample components, and assuming that loss of sample volume was equal to volumetric salt loss. The RETC code (van Genuchten et al., 1991) was used to estimate residual water content θr, saturated water content θs, and empirical van Genuchten parameters α, n, and m. These parameters were used to fit retention curves of the form

$$S_e = \frac{1}{\left[1 + (\alpha h)^n\right]^m}$$

[2.5]

(van Genuchten, 1980) to the measured data, where S_e is the effective degree of saturation or reduced water content ($0 \le S_e \le 1$), and h is the suction.

Consistency

The consistency limits, or Atterberg limits (Sowers, 1965), were determined by standard procedures of the American Society for Testing Materials (ASTM, 1992). A commercially available apparatus (FHF Strassentest, Baustoff-Prüfsysteme, Besigheim, Germany) was used to determine the liquid limit with use of the Casagrande method. A striking force was repeatedly applied to moist material in a bowl until a small furrow of defined width drawn through the sample closed. The number of strokes necessary to close the gap was counted. Several drops of water were subsequently mixed thoroughly with the material, and the procedure was repeated. Gravimetric water content was determined on subsamples following every repetition. A linear regression model of the form y = mx + b was fitted to the data, with x being the number of strokes, y being the gravimetric water content, and m and b being regression constants. From the regression model, the water content at 25 strokes was calculated and considered as the liquid limit. To determine the plastic limit, samples were rolled on a table surface into a cylindrical body the diameter of a pencil. This was further rolled until signs of crumbling became visible. At this point, gravimetric water content was determined, which was denoted as the plastic limit. The plasticity index was

calculated as the difference between water content at the liquid and plastic limit (see Sowers, 1965).

Erodibility and Erosion

The susceptibility of ALRP to water-induced erosion on the slopes of the mine-residue mound was assessed with the use of the Revised Universal Soil Loss Equation (RUSLE; Renard et al., 1997). This equation can be given as

$$A = R\ K\ LS\ C\ P \qquad [2.6]$$

where A = average annual soil loss (Mg ha^{-1}), R = rainfall erosivity index (kJ m^{-2} mm h^{-1}), K = soil-erodibility factor (Mg ha^{-1} h N^{-1}), LS = topographic factor (-), C = cropping-management factor (-), and P = conservation practice factor (-).

The factors needed for computational work with Eq.[2.6] were estimated following Schwertmann et al. (1987). The erosivity index R was calculated from the mean annual rainfall at the site of the mine-residue mound. The erodibility factor K of ALRP was estimated from its texture, organic matter content, aggregate size, and permeability class with use of a relation given by Schwertmann et al. (1987) as

$$K = 2.77 \cdot 10^{-6} \cdot M^{1.14} \cdot (12 - OM) + 0.043 \cdot (I - 2) + 0.033 \cdot (4 - J) \qquad [2.7]$$

where M = (% silt + % very fine sand) × (% silt + % sand), OM = % organic matter, I = class of aggregate size, and J = permeability class.

The value for M in Eq.[2.7] was calculated from the data of the particle size analysis for ALRP. Because of the high temperature under which ALRP is produced, it was assumed that ALRP did not contain organic matter (OM = 0.0). Before crushing and sieving the material for particle size analysis, aggregates of about 2 to 10 mm in diameter were observed. According to Schwertmann et al. (1987), this corresponds to a class of aggregate size of I = 3 in Eq.[2.7]. In view of results of hydraulic conductivity measurements, the permeability class was set equal to two (J = 2). Slope length and steepness factors L and S of the mound were derived from an analysis of the geometry. The geometry of the mound was

determined with the use of stereoscopic aerial photographs, a Digital Terrain Model of 5 m × 5 m cell resolution, and a cell-based geographic information system (GIS) integrated modeling technique (see Fischer and Hermsmeyer, 1999). The continuous function for slope steepness influence on soil loss (Nearing, 1997) was used to calculate S. Cropping management factor C and conservation practice factor P were assumed to be unity, because initially the ALRP-covered test field was bare and no conservation measures to reduce erosion were taken after the cover material was deposited on the slopes of the mound. With the RUSLE factors thus estimated, the mean annual material loss due to water erosion was calculated. Actual losses were not measured, but assessed visually after major rainfall events.

2.4 Results and Discussion

Moisture Content

During early stages of ALRP production at the Hannover plant, the material was dewatered under pressure. An average moisture content of about 35% was reached, which turned out to be too high for the material to be transported, particularly on upslope conveyor belts. It was found that a moisture content of the ALRP-FGDP mixture of 12 to 18% was yielding a product of optimal coherence. Because the available FGDP had a moisture content of less than 3% and the mixing ratio of ALRP and FGDP was 7:3, the moisture content of ALRP had to be less than 25%. Since 1998, a decanting centrifuge is operated to dewater ALRP to about 18% before the material enters the mixer. An average moisture content of 13% was determined in the material coming from the mixer, which is at the lower end of the optimum range. A sprinkler system has been installed to moisten the mixed material when dust is occurring.

Salt Content

Even salt-tolerable plants cannot grow in soils with a salt content of more than 1% (Bradshaw and Chadwick, 1980). Therefore, salt content of ALRP-FGDP mix is a key parameter when the material is to be used as a soil substitute on which to grow plants. Average salt content was found to be 50% in unwashed ALRP, 1.65% in unwashed FGDP, and 35.5% in the unwashed mixture (Table 2.2). Salt contents calculated from Ec measurements using Eq.[2.1] and loss of sample mass during particle size analysis varied by less than 4%. As

expected, instantaneous vegetation of fresh ALRP or ALRP-FGDP did not appear to be possible.

At 20°C, 357 g of sodium chloride is soluble in 1 L of water (Weast, 1987). Average annual rainfall at the site is about 640 mm, and average annual potential evaporation is 550 to 600 mm (Keller, 1978). If, for simplicity, potential evaporation is assumed to be equal to actual evaporation, this results in an average seepage rate of 90 mm a^{-1}. Since the BD of the mix is about 1 Mg m^{-3} (see below), a layer of 0.5 m thickness of ALRP-FGDP mix contains 172,500 g m^{-2} (i.e., 35.5%) of easily soluble components, predominantly NaCl. If seepage is salt-saturated until all salts are leached, 483 mm of seepage or at least 5.4 yr are needed to remove salts from a 0.5-m-thick layer to a plant-tolerable level, assuming piston flow to occur.

Particle Density, Bulk Density, and Total Porosity

PD of unwashed ALRP represented an average of the densities of its soluble (2.165 Mg m^{-3} for NaCl) and insoluble components (Table 2.2). Washed ALRP typically had PD of 3.05 to 3.08 Mg m^{-3} (Al = 2.69; Al_2O_3 = 3.965; $MgAl_2O_4$ = 3.60; SiO_2 = 2.65; CaF_2 = 3.18 Mg m^{-3}; Weast, 1987), while unwashed ALRP had densities ranging from 2.63 to 2.94 Mg m^{-3}. The density of FGDP was about 2.31 Mg m^{-3}. Densities of unwashed ALRP-FGDP mix (2.31 to 2.67 Mg m^{-3}) were between the values for NaCl and unwashed ALRP. The average value was 2.46 Mg m^{-3}. High and low values for both unwashed ALRP and unwashed ALRP-FGDP mix thus corresponded to those materials with the highest and lowest salt content. PD of main mineral soil components typically range from 2.5 to 2.8 Mg m^{-3} (Blake and Hartge, 1986b).

BD ranged from 0.56 Mg m^{-3} for washed FGDP to 0.93 Mg m^{-3} for ALRP (Table 2.2). High and low values within the group of unwashed materials corresponded to the respective PD values, suggesting that PD and percentage of primary particles, in particular salt content, rather than differences in structure were responsible for the observed BD values. BD of unwashed ALRP ranged between 0.88 and 0.99 Mg m^{-3}. Mineral soils typically have BD of 1.2 to 1.8 Mg m^{-3} (Brady and Weil, 1999).

Table 2.2 *Salt content, particle density, bulk density, and total porosity of unwashed and washed ALRP, FGDP, and ALRP-FGDP (7:3) mixture (N = 3 †).*

Material	Salt content Mean (%)	Salt content Range	Particle density Mean (Mg m^{-3})	Particle density Range	Bulk density Mean (Mg m^{-3})	Bulk density Range	Total porosity Mean (%)	Total porosity Range
Unwashed								
ALRP	50.0	45.0-55.0	2.77	2.63-2.94	0.93	0.88-0.99	66.4	62.4-69.9
FGDP	1.65	1.1-2.3	2.31	2.27-2.35	0.68	0.67-0.70	70.6	69.2-71.5
ALRP-FGDP	35.5	32.0-39.0	2.46	2.31-2.67	0.91	0.66-1.10	63.0	52.4-75.3
Washed								
ALRP	<0.05	-	3.07	3.05-3.08	0.93	0.92-0.93	69.8	69.5-70.1
FGDP	<0.05	-	2.31	2.27-2.35	0.56	0.55-0.57	75.7	74.9-76.6
ALRP-FGDP	<0.05	-	2.67	2.67-2.68	0.88	0.87-0.88	67.2	67.0-67.5

† The number of replicate measurements N in each case was three.

Average total porosity of ALRP, FGDP, and ALRP-FGDP mix was high, ranging from 63.0 to 70.6% for unwashed material and from 67.2 to 75.7% for washed material (Table 2.2). This resulted in low BD, even when PD was high (see Eq.[2.2]). A high total porosity should make ALRP-FGDP mix an excellent material for the uptake and storage of infiltrating rainwater that is to be withheld from seeping into the underlying salt-mine residue (NaCl). Also, after salts have been leached from the mix, it should provide physical properties that are favorable for root penetration.

Particle-Size Distribution

Particle-size analysis is a measurement of the size distribution of individual particles in a grainy material (Gee and Bauder, 1986). Particles of unwashed ALRP were separated according to size limits by wet sieving and Stokes' sedimentation. Both procedures involve intensive mixing of sample solids with water. Salts were leached, and the influence of solid salts on particle size distribution could not be detected. Material loss during the analysis was recorded and was assumed to equal initial salt content. Salt contents were within 4% of those determined from Eq.[2.1] (see Table 2.2). Particle-size distribution in Table 2.3 is listed in percentage by weight of dry, salt-free (or leached) samples.

Gee and Bauder (1986) suggested use of a correction factor when particle-size distribution of clay-size materials from laser-light methods (here: FGDP) is compared with that of sieved and sedimented materials (ALRP). Because mineralogy, particle shape, and PD all affect this factor, it is somewhat difficult to determine, and no computational correction was conducted in this study. Values from Table 2.3, however, support our visual impression that FGDP was both finer-grained and more powdery than ALRP.

The texture of both washed ALRP and FGDP resembled a silt loam, and hence so did the ALRP-FGDP mix. Natural soils of similar particle-size distributions are commonly rated favorable for plant growth, because they provide ample pore space to store plant-available water. This is consistent with results for porosity and moisture retention.

Table 2.3 *Particle-size distribution of washed ALRP, FGDP, and washed ALRP-FDGP.*

Class (mm)	% by weight of sample (excluding salts)			
	ALRP †		FGDP ‡	ALRP-FGDP §
	Mean	STD ¶	Mean	Mean
<0.002	9.0	2.60	25.3	15.0
0.002-0.0063	16.5	3.37	12.7	15.1
0.0063-0.02	19.3	3.28	29.2	22.6
0.02-0.063	17.5	3.48	22.8	19.2
0.063-0.2	22.6	4.12	9.9	18.0
0.2-0.63	13.0	4.52	0.1	8.8
0.63-2.0	2.1	1.66	0.0	1.3

† By sieving and sedimentation (N = 10).
‡ By laser-light scattering; data provided by the GfR Company.
§ Computed from mean values for ALRP and FGDP,
using mixing fractions (5.2:3) as weighting factors.
¶ Standard deviation.

Permeability to Air, Water, and Salt Solutions, and Saturated Hydraulic Conductivity

Densities and dynamic viscosities of aqueous solutions in equilibrium with ALRP, ALRP-FGDP mix, or FGDP (all unwashed) were 1.15, 1.12, and 1.01 Mg m^{-3}, and 1.51, 1.36, and 1.05 mPa s, respectively. To minimize the effect of fluid density and viscosity on permeability, and to make results comparable, intrinsic permeabilities were calculated from Eqs. [2.3] and [2.4]. Results are given in Table 2.4. According to Reeve (1965), the air-to-water permeability ratio reflects the magnitude of structure breakdown as a result of wetting. Air is a fluid that has little effect on structure. Water, being a polar liquid, reacts with the material to cause a change in structure, usually resulting in a decrease of permeability, and a k_a/k_w ratio > 1. Swelling, slaking, dispersion, deflocculation, and other processes disrupt the material's structure

upon wetting. A value of 1, which is rarely obtained in work with soils, indicates no change in structure. Values greater than 1 signify a deterioration of structure.

Air permeability ranged from 0.1 μ^2 for washed ALRP and the washed mix to 21.8 μ^2 for unwashed ALRP (Table 2.4). Soils typically have air permeabilities ranging from 0.1 to 18 μ^2 (Reeve, 1965). Intrinsic permeabilities as determined with salt solutions for unwashed samples were lower than air permeabilities for ALRP and ALRP-FGDP mix, yielding air-to-water permeability ratios of > 1. This signifies a structural disruption of the samples upon wetting. Air-to-water permeability ratio for unwashed FGDP was close to 1, indicating structure stability. This might indicate that FGDP, originating from a high-temperature combustion process, mainly consists of amorphous minerals that, much like glass beads, are inert to reactions with polar liquids. The same seems to be true for washed ALRP samples, indicating that the structural disrupture of unwashed (saline) samples upon wetting is mainly caused by salt particles. For soils, the band of values for air-to-water permeability ratio is extremely broad, ranging from 2 or 3 for stable soils to as much as 50,000 for unstable soils (Reeve, 1965).

Saturated conductivity of unwashed samples showed highest values for ALRP (294 cm d^{-1}), lowest for FGDP (75 cm d^{-1}), and intermediate values for the mix (156 cm d^{-1}, Table 2.4). This is in agreement with intrinsic permeabilities as determined with air or with a salt solution. Measured values were in a range that is often determined for fine sand (Klute and Dirksen, 1986).

Permeabilities, permeability ratios, and saturated hydraulic conductivities were higher for unwashed samples than for washed samples. This does not correspond to porosities, which were found to be higher for washed samples, and is unusual in comparison with most porous media. Air permeability, for example, usually depends largely on porosity: The larger the pore space, the higher the permeability (Evans, 1965). An explanation for the unusual behavior might be that space initially taken up by solid but soluble salts in dry unwashed samples becomes available to solute movement after saturation. It seems that solid salts led to an underestimation of original porosity. However, this does not explain why air permeabilities, which were measured on air dried samples, were also higher for unwashed than for washed samples (Table 2.4).

Table 2.4 *Intrinsic permeability to air (k_a), brine solution (k_s), and pure water (k_w), as well as saturated hydraulic conductivity (Ks) to brine solution (Ks_s) and water (Ks_w) of unwashed and washed ALRP, FGDP, and ALRP-FGDP (7:3) mixture (N = 3).*

Material	k_a		k_s		k_a/k_s		Ks_s	
	Mean	Range	Mean	Range	Mean	Range	Mean	Range
	(μ^2)		(μ^2)		(-)		(cm d^{-1})	
Unwashed								
ALRP	21.8	20.5-22.5	4.5	4.48-4.53	4.85	4.82-4.97	293.8	284.7-305.2
FGDP	0.9	0.74-1.01	0.9	0.80-1.02	0.94	0.85-0.99	74.7	70.1-78.9
ALRP-FGDP	7.2	5.3-8.6	2.2	1.90-2.45	3.24	2.98-3.51	155.5	145.4-171.2
Washed			k_w		k_a/k_w		Ks_w	
ALRP	0.1	0.09-0.13	0.1	0.09-0.14	0.85	0.78-0.89	11.2	9.5-12.4
FGDP	0.2	0.13-0.20	0.3	0.23-0.31	0.62	0.55-0.69	21.6	18.4-25.4
ALRP-FGDP	0.1	0.08-0.12	0.1	0.05-0.11	1.25	1.12-1.30	6.7	5.8-7.3

Moisture Retention

Water content at saturation was not measured, but estimated from porosity. Values ranged from 58.9 to 68.2% (Table 2.5), the lowest value being that of unwashed (saline) ALRP. Measured water content at 0.1 m of suction (the lowest suction samples were equilibrated to) was larger than estimated water content at saturation, but high and low water contents at 0.1 m of suction corresponded closely to high and low saturation values between samples. For salt-free samples, the 1.0 m-suction water content (representing field capacity, which is found in natural soils after gravity drainage has occurred following rain) was on average only 3.9% less than the 0.1 m-water content (Table 2.5). For unwashed ALRP, the difference was 16.8%. There was considerably less water in washed materials at 158 m of suction than at 3.0 m of suction (Table 2.5), indicating that a high percentage of water was held in small pores, or thin water films with little or no liquid continuity. The 158-m suction water content was highest for washed ALRP (24.3%). Plant-available water holding capacity of washed materials ranged from 36.3 to 55.7%, with a mean of 45.7%, which is higher than that of many well-aggregated soils high in organic matter. The highest value was that of the washed FGDP (55.7%).

This, again, may reflect a glassy, amorphous structure of the mineral components of this material. Rather fine-grained, FGDP can hold much water in its large pore space, but also easily releases this moisture under suction. The reason for this behavior is possibly the lack of expanding clay minerals in this particular material.

Equation [2.5] was used to calculate retention curves from the van Genuchten parameters given in Table 2.5. The quantities θr and θs are the fitted residual and saturated water contents, respectively. The residual water content θr specifies the maximum amount of water that will not contribute to liquid flow because of blockage from the flow paths or strong adsorption to the solid phase. van Genuchten et al. (1991) stated that θr is an extrapolated parameter, and hence may not necessarily represent the smallest possible water content, nor the water content at 158.49 m of suction. As starting values for θs and θr in the fitting procedure with the RETC code, water contents at 0.0 and 158.49 m of suction from Table 2.5 were selected. Values of R^2 for regressions of observed versus fitted values varied from 0.987 to 0.995.

Table 2.5 *Moisture retention, water-holding capacity, and van Genuchten parameters of unwashed and washed ALRP, washed FGDP, and washed ALRP-FGDP (7:3) mixture (N = 3, unless noted otherwise).*

	Volumetric water content (%)							
	Unwashed		Washed					
	ALRP †		ALRP		FGDP		ALRP-FGDP	
Suction (m)	Mean	Range	Mean	Range	Mean	Range	Mean	Range
0.0‡	58.9	-	62.3	-	68.2	-	59.7	-
0.1	61.3	55.3-69.2	64.6	64.0-65.0	72.1	71.7-72.5	65.0	64.8-65.1
0.32	n.d.	n.d.	62.6	61.3-63.6	69.3	69.1-69.8	63.6	63.3-63.9
0.6	48.5	40.9-62.9	61.3	60.8-62.0	68.2	67.8-68.7	62.4	62.1-62.9
1.0	44.5	35.4-57.4	60.6	60.0-61.2	67.7	67.3-67.5	61.8	61.2-62.5
3.0	31.0	21.8-44.4	59.1	58.2-60.4	62.4	61.7-63.8	60.8	60.0-61.8
158.49	n.d.	n.d.	24.3	24.0-24.7	12.0	11.5-12.2	16.8	16.3-17.1
Plant-available water	-	-	36.3	36.0-36.5	55.7	54.8-56.0	45.0	44.9-45.4
van Genuchten parameters								
θr (%)	17.0	-	0.0	-	0.0	-	0.0	-
θs (%)	60.3	-	62.8	-	69.7	-	62.6	-
α (m^{-1})	1.682	-	0.148	-	0.180	-	0.070	-
n (-)	1.674	-	1.299	-	1.523	-	1.543	-
m (-)	0.403	-	0.230	-	0.346	-	0.352	-

† N = 6. ‡ Volumetric water content at 0.0 m of suction was set equal to porosity calculated with Eq.[2.2], minus 5%, using average values for particle density from Table 2.2, and oven-dried sample weight from retention measurements. n.d.: not determined.

The inverse of the empirical parameter α (L^{-1}) is often referred to as the air entry value or bubbling pressure, i.e., the suction at which the material begins to release significant amounts of water, or the suction at which the water retention curve bends downward. To impose a restriction on the permissible values of the empirical constants m and n, the relation m = 1-1/n was selected (van Genuchten, 1980). Retention curves from fitted parameters given in Table 2.5 are shown in Fig. 2.1.

The relationship between water content and suction is a fundamental part of the characterization of the hydraulic properties of porous materials. The water retention function depends primarily on the texture or particle-size distribution of the material, and the structure or arrangement of the particles (Klute, 1986). Water retention curves in Fig. 2.1 reveal similar hydraulic behavior for all washed (salt-free) materials. The finest-grained material studied (FGDP) had the largest water content at low suctions, but the lowest water content at high suctions. Washed ALRP had a lower water content at low suctions, a higher water content at high suctions, and a similar bubbling pressure as FGDP. The ALRP-FGDP mix was intermediate. The unwashed-ALRP curve is considerably different from the washed-material curves in that it has a lower water content at low suctions and a lower air entry value.

Washed samples of all materials, including washed ALRP, did not reveal visible signs of swelling or shrinking. This indicates again that the material structures were relatively rigid, meaning that a decrease of water content required the entry of air. With unwashed ALRP samples, settling occurred during saturation and dewatering of samples, and totaled 23.3% of sample volume.

Because nonsoluble ALRP compounds (i.e., washed ALRP) are rigid, there was no reason to assume that the loss of volume of unwashed ALRP was the result of particle shrinking due to dewatering. Therefore, loss of sample volume most likely was due to dissolved and leached salts. Volumetric water content at different suctions was corrected for loss in total volume, assuming that salt loss was not larger than the visible loss of volume, i.e., assuming that the porosity remained constant. However, no measurements were conducted to test this assumption, and the water retention curve for unwashed ALRP, shown in Fig. 2.1 (and volumetric water contents given in Table 2.5), might not be totally free from artifacts.
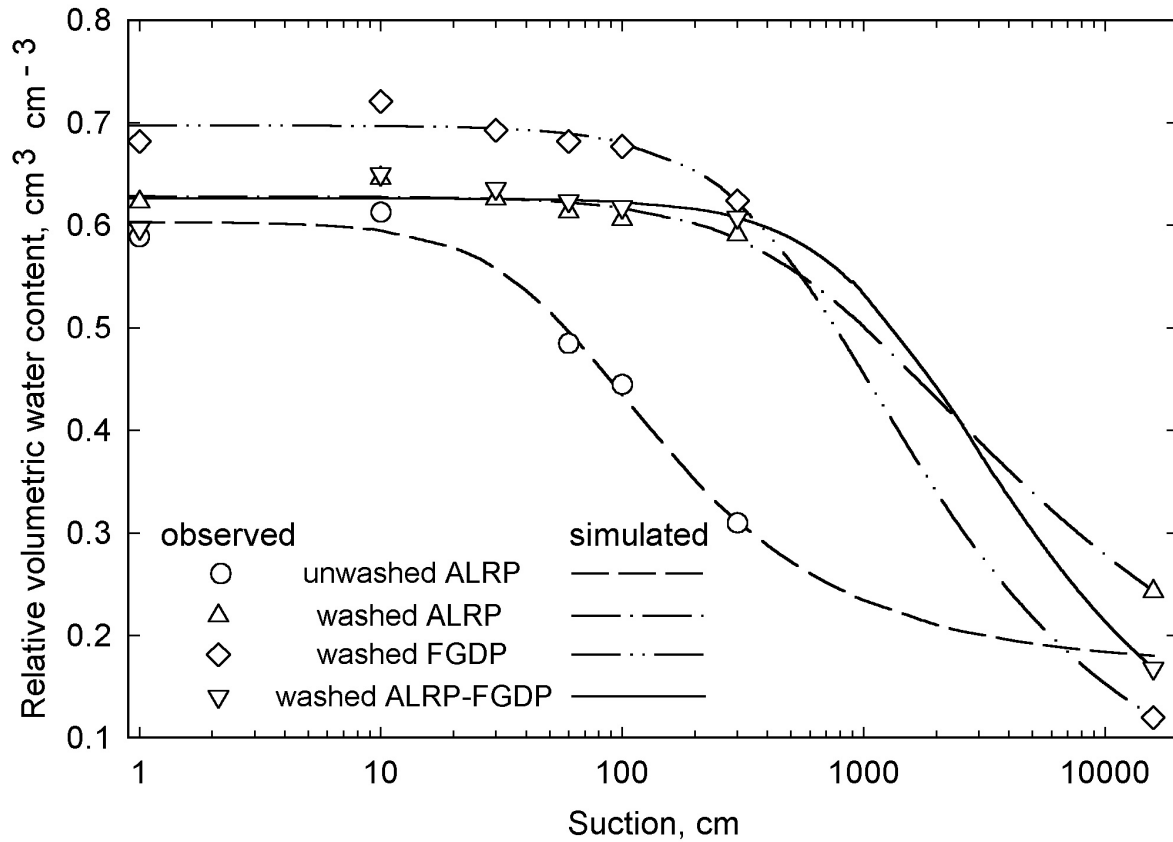
Fig. 2.1 *Moisture retention curves for unwashed and washed ALRP, and for washed FGDP and ALRP-FGDP (7:3) mixture. Measured data and van Genuchten parameters for the fitted curves are given in Table 2.5.*

Consistency

The Atterberg limits (liquid limit and plastic limit) and the plasticity index are measures of the ability of a porous material to be deformed across a range of moisture contents. The liquid limit is the gravimetric moisture content at which a material will flow when subjected to a striking force. It is an indirect measurement of shear strength. The higher the moisture content at the liquid limit, the lower the potential of the material to flow or slump under normal moisture conditions. Data and linear regression models fitted to the number of strokes necessary to close the furrow in the Casagrande apparatus in relation to corresponding water contents are given in Table 2.6.

Table 2.6 *Atterberg limits and plasticity index of unwashed and washed ALRP, FGDP, and ALRP-FGDP (7:3) mixture.*

Material	Model	R^2	Liquid limit % moisture †	Plastic limit % moisture	Plasticity index %
Unwashed					
ALRP	y = -0.1138 x + 24.378	0.95	21.5	19.3	2.2
FGDP	y = -0.3933 x + 44.680	0.86	34.8	32.2	2.6
ALRP-FGDP	y = -0.1583 x + 26.228	0.67	22.3	19.5	2.8
Washed					
ALRP	y = -0.0862 x + 56.252	0.42	54.1	47.6	6.5
FGDP	y = -0.8760 x + 74.658	0.93	52.8	43.2	9.6
ALRP-FGDP	y = -0.2101 x + 48.432	0.72	43.2	34.2	8.9

† Gravimetric moisture content y, at x = 25 strokes, calculated from the corresponding regression model.

Unwashed ALRP-FGDP mix samples had an average liquid limit of 22.3% moisture by weight. Because the moisture content of the material that is leaving the mixer is about 13%, it does not slump under normal moisture conditions. However, the liquid limit helps to explain why initially ALRP, dewatered under pressure to a moisture content of 35%, could not be transported upslope on a conveyor belt. The liquid limit of FGDP (34.8%) was well above the average moisture content of this material when it entered the mixer (< 3.0%). Water contents of all materials at the liquid limit are lower than water contents at 1 m of suction (≈ field capacity, see Table 2.5). After heavy rainfall, this may potentially lead to stability problems, because material may slump before it will be dewatered by gravity flow.

The plastic limit is the gravimetric moisture content of a material at which it will begin to exhibit plastic behavior. The higher the moisture content at the plastic limit, the less plastic the material will be at normal moisture contents. The plasticity index, the range of moisture contents over which the material is plastic, is only 2.2% for unwashed ALRP and 2.8% for unwashed ALRP-FGDP mix. This indicates that both materials change from nonplastic, via plastic, to liquid behavior over a very narrow range of water contents. Adding dry FGDP to ALRP dewatered in the decanting centrifuge to about 18% results in an average moisture content of 13% of the mix (see above). This seems to indicate

that the positive effect of adding FGDP results partly from reducing the initial moisture content of ALRP. The result is a nonplastic, granular material that flows evenly down the long slope of the high salt-mine residue mound, thus yielding a relatively homogeneous surface cover.

Liquid limits, plastic limits, and plasticity indices of all materials were considerably higher after washing (Table 2.6). This suggests that the stability of the proposed cover layer material will increase with decreasing salt content over time, under a humid climate. Chemical reactions in the moistened FGDP, similar to those occurring in gypsum or hydraulic cement, may contribute to an increase in stability. However, such reactions were not part of the research conducted during this study.

Erodibility and Erosion

With the rainfall erosivity index relation given by Schwertmann et al. (1987), the factor R in Eq.[2.6] was estimated as $R = 51.7$ kJ m^{-2} mm h^{-1}, for a mean annual rainfall at the site of 640 mm. For the erodibility factor of pure ALRP we calculated $K = 0.62$ Mg ha^{-1} h N^{-1}. Because the length of the relevant slope of the mound was 130 m and the mean angle of this slope was 36°, it was estimated that the topographic factor in Eq.[2.6] LS = 28.7. For C = 1 and P = 1, a value for the average annual ALRP loss due to erosion by water was calculated as $A = 919.9$ Mg ha^{-1}. When compared with common agricultural soils, both the calculated K-value and A-value are high. It is obvious that these calculations can only give a rough estimate about the erodibility and the possible erosion losses of ALRP as a cover material. However, the computational results were confirmed by observations during the initial stage of the project, when pure ALRP was used as cover material and considerable erosion was noticed. Therefore, ALRP was mixed with FGDP, and with an ALRP-FGDP cover layer, erosion practically ceased to exist. A possible reason is the formation of carbonate and silica cements in the mix. Fly ash materials, such as FGDP, frequently undergo pozzolonic reactions, which may have a strong erosion-reducing effect (the name of such reactions is derived from Pozzuoli, a city near Naples, Italy, where since Roman times it has been known that volcanic ashes, mixed with burned limestone, yield strong mortar and cement). For the ALRP-FGDP mix no K- or A-value was calculated, because RUSLE does not consider pozzolonic effects.

2.5 Conclusions

Physical properties of ALRP, mainly from a metallurgical point of view, have been reported previously (e.g., Manfredi et al., 1997). Our study, however, appears to be the first survey on some of the basic soil physical and hydraulic properties of ALRP and an ALRP-FGDP mixture. Our data show that the materials had physical and hydraulic properties that resemble those of fine-textured soils, with stable aggregates, and a nonplastic consistency. This applies in particular to the moisture retention curves. These curves were similar to those of fine-textured soils with predominantly small pores and a medium to high plant-available water-holding capacity. Also, it was possible to describe these curves with the van Genuchten (1980) model. Further, the investigated materials showed a surprisingly high permeability. PD and BD of the various materials appeared to reflect the ratio of the different components in the mixtures. The amount of apparently stable aggregates in the ALRP-FGDP mix was noteworthy and seemed to be the result of chemical interactions of FGDP and water. These possibly include the formation of carbonate and silicate cement. Our data, concerning the physical properties of the studied materials, in particular those of the ALRP-FGDP mixture, seem to indicate that these materials are suited to serve as cover materials, even on steep slopes of high salt-mine residue mounds.

Our ongoing research is focused on estimating the effectiveness of a proposed cover layer of ALRP-FGDP mix on a salt-mine residue mound in reducing the amount of discharge. To this end, a soil water simulation model is used. The measured hydraulic properties of the cover material are essential model parameters. However, so far all laboratory measurements of physical and hydraulic properties have been made on fresh material, and it is not clear how characteristics might change over time. For example, if the portion of FGDP added to ALRP was too high, the mix might develop a crust that cannot be penetrated by grass sprouts and roots. If it was too low, the material may not be stable on the long steep slopes of the mound under consideration. Hence, further studies and additional observations are necessary before a final evaluation of the physical and hydraulic properties of the studied materials can be made. The same applies to the chemical and mineralogical properties. Not until it has been shown that these properties are environmentally sound, can the use of ALRP be recommended as a soil substitute or mine residue cover. In view of the metallurgical origin of ALRP and some data on heavy-metal contents of comparable materials (Manfredi et al., 1997), we expect that chemical rather than physical attributes eventually may hinder the use of ALRP as a soil substitute.

2.6 References

Allen, T. 1981. Particle size measurement. 3rd ed. Chapman and Hall, New York.

ASTM (American Society for Testing Materials). 1992. Standard test method for liquid limit, plastic limit, and plasticity index of soils. D 4318. p. 94-104. *In* ASTM standards on soil stabilization with mixtures. ASTM, Philadelphia, PA.

Blake, G.R., and K.H. Hartge. 1986a. Bulk density. p. 363-376. *In* A. Klute (ed.) Methods of soil analysis. Part 1, 2nd ed. ASA and SSSA, Madison, WI.

Blake, G.R., and K.H. Hartge. 1986b. Particle density. p. 377-382. *In* A. Klute (ed.) Methods of soil analysis. Part 1, 2nd ed. ASA and SSSA, Madison, WI.

Bradshaw, A.D., and M.J. Chadwick. 1980. The restoration of land. The ecology and reclamation of derelict and degraded land. Studies in ecology Vol. 6. Blackwell Scientific Publications, Oxford, U.K. 317 p.

Brady, N.C. and R.R. Weil. 1999. The nature and properties of soils. 12th ed. Prentice Hall, Upper Saddle River, NJ.

Carlson, C.L., and D.C. Adriano. 1993. Environmental impacts of coal combustion residues. J. Environ. Qual. 22:227-247.

Cooper, L.R., R.L. Haverland, D.M. Hendricks, and W.G. Knisel. 1984. Microtrac particle analyzer: An alternative particle-size determination method for sediment and soils. Soil Sci. 138(2):138-146.

Corey, A.T. 1986. Air permeability. p. 1121-1136. *In* A. Klute (ed.) Methods of soil analysis. Part 1. 2nd ed. Agronomy 9, ASA and SSSA, Madison, WI.

Danielson, R.E., and P.L. Sutherland. 1986. Porosity. p. 443-462. *In* A. Klute (ed.) Methods of soil analysis. Part 1. 2nd ed. ASA and SSSA, Madison, WI.

Evans, D.D. 1965. Gas movement. p. 319-330. *In* C.A. Black (ed.) Methods of soil analysis. Part 1. Agronomy 9, ASA and SSSA, Madison, WI.

Federal Statistical Office Germany (Statistisches Bundesamt). 1997. Statistical yearbook for the Federal Republic of Germany. Metzler-Poeschel Publishers, Stuttgart (Germany).

Fischer, C., and D. Hermsmeyer. 1999. Digital photogrammetry and GIS in tailings and mine waste management. p. 77-86. *In* J.D. Nielsen et al. (eds.) Tailings and mine waste '99. A.A. Balkema, Rotterdam (the Netherlands) and Brookfield, VT.

Gee, G.W., and J.W. Bauder. 1986. Particle-size analysis. p. 383-411. *In* A. Klute (ed.) Methods of soil analysis. Part 1. 2nd ed. ASA and SSSA, Madison, WI.

Graziano, D., J.N. Hryn, and E.J. Daniels. 1996. The economics of salt cake recycling. p. 1255-1260. *In* W. Hale (ed.) Light metals 1996. TMS, Warrendale, PA.

Henzel, D.S., B.A. Laseke, E.O. Smith, and D.O. Swenson. 1982. Handbook for flue gas desulfurization scrubbing with limestone. *In* Pollution technology review, No. 94. Noyes Data Corp., Park Ridge, NJ.

Hryn, J.N., E.J. Daniels, T.B. Gurganus, and K.M. Thomaswick. 1995. Products from salt cake residue-oxide. p. 905-916. *In* P.B. Queneau and R.D. Peterson (eds.) Third International Symposium on Recycling of Metals and Engineered Materials. TMS, Warrendale, PA.

Jody, B.J., E.J. Daniels, P.V. Bonsignore, and D.E. Karvelas. 1992. Recycling of aluminum salt cake. Journal of Resour. Management and Technol. 20:39-49.

Kanabo, I.A.E., and R.I. Gilkes. 1992. Low-contaminant jarosite waste as a fertilizer amendment. J. Environ. Qual. 21:679-684.

Karvelas, D.E., E.J. Daniels, B.J. Jody, and P.V. Bonsignore. 1991. An economic and technical assessment of black-dross- and salt-cake-recycling systems for application in the secondary aluminum industry. Energy Systems Division, Argonne National Laboratory. Argonne, IL.

Keller, R. (ed.). 1978. Hydrological atlas of the Federal Republic of Germany (in German). Harald Boldt Publ. Co., Boppard, Germany.

Klute, A. 1986. Water retention: Laboratory methods. p. 635-662. *In* A. Klute (ed.) Methods of soil analysis. Part 1. 2nd ed. ASA and SSSA, Madison, WI.

Klute, A., and C. Dirksen. 1986. Hydraulic conductivity and diffusivity. p. 687-734. *In* A. Klute (ed.) Methods of soil analysis. Part 1. 2nd ed. ASA and SSSA, Madison, WI.

Laperche, V., and S.J. Traina. 1999. Flue gas desulfurization by-product weathering by acidic mine drainage. J. Environ. Qual. 28:1733-1741.

Lavoie, S., C. Dubé, and G. Dubé. 1990. The ALCAN plasma dross treatment process, a new salt-free dross processing technology. *In* J.H.L. van Linden, D.L. Stewart, and Y. Sahai (ed.) Second International Symposium on Recycling of Metals and Engineered Materials. The Minerals, Metals, and Materials Society, Point Clear, AL.

Lindo, P.V. 1997. Environmental impact on an agricultural soil of K, Al, and trace metals in an aluminum recycling by-product. Unpubl. Ph.D. thesis. Auburn University, Auburn, AL.

Logan, T.J., and B.J. Harrison. 1995. Physical characteristics of alkaline stabilized sewage sludge (N-Viro Soil) and their effects on soil physical properties. J. Environ. Qual. 24: 153-164.

Manfredi, O., W. Wuth, and I. Bohlinger. 1997. Characterizing the physical and chemical properties of aluminum dross. Journal of the Minerals, Metals, and Materials Society 49(2):48-51.

Nearing, M.A. 1997. A single, continuous function for slope steepness influence on soil loss. Soil Sci. Soc. Am. J. 61(3):917-919.

Rader, L.F., Jr., D.S. Reynolds, and K.D. Jacob. 1945. Greenhouse and laboratory experiments with nitrogen bearing aluminum dross as a fertilizer. J. Am. Soc. Agron. 37:1024-1032.

Rao, S., and P.R. Dawson. 1980. A state-of-the-art report on secondary aluminum processes with particular emphasis on fluxes and emission control. Warren Spring Laboratory, Department of Industry, Stevenage, United Kingdom Report LR 359 (ME), 82 pp.

Reeve, R.C. 1965. Air-to-water permeability ratio. p. 520-531. *In* C.A. Black (ed.) Methods of soil analysis. Agronomy 9, ASA and SSSA, Madison, WI.

Renard, K.G., G.R. Foster, G.A. Weesies, D.K. McCool, and D.C. Yoder (Coordinators). 1997. Predicting soil erosion by water: A guide to the revised universal soil loss equation (RUSLE). USDA Agriculture Handbook No. 703. U.S. Government Printing Office, Washington, DC.

Richards, L.A. (ed.) 1954. Diagnosis and improvement of saline and alkali soils. Agriculture Handbook No. 60. United States Department of Agriculture.

Schwertmann, U., W. Vogl, and M. Kainz. 1987. Bodenerosion durch Wasser. Vorhersage des Abtrags und Bewertung von Gegenmaßnahmen. Ulmer Verlag, Stuttgart, Germany (in German).

Sowers, G.F. 1965. Consistency. p. 391-399. *In* C.A. Black (ed.) Methods of soil analysis. Part 1. Agronomy 9, ASA, Madison, WI.

USGS (United States Geological Survey). 1999a. Minerals yearbook [Online]. Available: http://minerals.usgs.gov./minerals/pubs/commodity/recycle/index.html (posted 11 Nov. 1999, verified 26 Jan. 2000).

USGS (United States Geological Survey). 1999b. Minerals information. Aluminum statistics and information [Online]. Available: http://minerals.usgs. gov./minerals/pubs/commodity/ aluminum/index.html (posted 24 Jan. 2000, verified 26 Jan. 2000).

van Genuchten, M.Th. 1980. A closed-form equation for predicting the hydraulic conductivity of unsaturated soils. Soil Sci. Soc. Am. J. 44:892-898.

van Genuchten, M.Th., F.J. Ley, and S.R. Yates. 1991. The RETC code for quantifying the hydraulic functions of unsaturated soil. EPA/600/2-91-065. USEPA. Office of Research and Development, Washington, DC.

Weast, R. 1987. Handbook of chemistry and physics. 67th ed. CRC Press, Boca Raton, FL.

3. Lysimeter Study of Water Flow and Solute Transport in a Metallurgical Waste: I. Construction, Operation, and Data Acquisition

3.1 Abstract

In Germany, mounds of solid wastes from potash mining (rock salt, NaCl) produce annually large amounts of briny runoff which are conveyed into streams and rivers. This study was conducted to evaluate the feasibility and effectiveness of an initially saline, fine-grained aluminum recycling by-product as soil substitute in a surface barrier over mine wastes, and to collect data suitable to calibrate a water balance model. Also, the amount of seepage necessary to leach the material to plant-tolerable salinity needed to be estimated. Four free drainage lysimeters were monitored for three years under field conditions near Hannover, Germany. Two lysimeters were filled with a by-product from aluminum recycling, and the other two with a mixture of this by-product and a coal combustion waste. Precipitation, evaporation, discharge, as well as pressure head in three depths were measured continuously. Electrical conductivity in the discharge and in suction cup solutions from four depths was used to monitor desalinization. Mean annual discharge from the pure metallurgical waste and from the mixture was 39% and 24% of rainfall. Materials were sufficiently leached to support growth of ryegrass (*Lolium perenne*, L.) after 444 (pure metallurgical waste) and 281 mm (mix) of seepage, or 28 months of lysimeter operation. With respect to reducing seepage and supporting plant growth, the mix was the better material for an engineered mine-waste surface barrier. Results from this study are useful to calibrate a numerical water balance model, and in designing the final barrier thickness.

3.2 Introduction

By-production of solid wastes is unavoidable in many mining operations. In the potash mining industry of northern Germany, solid residues consist mainly of rock salt (NaCl). Although as much as 60% of these residues are returned to abandoned mine caverns, and some NaCl is sold as road salt, remaining wastes are piled up in mounds. Because of high salinity, tailings usually are void of vegetation. Under the country's humid climate, salt mine residue mounds annually produce large amounts of briny discharge. During and

after rainfall, such discharge is collected on clay base barriers and conveyed into rivers of low stream order. Thus, smaller local streams are relieved and dilution ratios are maximized. Covering potash mine tailings with soil or soil-like material and establishing a plant cover is one possibility to reduce the amount of discharge. It can be assumed that a soil and plant cover will enhance the evaporation from such mounds.

The research reported on was conducted at the Sigmundshall potash mine, operated by the K+S Company (Kali und Salz GmbH) near Hannover, Germany. Mining operations started in 1898, and residues are piled up in a mound next to the mine shaft. This mound is currently about 160 m high (120 m above the surrounding terrain), has steep (35°) slopes, and contains about 13.4 million m^3 of about 96% NaCl and 4% of mostly clay sized (< 0.002 mm) impurities (K+S, personal communication).

Instead of valuable soil material, industrial by-products may be used as cover materials for such mine tailings. This practice has the additional advantages of providing a low-cost method of disposal and a relief of limited landfill capacities. It has been suggested that fine-granular, so-called aluminum recycling by-product (ALRP) be used as soil substitute in a surface barrier for the Sigmundshall mine residue mound. ALRP is a waste material generated in large amounts during remelting of discarded aluminum products. To stabilize this material against erosion on the steep slopes of the mound, it may be mixed with flue gas desulfurization by-products (FGDP) of coal combustion. A description of the physical and hydraulic properties of ALRP and FGDP, which both are medium grained (silt-loam) materials, can be found in Hermsmeyer et al. (2001). Little is known about the water storage capacity of these materials and their performance in minimizing seepage into the underlying mine waste under field conditions. Unweathered ALRP itself is highly saline (40 to 50% NaCl). It is expected that under the humid field conditions of northern Germany easily soluble components will be leached from ALRP (or ALRP-FGDP mix) to a plant-tolerable level of salinity within a few years after application. To our knowledge, the process of desalinization of ALRP, and the amount of seepage needed to reach this level, have not been studied so far.

Field lysimeter studies are one way to evaluate (i) the performance of engineered surface barriers (Lutton et al., 1979; Phillips et al., 1988), and (ii) the leaching of chemicals through soil (Flury et al., 1998). Therefore, it was decided to construct at the Sigmundshall potash mine, a field lysimeter test facility, specifically to study infiltration of precipitation through ALRP and ALRP-FGDP mix barriers into underlying potash mine waste. The main objective of

this research was to assess the feasibility and the effectiveness of these two materials as protective barrier materials. The lysimeter design permits evaluation of one-dimensional flow of water and solute. This is the first of two papers to describe results from the lysimeter study, which examines water balance as precipitation is partitioned into evaporation, storage, and drainage (runoff is prevented by raised edges on the lysimeters). This paper is focused on lysimeter construction, operational complexities, and acquisition of data. Calibration and application of a numerical model to describe the measured data will be covered in a subsequent paper. Test results permit direct comparison of ALRP and ALRP-FGDP mix under local site conditions. The present study includes assessment of 1) seepage control, 2) barrier construction material, and 3) field monitoring of drainage and desalinization of ALRP and ALRP-FGDP mix. Results from the lysimeter facility can be used in determining a final barrier design.

3.3 Materials and Methods

Site and Design

We studied four free drainage lysimeters (L1 to L4) over a period of 35 months (1 Jul. 1997 to 31 May 2000). Lysimeters were installed on the Sigmundshall potash mine area. The installation site was located only about 15 m from the steep (34 to 36°) south-west facing slope of the unvegetated tailings mound. Fig. 3.1 (a and b) depicts a top and a cross-sectional view of the lysimeter setup and instrumentation. Table 3.1 shows details about the lysimeter experiment.

To build the lysimeter containers, a 4 by 4 m^2 frame of wooden walls was constructed on top of the natural soil surface. This has a south facing slope of about two to three degrees. The frame was subdivided by additional walls into subsections of 2 by 2 m^2. To the south of the structure, four 150 L plastic barrels to collect drainage from the lysimeters were lowered into the ground. One-inch (inner diameter) PVC outflow pipes were laid down under the walls to run laterally from the low side of the bottom of each container to the collection barrels. The pipes followed the slope of the soil surface under the installation.
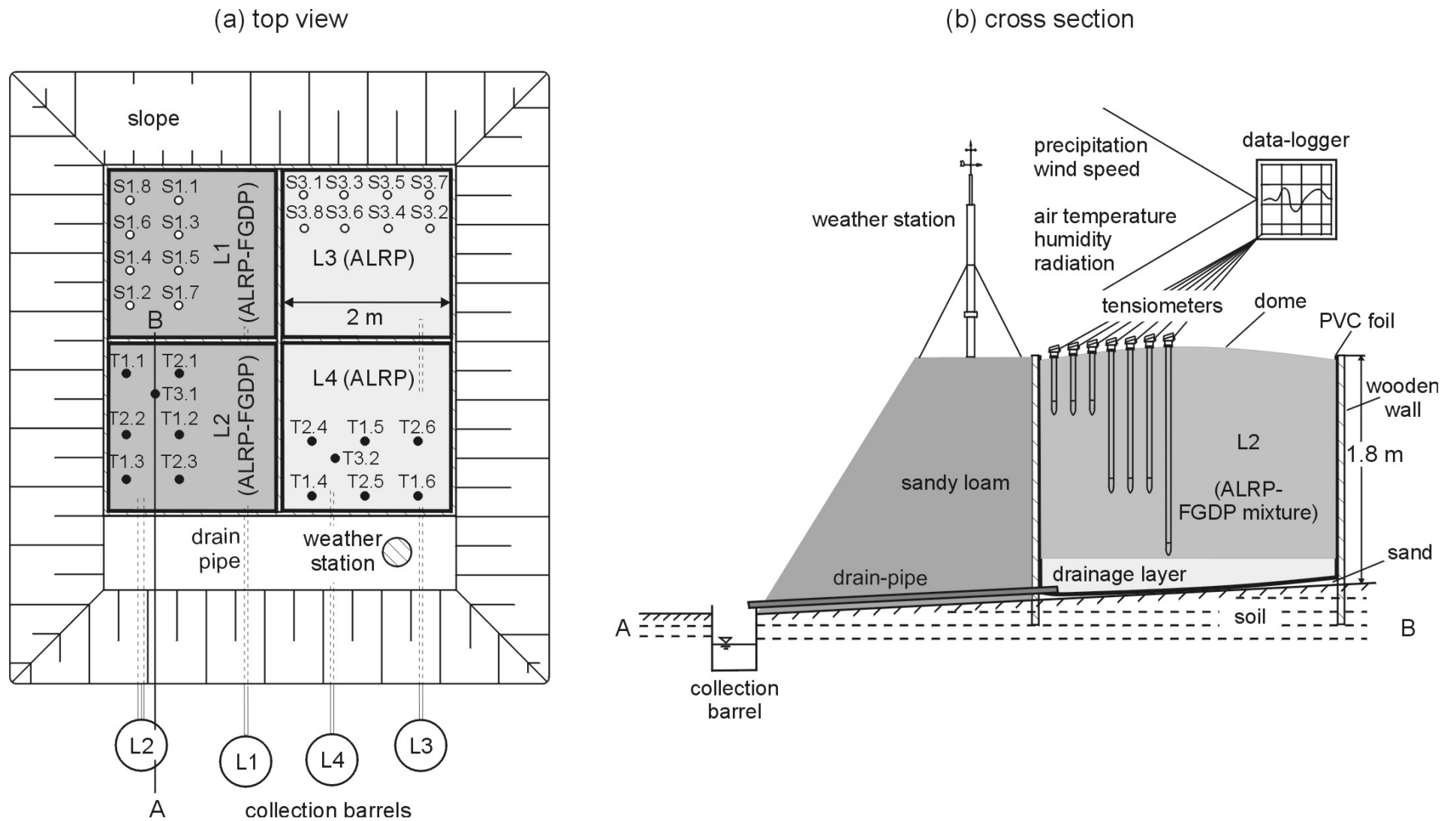
Fig. 3.1 *(a) Top view and (b) cross-sectional view of the lysimeter setup and instrumentation (not to scale).*

40

Sand was filled into each lysimeter to cover the soil surface to about 0.1 m. The sand surface was modelled to form an asymmetric bowl with its lowest point at the inflow end of the PVC pipe. A 2-mm thick impermeable PVC foil used for landscaping artificial garden ponds was applied to seal the inside of the containers. At the bottom of each container, over the lowest point of the sand bowl, a hole was cut into the foil to allow entrance of the drain-pipe into the lysimeter. To prevent leakage of water around the pipes into the underlying sand and soil, the PVC pipes and foil were welded together, and a piece of plastic coated wire was tightly wrapped around the foil and pipes at the inflow end of each pipe. With the same wire, plastic meshes of 1 mm openings placed over the inflow ends of the pipes were fastened to prevent solids from travelling out of the containers and into the drain-pipes.

Table 3.1 *Lysimeter (L1 to L4) study events in chronological order.*

Date	Event	Details
07/01/1997	lysimeters filled with saline materials	L1 & L2: ALRP-FGDP (7:3) mix L3 & L4: ALRP
07/31/1997	weather station and tensiometers installed	precipitation, wind; matric potential in L2 & L4: 0.60, 1.10, and 1.63 m depth
09/08/1997	suction cups installed; cups could be kept in lysimeters over the first (1997/98) winter period because of high salinity	L1 & L3: 0.15, 0.30, 0.60, and 1.10 m depth
01/21&22/1998	beginning of outflow, L3 & L4	
09/24/1998	beginning of outflow, L2	
10/15/1998	beginning of outflow, L1	
mid Oct. 1998	outflow almost ceased, L1, L3 & L4	outflow pipes blocked with salt crusts
11/26/1998	shallow (0.15 m) suction cups de-installed	beginning of 2nd frost-period
12/17/1998	outflow pipes washed, L1, L3 & L4	outflow: 62.4 (L1) to 100.3 mm d^{-1} (L4), outflow pipes sealed at end of day
12/23/1998	outflow pipes re-opened and washed, L1, L3 & L4	outflow: 29.0 (L4) to 51.9 mm d^{-1} (L3)
01/05/1999	outflow pipes washed, L1, L3 & L4	outflow: 40.1 (L1) to 50.8 mm d^{-1} (L3)
02/24&25/1999	outflow pipes washed, L1, L3, & L4	outflow: 31.2 (L4) to 36.4 mm d^{-1} (L1)
03/04/1999	shallow (0.15 m) suction cups re-installed	end of 2nd frost period

Table 3.1 *(continued)*.

Date	Event	Details
04/22/1999	1. fertilization and seeding, L1 to L4	1125 kg ha^{-1} phosphate (45% P_2O_5), 400 kg ha^{-1} ryegrass (*Lolium perenne*, L.)
06/03/1999	outflow ceased, L1 to L4	
08/01/1999	tensiometers recalibrated	tensiometer values before and after calibration did not vary considerably
08/10/1999	temperature, humidity, and radiation sensors added to weather station	see text
11/18/1999	2. fertilization and seeding, L1 to L4	1125 kg ha^{-1} phosphate (45% P_2O_5), 400 kg ha^{-1} ryegrass (*Lolium perenne*, L.)
12/16/1999- 01/06/2000	beginning of outflow, L3 (16.12.), L4 (23.12.), L2 (30.12.), L1 (06.01.)	
01/06/2000	grass sprouts from 2. fertilization and seeding visible	
01/13/2000	shallow (0.15 m) suction cups de-installed	Beginning of 3rd frost-period
01/13/- 01/27/2000	outflow pipes washed weekly, L1 to L4	Blockage of outflow pipes with salt crusts prevented
03/09/2000	shallow (0.15 m) suction cups re-installed	end of 3rd frost-period
03/16/2000	3. fertilization and seeding, L1 to L4	1250 kg ha^{-1} phosphate (45% P_2O_5), 200 kg ha^{-1} ryegrass (*Lolium perenne*, L.)
05/18/2000	outflow ceased, L1 to L4	

Filling

Each lysimeter had a cross-section of 2 by 2 m^2 and was 1.8 m high. The bottom 0.15 m were filled with a drainage layer of sand and fine gravel. In lysimeters L1 and L2, the top 1.63 m were filled with a mixture (7:3, on volumetrical basis) of saline ALRP and FGDP. In lysimeters L3 and L4, they were filled with saline ALRP. Materials were brought to the lysimeters from their production sites the day before they were filled into the containers. Using a front end loader, ALRP and FGDP were blended, both materials were homogenized, and filled into the lysimeters at a water content of approximately 0.25 cm^3 cm^{-3} (ALRP-FGDP mixture) and 0.35 cm^3 cm^{-3} (ALRP) on 1 Jul.

1997. During the mixing and filling procedures, the sharp smell of ammonia was noticable from the ALRP. Therefore, we were not able to work inside the containers to compact the materials. However, intermittently we did manage to spread the materials homogeneously over the cross-sectional area of the lysimeters with use of a shovel. Because we expected some settling of the materials, we finished the filling with a dome-shaped cap, which in the center of each lysimeter was about 0.15 m higher than the walls. At the edges, the filling was about 0.02 m lower than the walls to prevent surface runoff. To stabilize the wooden containers mechanically, and to insulate the lysimeters against temperature changes from the side walls, local soil material (sandy loam) was filled against the walls of the structure from the outside at an angle of about 30°. This outside soil was planted with grass to minimize erosion. During summer months, vegetation on the slopes around the lysimeters was repeatedly cut to keep it from growing higher than about 0.30 m.

Instrumentation and Measurements

Drainage from the lysimeters was collected in the plastic barrels which were covered with lids to prevent evaporative loss between sampling dates. The materials were allowed to settle for one month before sensors for auxiliary measurements were installed on 31 Jul. and 9 Aug. 1997 (see Table 3.1). Ceramic suction cups, 0.05 m long and 0.02 m in diameter, were vertically installed in lysimeters L1 (ALRP-FGDP mix) and L3 (ALRP) to collect solution from the 0.15-, 0.30-, 0.60-, and 1.10-m depths in two replicates per depth. Once per week, electrical conductivity (Ec) was measured in both the drainage and the suction cup solutions, and the volume of discharge was recorded. Pressure head was monitored with vertically installed pressure transducer tensiometers (UGT GmbH, Müncheberg, Germany) at the 0.60-, 1.10-, and 1.63-m depths in lysimeters L2 (ALRP-FGDP mix) and L4 (ALRP), with three replicates at 0.60 and 1.10 m, and one replicate at the 1.63 m depth (i.e., directly over the drainage layer). All initial installation depths were measured from the proposed horizontal surface of the profiles (at 0.02 m below the edges of the container walls) along the shafts of the instruments. To prevent preferential flow along the shafts, both suction cups and tensiometers were equipped with impermeable PVC collars (0.12 m in diameter) tightly surrounding the shafts at the soil surface.

The pressure transducer tensiometers were similar to those described by Long (1984). A cable ran down the shaft of each tensiometer to the pressure transducer, that was placed only 0.05 m above the porous ceramic cup. The water column inside the tensiometer was protected against moderate frost as it was located at some distance below the soil surface. To prevent contact of the pressure transducer with the highly saline, corrosive seepage solution, an impermeable rubber diaphragm was placed inside the tube under the pressure transducer. The tube was filled with silicon oil above this barrier.

A weather station, supplied with an automated data logger (UGT GmbH), recorded precipitation at 1 m height, wind speed and direction at 2 m above the lysimeter surface, and tensiometer values. Readings were repeated once per minute, and the logger was set to store hourly minimum, maximum and average values. With respect to precipitation, it was set to store hourly totals, respectively. In Jul. 1999, i.e. after two years of operation, sensors were added to the weather station to also record air temperature and relative humidity in a Young radiation screen, as well as solar radiation in 2 m above the lysimeter surface. For radiation measurements, a CNR 1 net radiometer (Kipp & Zonen B.V., Delft, The Netherlands) was used. This instrument was supplied with two CM3 pyranometers to record 305 to 2800 nm radiation (short wave or visible spectrum), and with two CG3 pyrgeometers to record 5000 to 50000 nm radiation (long wave or infrared). The CNR 1 was positioned with two sensors (one GM3 and one CG3) faced upwards, and the other two sensors faced downwards.

Vegetation and Fertilization

Because of the high initial salt content of ALRP (40 to 50%), lysimeters were practically bare until January 2000, i.e. during the first 30 months of our experiment. An attempt was made to sow lysimeters with ryegrass (*Lolium perenne*, L.) on 22 Apr. 1999, using the equivalent amount of 400 kg of seeds per ha. By this time, Ec in the 0.15 m suction cups, that initially ranged from 267 to 302 mS cm^{-1}, had dropped to less than 5 mS cm^{-1} after the wet 1998/99 winter season. Before sowing, we raked the lysimeter surfaces, which were still dome-shaped from the filling procedure, to horizontal planes. These planes were about 0.02 (L1 and L2, ALRP-FGDP mix) and 0.04 m (L3 and L4, ALRP) lower than the wooden frame walls, i.e. profile lengths were 1.63 (ALRP-FGDP mix) and 1.61 m (ALRP) from the surface to the top of the drainage layer at the time of the first seeding. During the dry spring and summer following the date of sowing, Ec continuously rose and was well above 160 mS cm^{-1} in the 0.15 m

depth by mid Aug. 1999. Most plants, that initially germinated and grew satisfactorily to about 1 cm height, wilted and died.

We made a second attempt to plant lysimeters to ryegrass on 18 Nov. 1999, when Ec in the suction cups at the 0.15 m depth was down to less than 5 mS cm^{-1} again after a fall period of ample rainfall and little evaporation. Seeds germinated in January, but sprouts grew slowly because of low temperatures. Some plants may have died from an occasional frost, and sowing was repeated again on 16 Mar. 2000. On this day, plants from the Nov. 1999 seeding were about 1.5 cm high, and only half the amount of seeds (200 kg ha^{-1}) was used as compared to the first two sowings. Phosphate fertilizer was applied to the lysimeter surfaces with every sowing. Amounts are listed in Table 3.1.

Operational Complexities

For several reasons we failed to collect a complete set of data from the suction cups. Because of the high initial salt content of ALRP, salt crystals occasionally clogged the tubes running down the inside of the suction cup shafts, thus preventing the establishment of a suction in the inside of the porous cup. To clean the tubes, suction cups were removed, tubes were rinsed with tap water, and cups were re-installed. To prevent suction cups from frost breakage, those from shallow depths were removed when Ec was low during the winters of 1998/99 and 1999/2000. Additionally, during summer, the lysimeter materials sometimes were too dry to let solution flow into the cups. Again this was especially true for shallow installation depths (0.15 and 0.30 m).

Salt crystals also formed in the one-inch PVC lysimeter drain-pipes. This was observed particularly during winter months, when the air temperature dropped below 5°C. From mid Oct. 1998, increasingly positive pressures were recorded in the deepest (1.63 m) tensiometer in L4, suggesting that a free water table was rising in this lysimeter. At the same time, in spite of ample rainfall, outflow from the lysimeters L1, L3, and L4 almost ceased. Outflow pipes of these lysimeters were blocked with salt crystals. After additional rainfall, all tensiometers in L4 showed large positive pressures and free water was visible in small puddles at the surfaces of L1, L3, and L4 about mid Dec. 1998. This indicated that these lysimeters had become nearly saturated. However, outflow did not cease from L2, and no large positive pressures were recorded in this lysimeter, except at the 1.63 m depth. This may have been because of the four lysimeters, L2 had the shortest and steepest outflow pipe, providing fast solution flow and little time for salt crystals to grow in this pipe.

On 17 Dec. 1998, we disconnected the drain-pipes of L1, L3, and L4 from the collection barrels, connected a hose to the outflow end of each pipe, and raised the hoses well above the surface of each lysimeter. A funnel was connected to the end of each hose and was held in place about 1 m over the lysimeter surface. To rinse salts from the outflow pipes, we carefully poured hot tap water into the funnels until they were filled, thus imposing a reverse positive pressure of a water column of approximately 3 m to the outflow end of the drain-pipes. Three to five liters of water were needed to fill each hose and funnel. About ten minutes after application, water levels decreased rapidly, audibly drawing air into the hoses.

After we disconnected the hoses, large amounts of solution rapidly flushed out of the lysimeters. For example, more than 100 mm (i.e., 400 L) flushed from L4 on 17 Dec. 1998, and the outflow rate was high until the end of that day. Simultaneously, tensiometer readings from L4 dropped sharply from high positive pressures to suction, or values close to suction. To prevent unrecorded drainage and overflow of the collection barrels, we stopped the outflow from lysimeters L1, L3, and L4 with rubber stoppers at dusk. On 23 Dec. 1998, we took out the stoppers, repeated the procedure of washing the pipes, and collected another 29 (L4) to 52 (L3) mm of drainage on that single day, before outflow rates decreased rapidly to relatively constant dripping. Washing was repeated twice during the 1998/99 winter season. Dates and subsequent outflow volumes are given in Table 3.1. The tap water used to wash the systems is not included in the tabulated outflow volumes. During the 1999/2000 winter season, washing of the drain-pipes was conducted before lysimeter outflow decreased from blockage. No increase of outflow rates occurred after the washing procedures and no positive pressures in the tensiometers were observed during that season.

Lysimeter surface heights lowered during the course of the experiment. This can in part be attributed to settling of the tested materials, as would also have occurred in an uncompacted natural soil or sand. Another reason may be the dissolution and subsequent leaching of solid phase salts (predominantly NaCl) from ALRP, especially from the upper part of the profile. No method was applied to distinguish between the two processes. As described above (see section titled 'Filling'), the surfaces of the lysimeter fillings were initially about 0.02 m lower than the top of the walls at the edges of the containers, but 0.15 m higher in the center. After raking the surfaces to horizontal planes at the date of the first seeding (22 Apr. 1999), these planes were about 0.02 (ALRP-FGDP) and 0.04 m (ALRP) lower than the top of the containers across the entire cross

section. By 16 Mar. 2000, surface heights had lowered another 0.03 (ALRP-FGDP), and 0.05 m (ALRP). In total, the surface in the center and near the edges of lysimeters L1 and L2 (ALRP-FGDP) was about 0.20 and 0.03 m lower than at the start of the experiment. Corresponding values for lysimeters L3 and L4 (ALRP) were 0.24 and 0.07 m. No significant differences in settling were observed between replicate lysimeters filled with the same material.

Computational

The lysimeter design enables a rough estimate of the water balance. To this end, precipitation, P can be partitioned into evaporation E, discharge D, and change of water storage in the profile, ΔS. For the entire period of experimentation, this relation can be described by the following form of the water balance equation:

$$P = E + D + \Delta S \qquad [3.1]$$

Because of the raised edges of the lysimeter containers, surface runoff was prevented and no term is needed in Eq.[3.1] to describe this part of the water balance. However, some adjustment of the measured data was necessary before they were useful to solve Eq.[3.1]. From recorded hourly values of weather data and soil water tension, daily averages or, in the case of precipitation and radiation, daily totals were computed.

Precipitation

For precipitation measurements, we used a rain gauge that, apart from its automatic registration unit (tipping scale), was very similar to the so-called Hellmann rain gauge commonly used by the German Weather Bureau (Deutscher Wetterdienst, DWD, Offenbach, Germany). Richter (1995) analyzed the systematic error of measurements conducted with the Hellmann rain gauge, which is mainly due to evaporation from the wet gauge wall, and to wind effects. In summary, these effects lead to measured values being lower than actual precipitation. Empirical monthly correction percentages for Germany were published by Richter (1995). These take into account regional effects (e.g. the longterm average percentage of snowfall from total precipitation), elevation, and sheltering of the rain gauge by local features. In general, correction

percentages are higher for winter months with snowfall and smaller raindrops (from predominantly advective atmospheric conditions), than for summer months with larger raindrops (from mostly convective atmospheric conditions). Correction values from Richter (1995) for north-central Germany are shown in Table 3.2.

Table 3.2 *Monthly correction percentages for precipitation measurements with unsheltered Hellmann rain gauge for north-central Germany (Richter, 1995).*

Month	%	Month	%
Jan.	27.5	Jul.	10.5
Feb.	29.0	Aug.	10.5
Mar.	23.6	Sep.	12.1
Apr.	18.2	Oct.	14.2
May	12.3	Nov.	19.1
Jun.	10.3	Dec.	22.7
Year			16.6

In northern Germany, most rain falls in connection with westerly winds. Due to channeling of such winds between the mine tailings mound and a nearby hedge, and because of its elevated position on top of the lysimeter installation, we assigned unsheltered conditions to the locality of our rain gauge. Following Richter (1995), we therefore added the correction percentages given in Table 3.2 to the measured daily totals of precipitation.

Evaporation and Water Content

To estimate evaporation, we used the combination method for potential evaporation, first proposed by Penman (1948). Daily values of actual evaporation can be derived from Penman's potential evaporation with use of the concept of drying stages of an initially wet surface (see Jury et al., 1991). Measurements to calculate Penman-evaporation were taken continuously during our experiment. The calculation of daily potential evaporation, and the complexities related to evaporation from saline materials, will be covered in a

second paper. However, a simple bookkeeper's approach can be used for a rough estimate of E in Eq.[3.1], especially when the time resolution is on the order of one year.

Because P and D are known from measurements, E can easily be calculated from Eq.[3.1] when ΔS is also known. In our experiment, we did not take measurements of water content. Time domain reflectrometry (TDR) is one method to measure water content. This method is highly dependent on the dielectrical constant of the tested material. The dielectrical constant is not only susceptible to water content, but also to the solution concentration. Therefore, and because of the corrosivity of the solution, TDR was not a feasible option to measure water content in the highly saline materials tested in our study. A neutron probe was not available. However, because the content and distribution of water in the profiles will be similar on days of subsequent years when the seasonal discharge from a lysimeter first starts or ceases, ΔS between such dates can be assumed close to zero. Estimates of yearly values of actual evaporation were obtained as the difference of cumulative precipitation and cumulative discharge between such dates.

Discharge

Following Richards (1954), we estimated solution concentration (c, mmol L^{-1}) and osmotic pressure potential (Ψ_o, cm) from measurements of Ec (mS cm^{-1}) in the suction cup and drainage solution as

$$c = 10.37 \, Ec^{1.065} \qquad [3.2]$$

and

$$\Psi_O = 365 \, Ec \qquad [3.3]$$

respectively. Assuming that Ec in the solutions was dominated by dissolved NaCl, we used the molecular weights of Na (22.9898) and Cl (35.435 g mol^{-1}; Weast, 1987) to calculate solution concentrations in g L^{-1} from Eq.[3.2]. Subsequently, the discharge volume of pure water, D in the solution outflow volume, V_S was estimated from

$$D \;=\; \frac{m_{H_2O}}{\rho_{H_2O}} \;=\; \frac{\rho_s V_s - c V_s}{\rho_{H_2O}} \qquad\qquad [3.4]$$

where m_{H_2O} is the mass of pure water in the discharge solution, c is in kg L^{-1}, ρ_{H_2O} is the density of water, which was assumed to be unity, and ρ_s is the density of the discharge solution. Values of ρ_s were estimated from a linear regression model of the form $\rho_s = 0.0007\,Ec + 1$ ($R^2 = 0.909$), which was derived empirically from measurements of ρ_s and Ec on 27 arbitrarily selected samples from suction cup and drainage solutions from all four lysimeters. These covered an Ec range from 25.7 to 306 mS cm^{-1}. A pycnometer method as described by Blake and Hartge (1986) was used for measurements of ρ_s. Values of D in units of L resulting from Eq.[3.4] were divided by the cross sectional area of the flow domain (4 m^2) to derive values in mm.

3.4 Results and Discussion

Precipitation and Discharge

Boundary condition results (precipitation and discharge) from the lysimeter experiment are shown in Figs. 3.2 (a and b). In Table 3.3, cumulative numbers for the entire length of the experiment (35 months or 1035 days) and mean annual values are given. Figure 3.2a depicts cumulative precipitation. Curves for both observed and corrected precipitation are plotted. For corrected precipitation, monthly correction percentages as listed in Table 3.2 were added to the observed data. The nearly constant slope of the cumulative precipitation curves is typical for the humid, oceanic climate at the site of our experiment.

From 1 Aug. 1997 to 31 May 2000, 1436 mm of precipitation were measured at the lysimeter facility (Table 3.3). When correction percentages from Table 3.2 are added, a total of 1687 mm, or an annual average of 595 mm, is obtained. According to Keller (1978) longterm average annual precipitation is 640 mm at the site.

Total and mean annual discharge from lysimeters L1 to L4 of salt solution (observed) and pure water (calculated from Eq.[3.4]) are listed in Table 3.3. Cumulative pure water discharge over time is shown in Fig. 3.2b. During the 1997/98 winter season, mean discharge from lysimeters L1 and L2 (ALRP-FGDP) was extremely small (1.1 mm by 1 May 1998), whereas discharge from lysimeters L3 and L4 (ALRP) started earlier (4.8 mm by 22 Jan. 1998) and was larger (28.2 mm by 1 May 1998). The difference between materials can be

attributed to the difference in initial water content. Little discharge was collected from both materials during the 1997/98 winter season as compared to the two following winters. This may be due to the physical capacity of the initially relatively dry materials to store water. Field capacity, defined as the water content at 1.0 m of suction, of ALRP and ALRP-FGDP was 60.6% and 61.8%, respecitvely (Hermsmeyer et al., 2001). For a profile height of 1.63 m, field capacity for ALRP was 988 mm. For ALRP-FGDP it was 1007 mm (Table 3.3). For comparison, rainfall was only 324 mm from 1 Aug. 1997 to 1 May 1998.

During the second (1998/99) winter, discharge from lysimeters L1, L3, and L4 was interrupted repeatedly by salt crystals blocking the outflow pipes between mid Oct. 1998 and 25 Feb. 1999 (see Table 3.1). Washing the salt from the drain pipes resulted in a sharp increase in discharge on 17 Dec. 1998, 23 Dec. 1998, on 5 Jan. 1999 and on 24 Feb. 1999 (see Fig. 3.2b and Table 3.1). Before these dates, discharge almost ceased and the curves of cumulative discharge approach horizontal lines. This is not true for lysimeter L2. The drain pipe of this lysimeter was not blocked and discharge flowed continuously. Overall, discharge was considerably larger from ALRP than from ALRP-FGDP during the 1998/99 winter season. Cumulative discharge by 1 May 1999 averaged 281 mm from L1 and L2 (ALRP-FGDP) and 437 mm from L3 and L4 (ALRP). Because lysimeters L1 (ALRP-FGDP), L3 and L4 (ALRP) were nearly saturated during the 1998/99 winter season, differences can no longer be assigned to differences in initial water content. It is more likely that they were caused by the different water storage capacity of the materials.

Discharge between replicate ALRP-FGDP lysimeters (L1 and L2) at the end of the 1998/99 winter season varied more (37.4 mm) than from replicate ALRP lysimeters (9 mm). Curves of cumulative discharge from lysimeters L1 and L2 run almost parallel from 1 Apr. 1999 to 31 May 2000. This indicates that discharge variations between L1 and L2 were mainly caused by different evaporation. Because L1 was nearly saturated, but L2 was unsaturated during the 1998/99 winter season, evaporation occurred near maximum, or potential rate from L1, but at a lower rate from L2.

During the third winter period (1999/2000) discharge was uninterrupted, and lysimeters were unsaturated. Between 1 Dec. 1999 and 1 May 2000, discharge averaged 125.5 mm from L1 and L2 (ALRP-FGDP) and averaged 208.5 mm from L3 and L4 (ALRP). The difference between materials (83 mm) was considerably larger than the difference between replicate lysimeters filled with ALRP-FGDP (15 mm) or ALRP (11 mm). Again, this reflects differences in water storage capacities between the two materials.
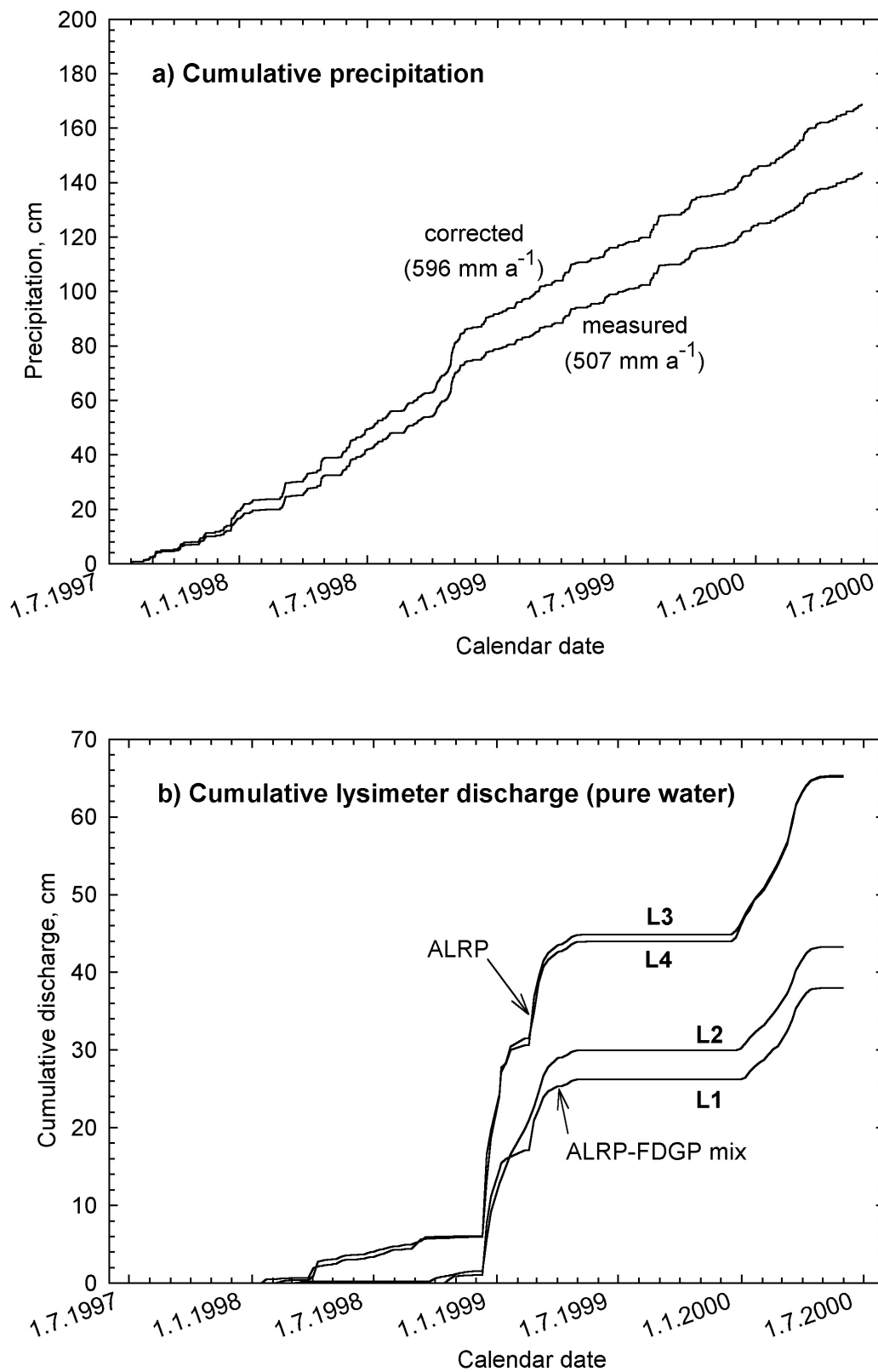
Fig. 3.2 *(a) Precipitation and (b) discharge from lysimeters L1 and L2 (ALRP-FGDP mix), and L3 and L4 (ALRP) over three years.*

Table 3.3 *Results from the lysimeter experiment after 1035 days (1 Aug. 1997 to 31 May 2000), and mean annual values.*

| | ALRP-FGDP mix | | | | ALRP | | | |
| | L1 | | L2 | | L3 | | L4 | |
	Total	Annual mean	Total	Annual mean	Total	Annual mean	Total	Annual mean
cumulative precipitation (observed), mm	1435.6	506.3	1435.6	506.3	1435.6	506.3	1435.6	506.3
cumulative precipitation (corrected), mm	1687.1	595.0	1687.1	595.0	1687.1	595.0	1687.1	595.0
discharge (salt solution), mm	399.0	140.7	450.3	158.8	684.3	241.3	686.2	242.0
discharge (pure water), mm	380.0	134.0	432.7	152.6	651.5	229.8	653.2	230.4
amount of salt leached, kg m^{-2} †	95.4	33.6	92.2	32.5	165.6	58.4	166.4	58.7
amount of salt leached, cm §	6.4	2.3	6.2	2.2	11.0	3.9	11.1	3.9
	%	mm ¶	%	mm ¶	%	mm ¶	%	mm ¶
field capacity, ‡	61.8	1007	61.8	1007	60.6	998	60.6	998

† To calculate total amount of salt leached from a lysimeter, multiply by 4.

‡ Results from laboratory analyses (see Hermsmeyer et al., 2001).

§ A bulk density of pure salt of 1.5 Mg m^{-3} was assumed.

¶ per profile length (1.63 m)

Discharge was higher from ALRP than from ALRP-FGDP in all three years of our experiment. This is in accordance with the fact that initial water content of ALRP-FGDP was lower, but field capacity was higher than that of ALRP (Hermsmeyer et al., 2001a).
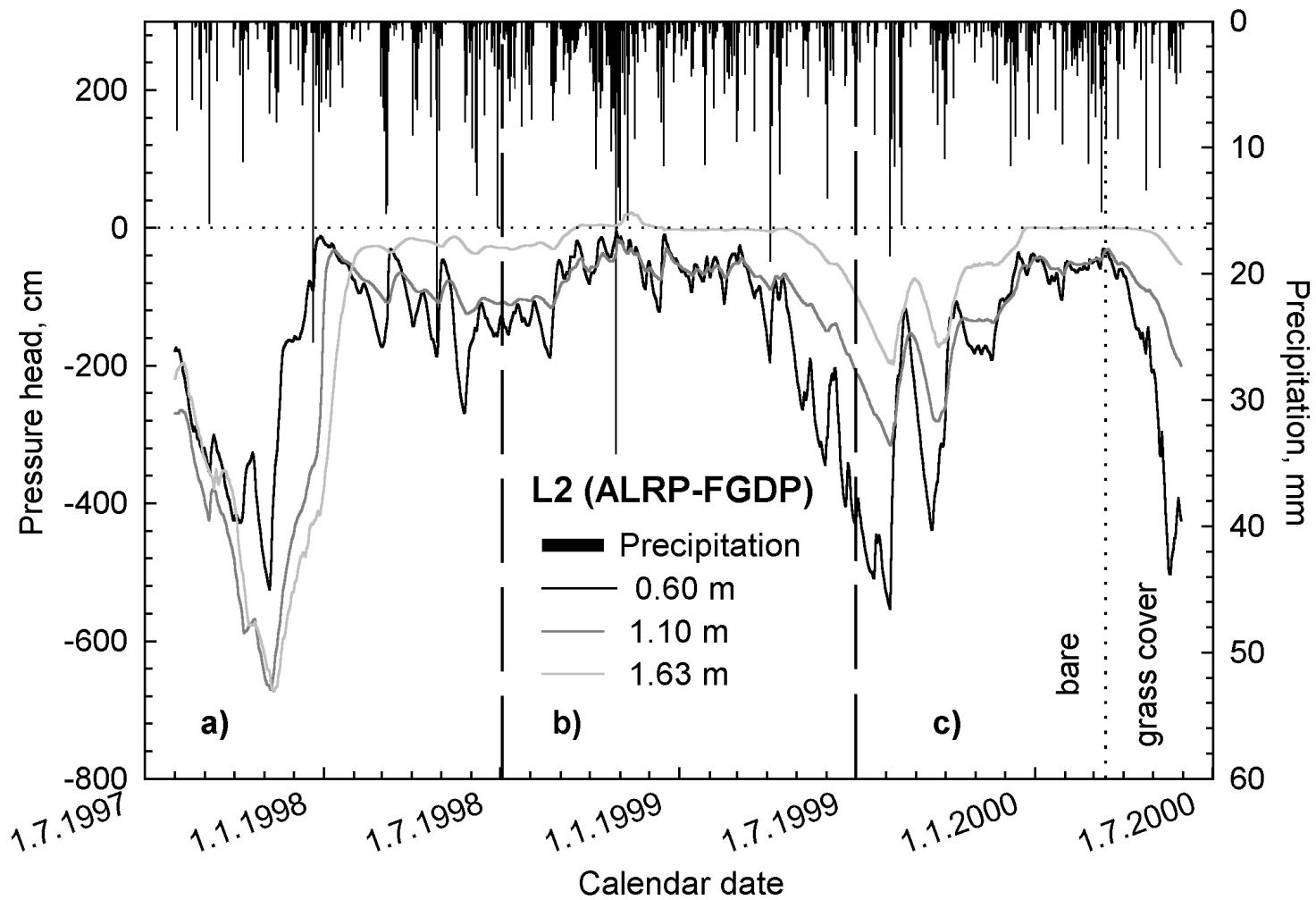
Pressure Head

Pressure heads (H-values) from tensiometer readings are shown in Fig. 3.3 and 3.4. In Fig. 3.3, daily averages of hourly values in lysimeter L2 (ALRP-FGDP) in the 0.60-, 1.10-, and 1.63-m depths are plotted. Values for the 0.60- and 1.10-m depths are replicates from three tensiometers per depth. In the 1.63 m depth, only one tensiometer was installed. Figure 3.4 depicts corresponding results from lysimeter L4 (ALRP). Daily totals of corrected precipitation are also shown in Figs. 3.3 and 3.4.

Pressure head was initially between -170 and -270 cm in ALRP-FGDP, and between -120 and -160 cm in ALRP. During the first late summer and fall (from Aug. to Nov. 1997), H-values decreased to values between -520 and -680 cm in ALRP-FGDP (0.60- and 1.63-m depths), and between -430 and -500 cm in ALRP (1.63- and 0.60-m depths). Only 118 mm of rain fell from 1 Aug. 1997 to 30 Nov. 1997. The decrease of H during this period is caused by drying of the profiles as a result of weather conditions.

Other processes may also have been involved in the drying of the profiles to such great depths. In natural soil profiles, precipitation and evaporation occur at the surface. This usually results in large amplitudes of near-surface pressure head during wetting and drying cycles, that are lessened deeper down in the profile. Such conditions were observed in our lysimeters from early spring, 1998 onwards (Figs. 3.3 and 3.4). However, before the spring of 1998 conditions in our lysimeters were different. The amplitude of pressure head was about as large in the 1.63- as it was in the 0.6-m depth in ALRP (Fig. 3.4). In ALRP-FGDP, the amplitude became even larger with increasing depth (Fig. 3.3), suggesting that the profile dried out more near the bottom than it did near the top. This may be a result of exothermal chemical reactions occuring in the fresh materials.

Other indications to such reactions were also observed: When instruments were installed in the lysimeters on 31 Jul. and 9 Aug. 1997 (Table 3.1), a steel auger was used to bore holes. The auger was distinctly heated after pulling it from ALRP-FGDP or ALRP, indicating that materials were chemically reactive.

Fig. 3.3 *Precipitation and average daily pressure head in the 0.60- 1.10-, and 1.63-m depths in lysimeter L2 (ALRP-FGDP) over three years.*
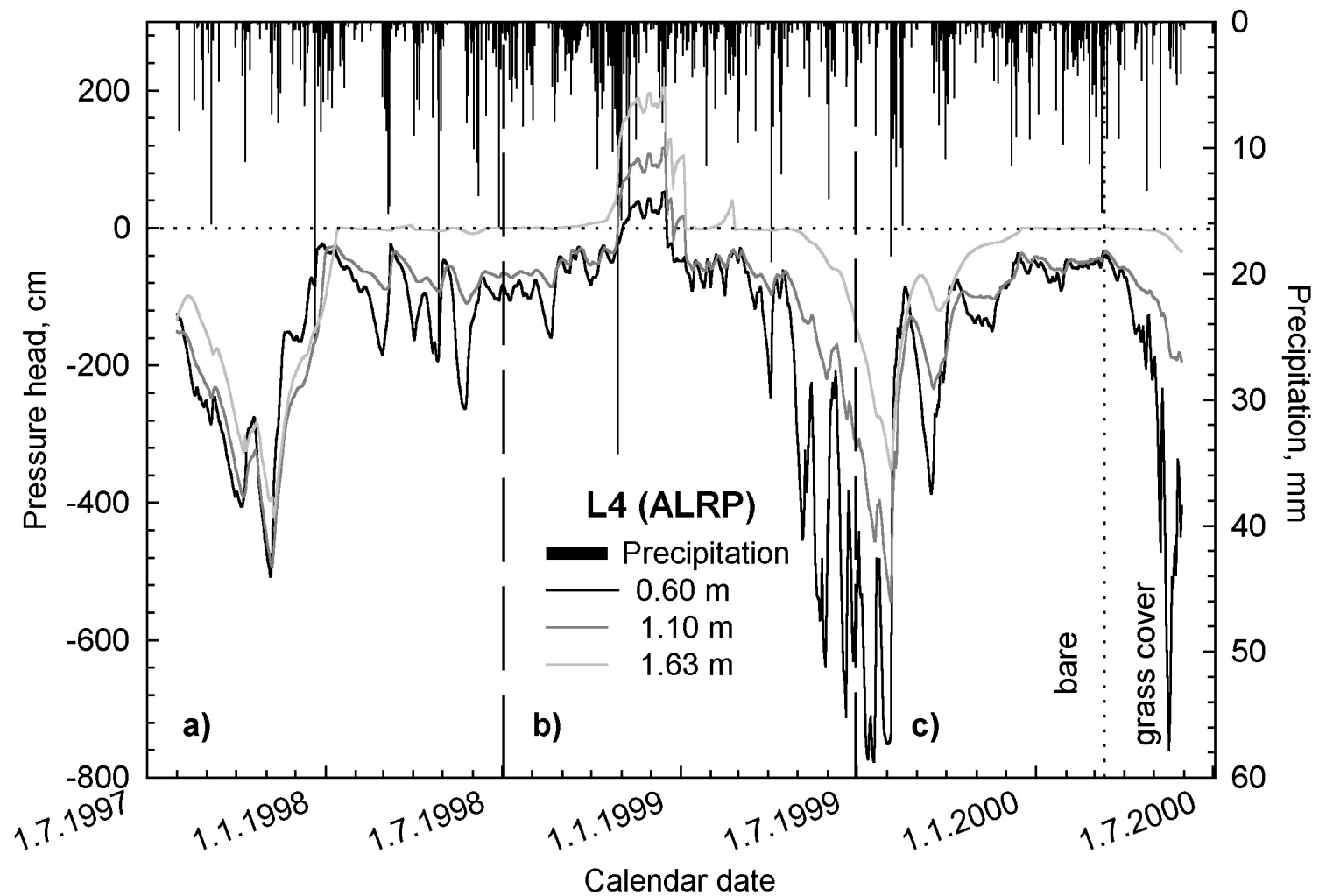
Fig. 3.4 *Precipitation and average daily pressure head in the 0.60- 1.10-, and 1.63-m depths in lysimeter L4 (ALRP) over three years.*

It is likely that high temperatures, caused by exothermal chemical reactions, resulted in evaporation not only from the surface but from throughout the profile. Also, chemical binding of water in hydrates, crystals, or both may have occurred. For example, water may have been chemically bound in gypsum, mortar-like compounds, or salts. The reversal of the commonly expected distribution of H with depth during early stages of our experiment may be the result of water movement in the vapor phase along a temperature gradient from deeper, more insulated, and hence warmer parts of the lysimeter to cooler, near-surface depths. In terms of the water balance equation, both chemical binding of water and water loss as a result of exothermal heating require additional terms in Eq.[3.1]. This leads to an equation with three unknowns, (i) change of water content from leaching and near-surface evaporation, (ii) change of water content from chemical binding of water, and (iii) change of water content from deep evaporation triggered by exothermal heating. Such an equation could not be solved with the limited information collected during our experiment. The loss of water from the pore system as a result of chemical reactions was not studied. Therefore, Eq.[3.1] can only be solved for periods when reactions had decreased to a degree where they had no significant effect on water storage.

During the winter of 1997/98, pressure head over the depths of the profiles was reversed to conditions that are commonly expected in chemically inert porous materials under humid field conditions (Fig. 3.3 and 3.4). This suggests that Eq.[3.1] can be solved with the information collected in our experiment from early spring 1998 onwards.

On 14 Jan. 1998, pressure head in the 1.63 m depth in L4 (i.e., in ALRP just above the gravel drainage layer) approached zero. The first discharge from this lysimeter was collected during the following control visit on 22 Jan. 1998. This close relation between times of discharge with times of zero tension near the bottom of the profiles was repeated in Apr. 1999, in Dec. 1999 and in May 2000 (compare Fig. 3.3 and 3.4, with Fig. 3.2b). Discharge occurred whenever near-bottom H-values approached zero. This is in agreement with the concept of a seepage face through which water can leave the saturated part of the flow domain. It has been found that this type of boundary condition often applies to lysimeters of finite length that are allowed to drain under gravity (Šimunek et al., 1998). When used in water balance modeling, a seepage face-type boundary condition assumes that the flux accross the bottom boundary is zero as long as the pressure head at the bottom of the profile is negative. Flux will be larger than zero as soon as the bottom of the profile becomes saturated.

The problem of drain pipes blocked by salt crystals during the 1998/99 winter season has been described in the section above titled 'Operational Complexities'. In terms of water balance modeling, the seepage face gradually changed into a zero flux-type boundary condition. Tables of free water rose in lysimeters L1, L3, and L4, and profiles were nearly saturated on 16 Dec. 1999, (the day before salt was first washed from the pipes). Because tensiometer cups were lower than the water table, increasingly positive pressures were measured in L4 from Sep. 1998 onwards (Fig. 3.4).

In a fresh-water system, the positive pressure monitored by a tensiometer installed below a water table is equal to the length of the column of free water above the tensiometer cup. In lysimeter L4, however, tensiometer readings during times of saturation of the profile or parts of the profile were larger than the lengths of column of free water. On 16 Dec. 1999 ponding was observed on the surface. The length of the water column above the tensiometer cup at the 1.63 m soil depth was about equal to the installation depth (163 cm), but the average of 24 hourly tensiometer readings on 16 Dec. 1999 was 205 cm. The difference can be explained by the high salinity of the solution. The density of a saturated NaCl solution is 1.21 Mg m^{-3} (Weast, 1987). If the average tensiometer reading is devided by 1.21, a length of a pure water column of 169.4 cm is obtained.

Whether tensiometer readings in the unsaturated case in the highly saline materials in our lysimeters also are effected by the density of the salt solution remains an open question. In agronomy and soil science, tensiometers are commonly used to study the water budget of arable soils that contain solutions of comparatively small concentrations. Possible effects of solution concentration, or solution density, on tensiometer readings are neglected in most studies. To our knowledge, no paper has been published to describe such effects, and further research is needed to clarify this point. However, solution concentrations were equally high in ALRP-FGDP and in ALRP over long periods of our study. Tensiometer readings should therefore be comparable between materials, even if possible effects of solution concentration or density are neglected.

For the years 1999 and 2000, i.e., after chemical reactions that may have consumed water from the pore system had ceased, a seasonal cycle is clearly visible in the tensiometer data. During summer, H-values were considerably lower than during winter. Between materials, summer values of H in ALRP were generally lower in all depths than in ALRP-FGDP. For example, during the summer of 1999 in the 1.63 m depth, the lowest daily mean H-value was

-353 cm in ALRP (on 5 Aug.), and -199 cm in ALRP-FGDP (on 8 Aug.). Although tensiometer depths were rather large, H-values increased rapidly after rainfall events. Variation in H-values between rainstorms was considerably larger in ALRP than in ALRP-FGDP. This is especially true for the 0.60-m depth. However, periods with zero tension near the bottom of the profiles (1.63 m depth) were almost identical in both materials after the 1998/99 winter season (Fig. 3.3 and Fig. 3.4), and so were periods with flow and no-flow of discharge (Fig. 3.2b).

Evaporation

Because the amount of water that was presumably consumed from the pore system by chemical reactions is unknown, trustworthy values of E cannot be determined with use of Eq.[3.1] for the first discharge season (or year) of our experiment. During the second year (1998/99), the outflow pipes of L1, L3, and L4 were at times blocked, again preventing unequivocal solution of Eq.[3.1] for E. Our bookkeeper's approach to E is therefore only applicable to the third discharge season (1999/2000). Results are shown in Table 3.4.

In rows A and B of Table 3.4, the last days of the 1998/99 and 1999/2000 winter seasons are listed on which we collected discharge. In row C the number of days between these dates is given. Assuming that water content in the profiles was similar on these two dates (i.e., ΔS of Eq.[3.1] was close to zero), we calculated cumulative actual evaporation as the difference between cumulative corrected precipitation and cumulative pure water discharge. Results are listed in row F of Table 3.4. In row G, we computationally extended results to the duration of one year and we also give average daily evaporation rates.

Mean annual evaporation from lysimeters L1 and L2 (ALRP-FGDP, 425 mm) was considerably larger than from lysimeters L3 and L4 (ALRP, 337 mm). The difference between materials (88 mm) was considerably larger than the difference between replicate lysimeters with the same filling (L1 and L2: 16 mm; L3 and L4: 19 mm). More water was was returned to the atmosphere via evaporation from ALRP-FGDP than from ALRP. This suggests that ALRP-FGDP is the material better suited as soil substitute in a mine waste surface barrier.

Table 3.4 *Evaporation from lysimeters L1 to L4, as calculated with Eq.[3.1].*

row		ALRP-FGDP		ALRP	
		L1	L2	L3	L4
A	last day with discharge from 1998/99 winter season	21 May 1999	21 May 1999	6 May 1999	14 May 1999
B	last day with discharge from 1999/2000 winter season	11 May 2000	11 May 2000	11 May 2000	11 May 2000
C	number of days from A to B	356	356	371	363
D	cumulative corrected precipitation from A to B, mm	540.1	540.1	555.4	540.1
E	cumulative pure water discharge from A to B, mm	117.6	132.9	203.0	213.7
F	cumulative evaporation from A to B, mm	422.5	407.2	352.4	326.4
G	average annual / daily evaporation, mm †	433.2 / 1.19	417.5 / 1.14	346.7 / 0.95	328.2 / 0.90

† Estimated from row C and row F.

Desalinization

The specific electrical conductivity, Ec in discharge solutions was high throughout the experiment. In the brine collected from ALRP-FGDP, Ec averaged 266 mS cm^{-1} whereas in the discharge from ALRP it was 287 mS cm^{-1}. Assuming, for simplicity, that Ec was solely caused by NaCl, the amount of salt leached from lysimeters was calculated from Ec, discharge volume, Eq.[3.2], and a variation of Eq.[3.4]. Results (in kg NaCl per square meter of the lysimeter surface) are listed in Table 3.3. For convenience, values in units of cm of NaCl are also shown. To calculate such values, a bulk density of the saline components of 1.5 Mg m^{-3} was assumed. For comparison, the density of NaCl is 2.165 Mg m^{-3} (Weast, 1987), and bulk densites of ALRP and ALRP-FGDP were 0.93 and 0.88 Mg m^{-3} (Hermsmeyer et al., 2001a). The amount of salt leached over the course of the experiment adds up to 0.06 to 0.07 m from ALRP-FGDP, and to 0.11 m from ALRP. This accounts for one third to one half of the surface settling observed in the lysimeters and is in good agreement with the differences in settling between materials (see section above titled 'Operational Complexities').
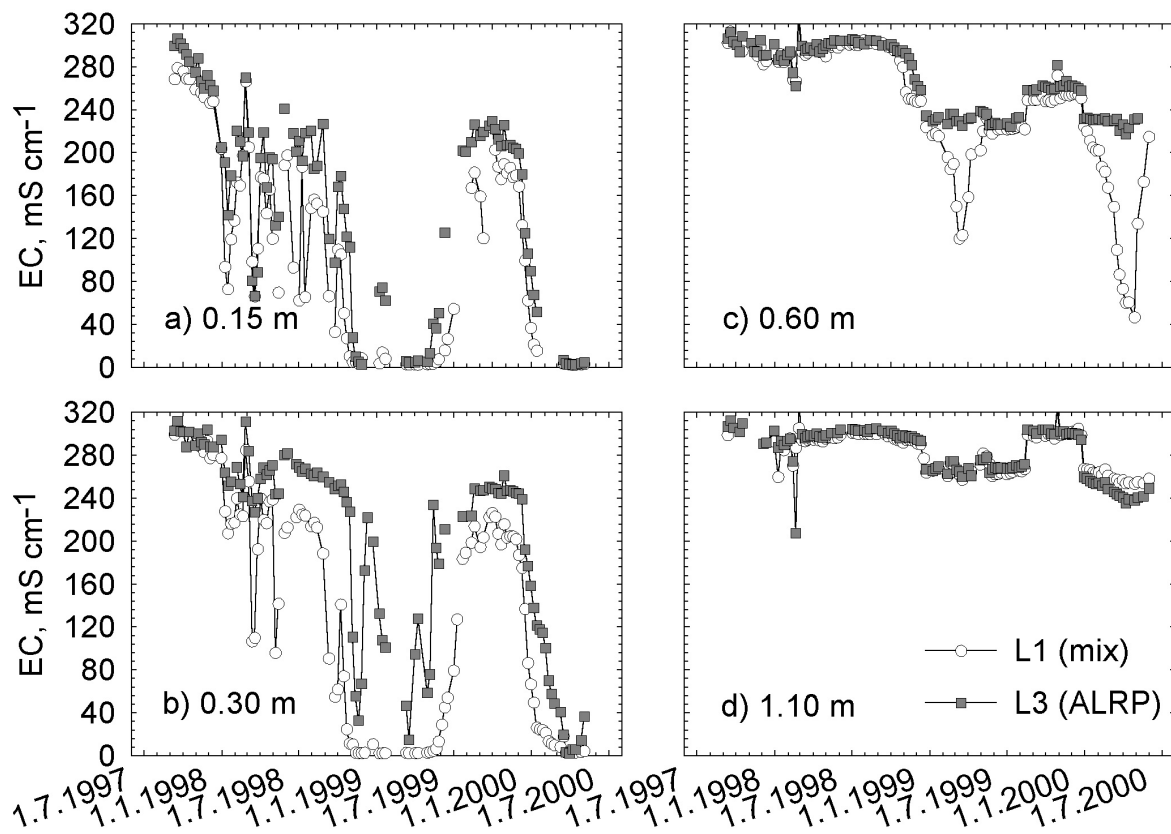
Fig. 3.5 (a to d) *Electrical conductivity (Ec) in lysimeters L1 (ALRP-FGDP mix) and L3 (ALRP) over three years. (a) in the 0.15-, (b) in the 0.30-, (c) in the 0.60-, and (d) in the 1.10-m depth.*

Results of Ec measured in suction cup solutions from the two materials from the 0.15-, 0.30-, 0.60-, and 1.10-m depths are shown in Fig. 3.5(a to d). For each depth and material, mean values from two replicate cups are given. Because of the high salt content of unweathered ALRP (40-50%), Ec initially was very high (about 300 mS cm^{-1}) in both materials and in all depths. In the shallow depth of 0.15 m, a period of pronounced scattering of Ec followed from Dec. 1997 to Nov. 1998. In both materials, with every major rainfall event, the briny solution was diluted and Ec decreased sharply. Subsequently, new salt was dissolved from the solid phase, and the water content in the profiles was depleted by evaporation during dry periods. Consequently, concentration and Ec increased. In the 0.30 m depth, scattering is also visible, but both low and high Ec values are higher than in the 0.15 m depth. At 0.60 and 1.10 m depth, Ec remained high and little scattering occurred during the same period.

From late fall 1998 onward, a seasonal dependency is clearly visible in the Ec data: In the 0.15- and 0.30-m depths, values are much lower during winter and spring months than during summer and fall. This can mainly be attributed to changes in water content. During the warm season, moisture is depleted because of high evaporation, and salt concentration increases. Capillary rise of high concentration solution from greater depths to the (by this time) mostly salt free upper parts of the profile may also lead to concentrations rising during summer. Towards the end of the 1998/99 winter season much of the solid phase salt was leached from the 0.15 m depth, causing Ec to stay low until the end of April 1999. Only after the onset of summer did Ec rise again. For the 0.30 m depth, the same is true for L1 (ALRP-FGDP), but not for L3 (ALRP). In ALRP at 0.30 m depth, Ec was still mostly dependent on wetting and drying cycles caused by individual rainstorms. This is explained by the fact that the initial salt content of ALRP was considerably higher (40 to 50%) than that of ALRP-FGDP (32 to 39%, Hermsmeyer et al., 2001).

From the winter of 1998/99 onward, Ec values in the 0.15- and the 0.30-m depths in both materials became more and more dependent on a seasonal cycle which was repeated during the winter of 1999/2000. After the onset of this seasonal cycle, periods of low and high Ec were in phase with periods of discharge flow and no-flow from the lysimeters (compare Fig. 3.2b and 3.5). This is true even for the 0.60- and the 1.10-m depths, although this far down in the profile a large supply of solid phase NaCl was available even at the end of the experiment. Nevertheless, almost instant decreases of Ec were observed in the 0.60- and in the 1.10-m depths on the dates of the start of solute percolation from both materials (e.g. 23 Dec. 1999; see Fig. 3.2b and 3.5, c and d). Ec increased again after discharge had stopped, although with a time lag. The seasonal fluctuation of Ec in the 0.60- and 1.10-m depths may be caused by differences between flow concentration and resident concentration of the solution.

On most sampling dates and depths, Ec was higher in L3 (ALRP) than in L1 (ALRP-FGDP). Differences between materials were most prominent in the 0.60 m depth during the 1998/99 and the 1999/2000 winter seasons (Fig. 3.5c). Even though more salt was leached from ALRP than from ALRP-FGDP (Table 3.3), Ec approached considerably lower values in ALRP-FGDP than in ALRP during these two winters. This is explained by the fact that initial salt content was lower in ALRP-FGDP than in ALRP. Ec and concentration are not only a result of salt content, but also of water content. Because the amount of

water leached from ALRP was larger than from ALRP-FGDP, the amount of water stored in ALRP was less than in ALRP-FGDP.

3.5 Conclusions

Mean annual pure water discharge from lysimeters L3 and L4 (ALRP) in three consecutive years was 230 mm, or 39% of the mean annual rainfall during that period. Discharge was further reduced when seven volumetric parts of ALRP were mixed with three parts of FGDP: Average discharge from lysimeters L1 and L2 was 143 mm, or 24% of rainfall. We conclude that, with respect to water balance, ALRP-FGDP is better suited as soil substitute in a mine waste surface barrier.

Because the amount of surface settling observed with ALRP was larger than with ALRP-FGDP, the same may be concluded with respect to structural stability of materials, e.g. against water induced erosion. Settling was at least partly the result of solid phase salts being leached from the materials. The amount of salt leached was larger from ALRP (59 kg m^{-2} a^{-1}), i.e., the material with the surface that settled more, than from ALRP-FGDP (33 kg m^{-2} a^{-1}). However, conclusions about structural stability cannot be drawn from lysimeter experiment results only. Testing of soil mechanical properties is necessary to study structural stability.

In our experiment under humid field conditions, surface layers of both ALRP and ALRP-FGDP were desalinized enough to support growth of ryegrass after 28 months, 1361 mm of rainfall, or 281 (ALRP-FGDP) and 444 mm (ALRP) of discharge. At 20°C, 357 g of NaCl is soluble in 1 L of water (Weast, 1987). If, for simplicity, discharge is assumed to be salt saturated throughout the experiment, 100.3 kg of NaCl were leached from ALRP-FGDP on the day that ryegrass was established (18 Nov. 1999), whereas 158.5 kg were leached from ALRP. The initial NaCl content of ALRP of about 45% was diluted to about 35% when this material was blended with FGDP. Therefore, less seepage was necessary to leach ALRP-FGDP to a plant tolerable level of salinity. In both materials the amount of NaCl leached by 18 Nov. 1999 should account for a mostly salt-free surface layer of about 0.30 m. Piston flow conditions were assumed to estimate this value.

Differences in Ec (i.e., concentration) between materials were clearly visible in suction cup solutions, and were most pronounced in the 0.60 m depth. In this depth, Ec was considerably lower in ALRP-FGDP during the second and third winter seasons. In future years plants will therefore be likely to root deeper

in ALRP-FGDP than in ALRP. This will provide a larger potential to enhance transpiration and to minimize seepage from ALRP-FGDP than from ALRP.

Compared to non-saline soils, water balance observations in highly saline materials are complex. Field measurements of water content are difficult to obtain. Variations in salt solution density and concentration may influence pressure head readings taken with tensiometers. At concentrations near saturation, salt crystals may block the pores of a ceramic tensiometer cup and may impose an impedance on water movement through the ceramic. This would be likely to result in a concentration gradient in the solution between the inside and outside of the cup, followed by an osmotic pressure gradient and, in turn, a feed back on water movement through the cup. Further reseach is needed to estimate the net effect of such processes on pressure head readings.

A numerical model to describe water balance is most easily calibrated to measured data when all components of the water balance equation are well known. During the first year of our experiment, exothermal chemical reactions apparently consumed uncontrolled amounts of water from the pore system of the tested materials. The water balance equation could therefore not be solved unambiguously for that year. During the second year, because of the blocking of outflow pipes by salt crystals, bottom boundary conditions in three out of our four lysimeters gradually changed from a seepage face to a zero flux boundary condition. This is inconvenient to take into account in numerical water balance modeling. During the third year of our study we collected water balance data suitable to calibrate a numerical model based on a short (e.g. daily) time step. Model calibration will be described in a following paper.

3.6 References

Blake, G.R., and K.H. Hartge. 1986b. Particle density. p. 377-382. *In* A. Klute (ed.) Methods of soil analysis. Part 1, 2nd ed. ASA and SSSA, Madison, WI.

Flury, M., M.V. Yates, W.A. Jury, and D.L. Anderson. 1998. Variability of solute transport in field lysimeters. *In* F. Führ (ed.) The lysimeter concept: environmental behavior of pesticides. Developed from a symposium sponsored by the Division of Agrochemicals, at the 213th National Meeting of the American Chemical Society, San Francisco, CA, 13-17 Apr. 1997. American Chemical Society, Washington, D.C.

Hermsmeyer, D., R. Diekmann, R.R. van der Ploeg, and R. Horton. 2001. Physical properties of a soil substitute derived from an aluminum recycling by-product. Manuscript submitted for publication.

Jury, W.A., W.R. Gardner, and W.H. Gardner. 1991. Soil physics. 5th ed. John Wiley and Sons. New York, NY.

Keller, R. (ed.) 1978. Hydrological atlas of the Federal Republic of Germany (in German). Harald Boldt Publ. Co., Boppard, Germany.

Long, F.L. 1984. A field system for automatically measuring soil water potential. Soil Sci. 137:227-230.

Lutton, R.J., G.L. Regan, and L.W. Jones. 1979. Design and construction of covers for solid waste landfills. EPA 600/2-79/165, U.S. Environmental Protection Agency, Cincinnati, Ohio.

Penman, H.L. 1948. Natural evaporation from open water, bare soil and grass. Proc. Roy. Meteorol. Soc. A. 193:120-145.

Phillips, S.J., M.S. Ruben, and R.R. Kirkham. 1988. Engineered surface barriers for waste disposal sites: lysimeter facility design and construction. U.S. Department of Energy, Assistant Secretary for Defense Programs.

Richards, L.A. (ed.) 1954. Diagnosis and improvement of saline and alkali soils. Agriculture Handbook No. 60. United States Department of Agriculture.

Richter, D. 1995. Results of methodological studies to correct the systematic measurement error of the Hellmann rain gauge. Reports of the German Weather Bureau, No. 194. Deutscher Wetterdienst DWD, Offenbach, Germany (in German).

Šimunek, J., M. Šejna, and M.Th. van Genuchten. 1998. The HYDRUS-1D software package for simulating the one-dimensional movement of water, heat, and multiple solutes in variably-saturated media. Version 2.0. U.S. Salinity Laboratory, Agricultural Research Service, U.S. Dept. Of Agriculture, Riverside, CA.

Weast, R. 1987. Handbook of chemistry and physics. 67th ed. CRC Press.

4. Lysimeter Study of Water Flow and Solute Transport in a Metallurgical Waste: II. Model Calibration and Application

4.1 Abstract

The longterm water balance of engineered surface barriers affects the amount of seepage into underlying waste materials. Lysimeter experiments are one means to estimate water balance components of such barriers, but it is difficult to assess longterm hydrological behavior from short-time lysimeter observations. This study was conducted to quantify longterm average seepage from a surface barrier into solid tailings from potash mining (rock salt, NaCl). Fine-grained aluminum recycling by-product and a mixture of this by-product and coal combustion waste were tested as soil substitutes in construction of a surface barrier for such tailings. Shortterm (294 d) data from lysimeters filled with these materials were used to calibrate a numerical water flow model (HYDRUS-1D). Actual evaporation was estimated from potential (Penman-) evaporation with the drying-stage approach. In combination with 31-yr-long weather records, the calibrated model was used to predict longterm seepage rates from the tested materials. Cumulative lysimeter discharge during the calibration period was adequately described by the model. Predicted longterm average annual discharge was 237 mm from the aluminum waste and 186 mm from the mix, or 31% and 24% of the longterm mean annual precipitation (764 mm). Rainfall was about 30% less than average during the calibration period. Calculated annual actual evaporation from the mix was only 11 mm short of potential evaporation. Thus it appears that the mix will effectively reduce seepage into the underlying waste.

4.2 Introduction

In industrial societies, large amounts of solid wastes are produced. Industrial, municipal, or radioactive wastes, as well as mine wastes and tailings, are often stored in landfills or piled up in mounds. Frequently, landfills and waste mounds are potentially hazardous to human health and / or the environment. Wind- and water-induced erosion of particles, leaching of solutes, and emission of gases are processes involved in the dissipation of potentially toxic substances from waste storage sites. Substances may travel into surrounding soils, surface water or groundwater resources, and the atmosphere.

Engineered surface barriers are one possibility to inhibit or to reduce all or most of the processes involved in spreading potentially hazardous substances. When a landfill or waste mound is covered with soil, or soil-like material, the underlying waste material is protected from the attacking forces of wind and rain. Such forces can then no longer mechanically separate particles from the surface of the waste material. When plants grow on a surface barrier, seepage into the underlying waste material is reduced, because water stored in the barrier is transferred to the atmosphere via transpiration. In layered surface barrier systems, gases that may be produced in the waste material below can be trapped and transmitted to a central gas stack (or stacks), where they are evacuated and may be burned or otherwise treated.

Environmental regulations in many countries require the application of engineered surface barriers after the storage capacity of a waste disposal site is exhausted. Barriers may consist of a single recultivation layer to support plant growth, or a combination of several layers. For example, a barrier system may consist of (from top to bottom) a recultivation layer, a water drainage layer to collect seepage and drain it laterally (e.g., into a ditch), a plastic foil and / or a mineral clay layer to prevent seepage flow into the underlying waste material, and a gas drainage layer.

Because toxic substances in many waste materials are resistant to decomposition, longterm performance of applied surface barriers is essential. As the layering of a surface barrier may be complex, and because a wide range of materials is used in barrier construction, evaluating the longterm performance of a barrier is not an easy task. At times, industrial by-products from one process may be used in constructing a surface barrier over waste materials from another process. This practice provides a low-cost method of disposal, decreases the overall need for landfill capacity, and saves valuable soil resources that would otherwise be used in surface barrier construction. When industrial by-products are used in constructing a barrier, their hydrological properties must be known in order to evaluate longterm barrier performance.

With respect to hydrological performance, lysimeter studies are one method to assess the feasibility and effectiveness of a particular surface barrier under the field conditions of a particular site. Infiltration of precipitation, water storage, evaporation, transpiration, and the remaining seepage water flow into an underlying waste material can all be monitored in lysimeter experiments (Gee et al., 1993). When lysimeters of identical dimensions, but filled with different materials, are operated side-by-side in the field, discharge can be compared directly. But, because leaching of water through soil is a slow process, lysimeter

studies are time consuming and cumbersome. Also, the number of lysimeters and surface barrier design variations that can be observed in such studies is limited. Based on results of lysimeter studies alone, it is difficult to assess longterm barrier performance and to make decisions about materials, or about the thickness of individual layers or the entire surface barrier.

An effective approach for evaluating longterm barrier performance of seepage control is to couple shortterm data from lysimeter studies with extended model simulations. The shortterm data are used to calibrate the model. In combination with longterm weather records, the calibrated model subsequently can be used to predict longterm seepage rates. Examples of models that may be used in longterm barrier performance evaluation are the Hydrologic Evaluation of Landfill Performance (HELP) model (Schroeder et al., 1994), SoilCover (Unsaturated Soils Group, 1997), HYDRUS-1D (Šimunek et al., 1998), and HYDRUS-2D (Šimunek et al., 1999).

The present study assesses the longterm hydrological performance of a proposed surface barrier for the rock salt (NaCl) waste mound of the Sigmundshall potash mine near Hannover, Germany. The mine and waste mound are operated by the K+S Company (Kali und Salz GmbH). The rock salt mound is currently bare and produces annually 150,000 to 200,000 m^3 of briny discharge (K+S, personal communication), which is conveyed into a local river.

In the work reported on here, the HYDRUS-1D model was calibrated to water balance data collected from lysimeters filled with two different, saline industrial waste materials that were proposed to cover the rock salt mound: fine-granular aluminum recycling by-product (ALRP), and a mixture of such waste and flue gas desulfurization by-product (FGDP) of coal combustion. ALRP is a by-product of the industrial processing of so-called black dross and salt cake, which in turn are wastes of the recycling process of discarded aluminum products. The K+S Company operates at the Sigmundshall mine, a facility that produces annually about 90 kt of ALRP. In the lysimeter study, it was shown that under humid conditions both ALRP and ALRP-FGDP are supportive of plant growth after an initial period of desalinization. A description of the physical and hydraulic properties of the materials, and a description of the lysimeter experiment and collected data can be found in two earlier papers (Hermsmeyer et al., 2001 a, b).

Subsequent to calibrating the model to the lysimeter data, 31-yr records of a nearby weather station were used to calculate expected longterm seepage rates from the two materials on the basis of a daily timestep. The calibrated model may be used in estimating the effect of changes in surface barrier properties and

in determining the final barrier design. For example, effects of different barrier thicknesses, or effects of variations in the growth and distribution of plant roots, may be estimated by changing corresponding parameters in the calibrated model.

4.3 Materials and Methods

Lysimeter Experiment

We studied four free-drainage lysimeters (L1, L2, L3, and L4) under field conditions. The lysimeters were constructed at the site of the Sigmundshall mine and were embedded in small, 2-m-high artificial hills. Each lysimeter had a square surface of 4 m^2 and was 1.8 m deep. The bottom 0.15 m consisted of a drainage package of sand and fine gravel. In lysimeters L1 and L2, the 1.63-m soil profile consisted of a single layer of a mixture of ALRP and FGDP (7:3, on a volumetric basis). In lysimeters L3 and L4, it consisted of a single layer of ALRP. Both materials originated from industrial processes. To prevent runoff, the top 0.02 m of all four lysimeters were not filled. Drainage water from the lysimeters was collected in buried barrels, which were covered with lids to prevent evaporation between sampling dates. Sampling, in general, was done once a week. We filled the lysimeters on 1 Jul. 1997 and allowed them to settle for 2 yr before we started to collect data for the calibration of the model on 11 Aug. 1999. Lysimeter surfaces were initially bare, but they were sown with ryegrass (*Lolium perenne*, L.) in early spring, 2000. Data collection ended on 31 May 2000, i.e., after 294 d. We refer to the period from 11 Aug. 1999 to 31 May 2000 as the calibration period.

At the end of the lysimeter experiment, we took undisturbed samples from the 0.05-, 0.15-, 0.30-, 0.60-, 0.90-, 1.10-, 1.40-, and 1.60-m depths of lysimeters L1 and L3 in cylinder rings of 0.05-m diameter with three replicates per depth. On these, we determined bulk density following a method described by Blake and Hartge (1986). Volumetric moisture content was determined by weighing samples before and after drying them to constant weight at 105 °C.

Pressure head was measured in lysimeters L2 (ALRP-FGDP) and L4 (ALRP) with vertically installed tensiometers at the 0.6-, 1.10-, and 1.63-m depths, with three replicates at the 0.6- and 1.10-m depths, and one instrument at the 1.63-m depth. For the 0.6- and 1.10-m depths, the average of three tensiometers was used to represent the pressure head at each depth. Tensiometers were connected to an automated data logger, which was set to

store hourly minimum, maximum, and average values of one reading per minute.

A weather station was connected to the same data logger with the same setting. The station was supplied with instruments to record air temperature and relative humidity, wind speed and direction, and downward and upward longwave and shortwave radiation. Measurements were taken in 2 m above the lysimeter surface, i.e., in 4 m above the terrain surrounding the lysimeter setup. Precipitation was recorded in 1 m above the lysimeter surface. With respect to precipitation, the logger was set to store hourly totals. Details of the lysimeter study and resulting data have been reported by Hermsmeyer et al. (2001b).

Laboratory Experiment

Soil physical and hydraulic properties of the tested materials were studied in the laboratory prior to the lysimeter experiment. Details of the laboratory study have been reported by Hermsmeyer et al. (2001a), and only a short summary appears here. The solid phase salt content of ALRP and ALRP-FGDP consisted predominantly of NaCl and was estimated from measurements of electrical conductivity (Ec) in solutions equilibrated with the materials. Salt content was about 45% in unweathered ALRP, and about 35% in the unweathered mix, i.e., the salt content of ALRP was decreased by blending this material with FGDP, which has a relatively low salt content (1.65%). After 2 yr of settling and seepage water flow under field conditions, salt content in the upper 0.3 m of lysimeters with both fillings (ALRP and ALRP-FGDP) had decreased sufficiently to support plant growth (Hermsmeyer et al., 2001b).

Saturated hydraulic conductivity K_s, of ALRP and ALRP-FGDP, was measured on packed core samples of 0.05-m diameter using the constant head method of Klute and Dirksen (1986). Because of the high salt content of ALRP, measurements were conducted on unwashed samples using a brine solution and were repeated on samples washed free of salt using water. Six consecutive measurements were taken on each of three replicate samples of each material in both the unwashed and washed condition (72 measurements in total).

The drying branch of the water retention curve also was measured on packed core samples of ALRP and ALRP-FGDP on a porous ceramic plate and in a kaolin box with a hanging water column in steps of 0.1, 0.3, 0.6, 1.0, and 3.0 m. A pressure plate apparatus was used to drain washed samples of 0.01-m height at 158 m of suction.

The Rosetta software (Schaap, 1999) was used to derive a set of water retention curves for the two materials. During this pedo-transfer function approach, we used results from laboratory measurements of particle size distribution, of bulk density, and of water content at 0.3 and at 158 m of suction to estimate water retention parameters. Values of particle size distribution and of water content were taken from Hermsmeyer et al. (2001a). Bulk density values were used as determined for eight depths of the profiles at the end of the lysimeter experiment.

Governing Equations, and Initial and Boundary Conditions

One-dimensional isothermal Darcian water flow in variably-saturated, rigid porous media was assumed. This is expressed by the following (extended) form of the Richards equation:

$$\frac{\partial \theta}{\partial t} = \frac{\partial}{\partial z}\left[K\,(\partial h/\partial z) + K \right] - S(h) \qquad [4.1]$$

where θ is the volumetric water content ($m^3\,m^{-3}$), t is time (d), z is a vertical space coordinate (m) positive downward, h is the water pressure head (m), K is the hydraulic conductivity ($m\,d^{-1}$), and S(h) is a sink term ($m^3\,m^{-3}\,d^{-1}$). The quantity S(h) describes root water uptake and is defined as the volume of water removed from a unit volume of soil per unit time. The quantity S(h) equals zero in a bare profile, i.e., during most of our calibration period. For periods with vegetation, we used the concept of Feddes et al. (1978) to derive values of S(h) (see section below titled "Longterm Weather Records and Longterm Modeling"). Initial and boundary conditions applied to the lysimeter experiment were as follows:

$$h(z,t) = h_i(z) \qquad\qquad , \text{at} \quad t = 0, \qquad [4.2]$$

$$-K\left(\frac{\partial h}{\partial z} - 1\right) = 0 \qquad\qquad , \text{at} \quad z = 0, \qquad [4.3]$$

and

$$h(z,t) = h_L(t) \qquad\qquad , \text{at} \quad z = L \qquad [4.4]$$

where $h_i(z)$ is the initial pressure head (m) at depth z, L is the coordinate of the bottom of the lysimeter, and h_L is the pressure head (m) at the bottom of the lysimeter. Equation [4.1], subject to the initial and boundary conditions given previously, was solved numerically using the HYDRUS-1D code (Šimunek et al., 1998). To describe initial and boundary conditions, we used results from measurements of our lysimeter experiment. Daily average values of tensiometer readings from day one of the calibration period were used as initial values for h_i in tensiometer installation depths. Values of h_i for profile depths with no tensiometers were estimated by linear interpolation of the measured values over depth.

To describe upper boundary atmospheric conditions during the calibration period, we used daily values of precipitation and evaporation derived from measurements of the lysimeter weather station. Daily totals of measured precipitation were corrected for the systematic error due to evaporation from the wet wall of the rain gauge and to wind effects. We added to the measured daily totals of precipitation the empirical monthly correction factors (percentages) for north-central Germany, as published by Richter (1995). Details are given in Hermsmeyer et al. (2001b). To derive daily values of actual evaporation from the lysimeter surfaces, we used the combination method of Penman (1948) and the concept of different stages of drying of an initially wet surface (see following section titled "Evaporation").

During the lysimeter experiment, we found that discharge occurred whenever the tension near the bottom of the profile approached zero (Hermsmeyer et al., 2001b). This is in agreement with the concept of a seepage face through which water can leave the saturated part of the flow domain. This often applies to lysimeters that are allowed to drain under gravity (Šimunek et al., 1998). The seepage-face concept implies that the flux across the bottom boundary will only be larger than zero when this boundary is saturated, i.e., when h_L approaches zero. In our model application we applied seepage face-type conditions to the bottom boundary of the lysimeters.

The unsaturated hydraulic properties of the tested materials were approximated by the following equations (van Genuchten, 1980):

$$S_e(h) = \frac{\theta(h) - \theta_r}{\theta_s - \theta_r} = \frac{1}{\left[1 + |\alpha h|^n\right]^m} \qquad , \text{for} \quad h < 0 \qquad [4.5]$$

$$\theta(h) = \theta_s \qquad\qquad , \text{for} \quad h \geq 0 \qquad [4.6]$$

and

$$K(\theta) = K_s S_e^{0.5} \left[1 - \left(1 - S_e^{1/m}\right)^m \right]^2 \qquad [4.7]$$

where n and α are the van Genuchten parameters, K_s is the soil hydraulic conductivity at saturation (m d^{-1}), S_e is the effective water content, $m = 1 - 1/n$, and θ_r and θ_s are the residual and saturated water content (m^3 m^{-3}), respectively.

Model Calibration and Inverse Procedure

Our main objective during model calibration was to match, as closely as possible, calculated values of the cumulative flux across the bottom boundary with discharge data measured in the lysimeter study. Many water balance models allow for the calculation of discharge from a set of initial and boundary conditions and the hydraulic properties of the flow domain material (or materials). In addition to this, the HYDRUS-1D software allows for estimation of soil hydraulic properties, e.g., from discharge data, by minimization of a statistical objective function. This approach is called inverse modeling, or inverse procedure.

During inverse modeling, an initial set of hydraulic properties must be given. For this we used values of θ_r, θ_s, α, n, and K_s, as estimated with the Rosetta model (Schaap, 1999) from laboratory measurements of particle size distribution, bulk density, and water retention for eight depths of the lysimeter profiles. The packed materials in the large field lysimeters may have differed from the ones in the laboratory cylinders, and our laboratory results may have been affected by high salt contents. Therefore, hydraulic properties as derived from the laboratory studies may not adequately describe field lysimeter conditions. We used the inverse capabilities of the HYDRUS-1D software to optimize the hydraulic properties of the tested materials from lysimeter outflow data.

The estimated parameters were assumed to be independent and uniformly distributed. The HYDRUS-1D software uses the following objective function to minimize differences between measured and calculated values (Šimunek et al., 1998):

$$\Phi(b,q,p) = \sum_{j=1}^{m_q} v_j \sum_{i=1}^{n_{qj}} w_{i,j} \left[q_j^*(x,t_i) - q_j(x,t_i,b) \right]^2 +$$

$$\sum_{j=1}^{m_p} \bar{v}_j \sum_{i=1}^{n_{pj}} \bar{w}_{i,j} \left[p_j^*(\theta_i) - p_j(\theta_i,b) \right]^2 + \qquad [4.8]$$

$$\sum_{j=1}^{n_b} \hat{v}_j \left[b_j^* - b_j \right]^2$$

where the first term on the right-hand side (RHS) of Eq.[4.8] represents deviations between measured and calculated space-time variables (in our problem, values of the cumulative flux versus time across the bottom boundary). In this term, m_q is the number of different sets of measurements, n_{qj} is the number of measurements in a particular measurement set, $q_j^*(x,t_i)$ represents specific measurements at time t_i for the *j*th measurement set at location $x(r,z)$, $q_j(x,t_i,b)$ are the corresponding model predictions for the vector of optimized parameters b, and v_j and $w_{i,j}$ are weights associated with a particular measurement set or point, respectively. The second term on the RHS of Eq.[4.8] represents differences between independently measured and predicted hydraulic properties, whereas the terms m_p, n_{pj}, $p_j^*(\theta_i)$, $p_j(\theta_i,b)$, $\bar{v}_j$, and $\bar{w}_{i,j}$ have similar meanings as for the first term, but now for the hydraulic properties of the medium. The last term on the RHS of Eq.[4.8] represents a penalty function for deviations between prior knowledge of the hydraulic parameters, b_j^*, and their final estimates, b_j, with n_b being the number of parameters with prior knowledge, and $\hat{v}_j$ representing preassigned weights. We assigned a value of 1 to all weighting factors of Eq.[4.8], v_j, $w_{i,j}$, $\bar{v}_j$, $\bar{w}_{i,j}$, and $\hat{v}_j$. Minimization of the objective function is accomplished by using the Levenberg-Marquardt nonlinear minimization method, which is a weighted least squares approach based on Marquardt's maximum neighborhood method (Marquardt, 1963). For further details, see Šimunek et al. (1998).

To limit the number of estimated parameters, we assessed θ_r, θ_s, α, n, and K_s separately (one inverse model run per parameter and eight profile depths) and isolated the parameter with the highest reduction of differences between measured and (inversely) simulated cumulative discharge curves for the calibration period.

Evaporation

To describe atmospheric conditions at the upper boundary of our lysimeters, daily values of actual evaporation are needed. These can be derived from potential evaporation. We used the combination method first proposed by Penman (1948) to estimate daily values of potential evaporation Ep (mm) from the surface of our lysimeters using the following equation:

$$Ep = \frac{s}{s+\gamma} \ \frac{Rn-G}{L} \ + \ \frac{\gamma}{s+\gamma} \ 0.063 \left(1+1.08 \, u_2\right)\left[e_s(T)-e\right]S_R \qquad [4.9]$$

In Eq.[4.9], s (hPa K^{-1}) is the slope of the temperature-dependent saturation vapor pressure curve, which according to DVWK (1996) can be calculated as

$$s = \frac{\partial e_s}{\partial T} = e_s(T) \ \frac{4284}{\left(243.12+T\right)^2} \qquad , \text{over water} \qquad [4.10a]$$

and as

$$s = \frac{\partial e_s}{\partial T} = e_s(T) \ \frac{6123}{\left(272.62+T\right)^2} \qquad , \text{over ice} \qquad [4.10b]$$

where T is temperature (°C) and e_s is saturation vapor pressure (hPa). For the psychrometer constant γ, values of 0.655 and 0.576 hPa K^{-1} were used over water and ice, respectively. The temperature-dependent saturation vapor pressure, e_s, was calculated as (see Sonntag, 1994)

$$e_s(T) = 6.11 \ \ \exp\left(\frac{17.62 \, T}{243.12+T}\right) \qquad , \text{over water} \qquad [4.11a]$$

and as

$$e_s(T) = 6.11 \ \ \exp\left(\frac{22.46 \, T}{272.62+T}\right) \qquad , \text{over ice} \qquad [4.11b]$$

For simplicity, a threshold air temperature value of 0 °C was used to separate periods in which either Eqs.[4.10a] and [4.11a], with $\gamma = 0.655$, were

used or Eqs.[4.10b] and [4.11b], with $\gamma = 0.576$ hPa K^{-1}. From calculated values of $e_s(T)$ and measurements of the relative humidity, H, values of the actual vapor pressure, e, were calculated with use of the expression

$$e = e_s(T) \frac{H}{100}$$
[4.12]

The expression $(Rn - G) / L$ in Eq.[4.9] is part of the energy term of the combination method (the first term on the RHS of Eq.[4.9]), with Rn being the net radiation flux, G being the soil heat flux (both Rn and G are in W m^{-2}), and L (W m^{-2} mm^{-1} d) being the specific heat of evaporation of water. To calculate L from air temperatures above 0 °C, we used the expression (see DVWK, 1996)

$$L = (28.9 - 0.028\ T)$$
[4.13]

For temperatures below 0 °C, we used a constant value of 32.8 W m^{-2} mm^{-1} d for L. Koitzsch et al. (1990) showed that for northern Germany the quantity $(Rn - G)$ is approximately equal to 0.6 Rg, where Rg (W m^{-2}) is the hourly average of the daily total of (shortwave) global radiation. Accordingly, we used the expression of Koitzsch et al. (1990) to estimate the energy term of Eq.[4.9].

In Eq.[4.9], u_2 (m s^{-1}) denotes wind speed at 2 m above the ground. Our anemometer was installed at 2 m above the lysimeter surface, which was about 4 m above the surrounding terrain. To account for the increase in wind speed with increasing elevation, we used an equation proposed by Häckel (1990), which can be given as

$$u_2 = u_4 \left(\frac{h_{u_2}}{h_{u_4}} \right)^C$$
[4.14]

where h_{u_4} (m) is the elevation of installation and h_{u_2} (m) is the objective elevation of the anemometer, and u_2 and u_4 are wind speeds in these elevations. In our case, $h_{u_4} = 4$ m and $h_{u_2} = 2$ m (see previous section titled "Lysimeter

Experiment"). The exponent C is a dimensionless empirical factor depending on the surface roughness of the surrounding terrain, including urban development and vegetation. According to Häckel (1990), C ranges from 0.13 for flat terrain with no or few obstacles to 0.67 for rough terrain with extremely large obstacles, e.g. inner-city areas. Because our lysimeters were set up next to the large potash mine tailings mound that caused channeling and turbulence in the air flow around it, we used C = 0.67.

The quantity S_R in Eq.[4.9] is the ratio of the number of daylight hours, N, and the number of daylight hours at equinox (12 h). We calculated N from the hour angles of the Sun at sunset T_s, and at sunrise T_r, using the following equation:

$$N = (12/\pi)(T_s - T_r) \qquad [4.15]$$

For further details about the calculation of N, see Swift (1976).

To estimate daily values of actual evaporation Ea (mm) from an initially wet and bare soil, we used the concept of the different stages of a drying soil (see Idso et al., 1974; Shouse et al., 1982; Jury et al., 1991). During the first stage, the upward flow of water in the wet soil is assumed to be high enough to sustain the evaporative demand of the atmosphere, and hence Ea is equal to Ep. This stage lasts for a period of t_c days after irrigation or rainfall has ceased. Evaporation and seepage deplete the soil near its surface, and the soil dries out to a point where the subsequent rate of water loss is controlled by the soil. At this point the second, or falling rate stage of drying begins.

Black et al. (1969) and Ritchie (1972) stated that during the falling rate stage cumulative actual evaporation (Ea_{cum}) is proportional to the square root of time passed since the onset of that stage. These authors provided an equation to estimate summer values of Ea on consecutive days. In our study, however, daily values of Ea were needed for the entire year. Following DVWK (1996), we applied an extended form of the square-root-of-time approach to estimate Ea on consecutive days as follows:

$$Ea = \frac{\beta}{(t - t_c)^{1/2}} Ep \qquad , \text{ for } \quad t > t_c \qquad [4.16]$$

In Eq.[4.16], $(t - t_c)$ is the time (in d) after the onset of the second (drying) stage, and β (in $d^{-1/2}$) is a constant that is dependent on the hydraulic properties of the soil. To solve Eq.[4.16], values of Ep from Eq.[4.9] can be used, but values of t_c and values of β must be estimated.

To determine values of $t - t_c$, we analyzed daily totals of (corrected) precipitation. Following Shouse et al. (1982), we assumed that Ea = Ep during the first 2 d after a rainfall event of 10 mm or more. We counted the days after such an event, assigning a value of 1 to the day the rainfall was recorded and to the two following days $(t - t_c = 1)$. For each additional day without rain, we added a value of 1 $(t - t_c = 2, 3, ...)$. For days with little rainfall (< 10 mm), we added a value of 0.

For β, a value of 0.5 has been recommended for sandy soils (DVWK, 1996). ALRP and ALRP-FGDP are materials finer than sand. We assumed that capillary rise and evaporation, and hence values of β, are higher for ALRP and ALRP-FGDP than for sand. To determine actual values of β, we repeated direct (or "forward") runs of the HYDRUS-1D model with values of β increasing between model runs, until visually the best fit of measured and calculated cumulative lysimeter discharge was obtained. As an initial value of β we used 0.5. We increased β in steps of 0.1 between model runs. This was done prior to optimizing material hydraulic parameters by inverse modeling.

For the calibration period, we calculated Ea from Eq.[4.16] with values of $t - t_c$ and values of β thus derived. In cases in which calculated values for Ea were larger than Ep (from Eq.[4.9]), we set Ea = Ep. For example, with a value of $\beta = 2.0 \ d^{-1/2}$, this occurs on days with $t - t_c \le 3$ d.

Longterm Weather Records and Longterm Modeling

Daily averages of temperature, relative humidity, and wind speed, as well as daily totals of precipitation and bright sunshine of 1 Jan. 1967 to 31 Oct. 1996 (11,672 d) were used to determine atmospheric boundary conditions for longterm model simulations. The daily totals were from a reference weather station operated by the German Weather Bureau at the Hannover airport, 25 km northeast of the Sigmundshall mine.

We applied the same procedure to the longterm precipitation data as to the lysimeter precipitation data to correct for the systematic error in rainfall measurements. To calculate daily values of longterm potential evaporation we used Eq.[4.9]. But because values of Rn are not measured at the Hannover airport, we determined Rn from daily values of duration of bright sunshine

(measured at the airport), using the following empirical equation given by Ångstrom (1924) and Kimball (1927), and modified by Black et al. (1954):

$$Rn = (A + B\, n_a/N_p)\, R_{st} \qquad [4.17]$$

In Eq.[4.17], R_{st} is the daily extraterrestrial shortwave radiation flux, n_a/N_p is the ratio of actual/potential daily duration of bright sunshine, and A and B are regressions coefficients. Yearly average values of A and B have been determined for numerous weather stations in Europe by Palz and Greif (1996). As suggested by these authors, we used values of 0.19 and 0.55 for A and B, respectively, to determine Rn from sunshine duration measurements at the Hannover airport. For details on determining values of R_{st} and N_p, see Zaradny and van der Ploeg (1982).

To reduce values of Ep to values of actual transpiration Ea for a grass cover, we used the water uptake reduction model of Feddes et al. (1978), which is implemented in the HYDRUS-1D software. According to this stress-response function, water uptake by roots is assumed to be zero close to saturation, i.e., wetter than some arbitrary anaerobiosis point, h_1. For $h < h_4$ (the wilting point pressure head), water uptake also is assumed to be zero. Water uptake is assumed to be optimal between h_2 and h_3, whereas for pressure heads between h_3 and h_4 (or h_1 and h_2), water uptake decreases (or increases) linearly with h. We assumed values of 0.1, 0.25, 10, and 80 m of suction for h_1, h_2, h_3, and h_4, respectively. In addition, we assigned a relative root density of one to the upper 0.4 m of the lysimeter profiles for both materials in the longterm modeling, and a linear decrease of root density from one to zero from the 0.4- to 0.5-m soil depth.

4.4 Results and Discussions

In Table 4.1, laboratory values of particle size distribution and of water content at 0.3 and 158 m of suction are listed for ALRP-FGDP and for ALRP (see Hermsmeyer et al., 2001a). Results from measurements of bulk density in eight depths of lysimeters L1 (ALRP-FGDP) and L3 (ALRP) are shown in Table 4.2. As a result of compaction, bulk density increased with depth in both lysimeters. Except near to the surface (0.05-m depth), bulk density was higher in ALRP than in ALRP-FGDP. This is in agreement with results from laboratory

analyses conducted on packed cylinder ring samples. Average bulk density of such samples was 0.93 Mg m^{-3} for ALRP and 0.88 Mg m^{-3} for ALRP-FGDP (Hermsmeyer et al., 2001a). Values from Tables 4.1 and 4.2 were used as input parameters for the Rosetta model to derive a set of eight water retention curves for each material for the sampling depths listed in Table 4.2. Values of θ_r, θ_s, α, n, and K_s, as estimated with the Rosetta model, are listed in Table 4.3.

Table 4.1 *Particle size distribution and water content at 0.3 and 158 m of suction for ALRP-FGDP and ALRP (data from Hermsmeyer et al., 2001a).*

	ALRP-FGDP	ALRP
% Sand	28.1	37.8
% Silt	57.4	53.3
% Clay	15.0	9.0

	Water Content, m^3 m^{-3}	
at 0.3 m	0.636	0.626
at 158 m	0.168	0.243

Table 4.2 *Bulk density and water content of ALRP-FGDP and ALRP at the end of the calibration period in eight profile depths (average values from three replicate measurements per depth).*

Sampling Depth, m	Bulk Density, Mg m^{-3}		Water Content, m^3 m^{-3}	
	L1 (ALRP-FGDP)	L3 (ALRP)	L1 (ALRP-FGDP)	L3 (ALRP)
0.05	0.65	0.64	0.28	0.36
0.15	0.66	0.86	0.28	0.49
0.30	0.71	0.87	0.26	0.41
0.60	0.98	1.14	0.27	0.28
0.90	0.98	1.24	0.29	0.28
1.10	1.10	1.19	0.36	0.28
1.40	1.14	1.21	0.35	0.28
1.60† / 1.55‡	1.19	1.40	0.38	0.29

†: for ALRP-FGDP, ‡: for ALRP (sampling depths differ between materials because of different amounts of settling during the course of the experiment).

Table 4.3 *Values of θ$_r$, θ$_s$, α, n, and K$_s$ for ALRP-FGDP and ALRP.*

				L1 (ALRP-FGDP)		
No. †	Assigned to Depth, m	θ$_r$ m^3 m^{-3}	θ$_s$ m^3 m^{-3}	α m^{-1}	n -	K$_s$ · 10^{-2} m d^{-1}
1	0.00-0.10	0.154	0.639	0.10§ / 0.039¶	2.530	50.7
2	0.10-0.23	0.155	0.638	0.10 / 0.873	2.550	49.1
3	0.23-0.45	0.161	0.631	0.09 / 0.176	2.650	41.4
4	0.45-0.75	0.183	0.601	0.05 / 0.028	3.177	12.4
5	0.75-1.00	0.183	0.601	0.05 / 0.190	3.177	12.4
6	1.00-1.25	0.186	0.588	0.04 / 0.010	3.434	5.7
7	1.25-1.50	0.186	0.584	0.04 / 0.011	3.524	4.2
8	1.50-1.60	0.186	0.579	0.03 / 0.018	3.636	2.9

				L3 (ALRP)		
No. ‡	Assigned to Depth, m	θ$_r$ m^3 m^{-3}	θ$_s$ m^3 m^{-3}	α m^{-1}	n -	K$_s$ · 10^{-2} m d^{-1}
1	0.00-0.10	0.146	0.652	0.13 / 0.016	2.190	49.6
2	0.10-0.23	0.163	0.616	0.07 / 0.010	2.582	22.1
3	0.23-0.45	0.164	0.614	0.07 / 1.258	2.601	21.0
4	0.45-0.75	0.167	0.576	0.04 / 0.171	3.050	3.7
5	0.75-1.00	0.164	0.562	0.03 / 0.018	3.213	1.9
6	1.00-1.25	0.165	0.569	0.03 / 0.010	3.130	2.6
7	1.25-1.50	0.165	0.566	0.03 / 0.250	3.163	2.3
8	1.50-1.55	0.160	0.540	0.02 / 0.043	3.452	0.7

†: Numbers refer to curve numbers in Fig. 4.1.
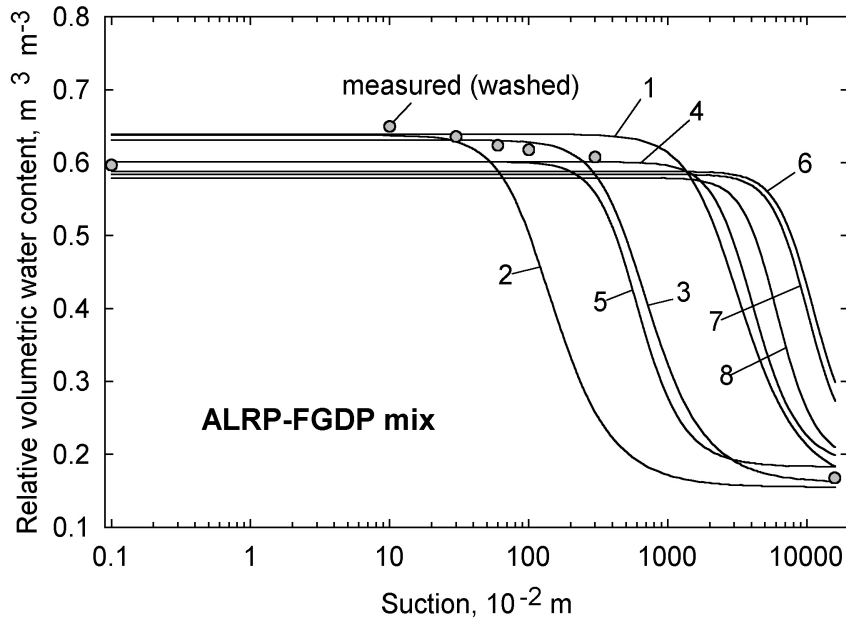‡: Numbers refer to curve numbers in Fig. 4.2.
§: From Rosetta model.
¶: From HYDRUS-1D inverse procedure.

As a result of bulk density increasing with depth (Table 4.2), residual water content, θ_r, also increases, but the water content at saturation, θ_s, and the saturated hydraulic conductivity, K_s, decrease. This can be attributed to a decrease of the number and the width of pathways for the flow of water with an increase of bulk density (= decrease of porosity).

The inverse of the parameter α is often referred to as the air entry value or bubbling pressure, i.e. the suction at which the material begins to release significant amounts of water, or the suction at which the water retention curve bends downward. During inverse modeling, we found that α was the most effective single parameter to be reestimated when matching calculated and measured values of cumulative lysimeter discharge. In Table 4.3, values of α resulting from the Rosetta model and from the HYDRUS-1D inverse approach are listed. For both materials, values of α from the Rosetta model gradually decrease with depth (i.e., with increasing bulk density), meaning that the bubbling pressure increased: The higher the compaction, the higher is the suction necessary to draw water from the pore space. However, values of α from the inverse approach are not that easy to interpret. For ALRP-FGDP, values of α ranged from 0.01 to 0.873 m^{-1} (or bubbling pressures from 100 to 1.145 m); for ALRP α ranged from 0.01 to 12.58 m^{-1} (or bubbling pressures from 100 to 0.079 m). For both materials, inversely estimated values of α seemed to change arbitrarily with depth.

Figure 4.1 depicts the set of water retention curves derived for lysimeter L1 (ALRP-FGDP), Fig. 4.2 shows curves for lysimeter L3 (ALRP). Curves are visualizations of Eq.[4.5] with values of θ_r, θ_s, n, and K_s, as well as α from the HYDRUS-1D inverse approach as listed in Table 4.3. Measured values of water retention (from Hermsmeyer et al., 2001a) are also shown in Figs. 4.1 and 4.2. For ALRP-FGDP, measurements were taken on salt-free (or washed) samples. For ALRP, they were taken on saline (unwashed) and on salt-free samples. Figures 4.1 and 4.2 show that values of water retention measured on washed samples are close to the center of the range of values inversely estimated from lysimeter outflow curves for eight profile depths. Measured water retentions of unwashed ALRP are close to the inversely estimated water retention curve with the maximum value of α (Fig. 4.2). In summary, the variation of water retention curves with depth in Figs. 4.1 and 4.2 is a result of increasing bulk density, but mostly of the variability of inversely estimated values of α.

Fig. 4.1 *Water retention curves for eight profile depths of ALRP-FGDP as calculated from particle size distribution, bulk density, measured water retention at 0.3 and 158 m of suction, and inversely estimated values of α. Curve numbers refer to lysimeter depths (see Table 4.3).*
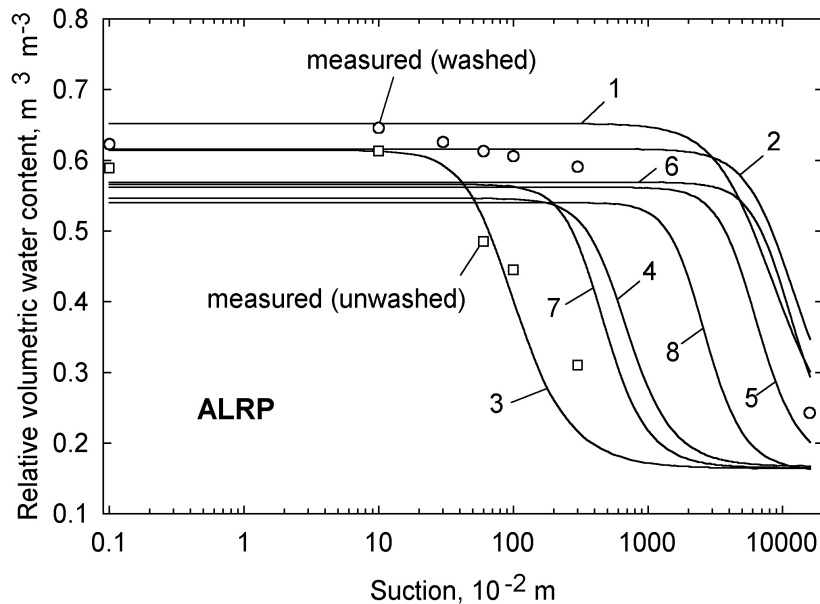
Fig. 4.2 *Water retention curves for eight profile depths of ALRP as calculated from particle size distribution, bulk density, measured water retention at 0.3 and 158 m of suction, and inversely estimated values of α. Curve numbers refer to lysimeter depths (see Table 4.3).*
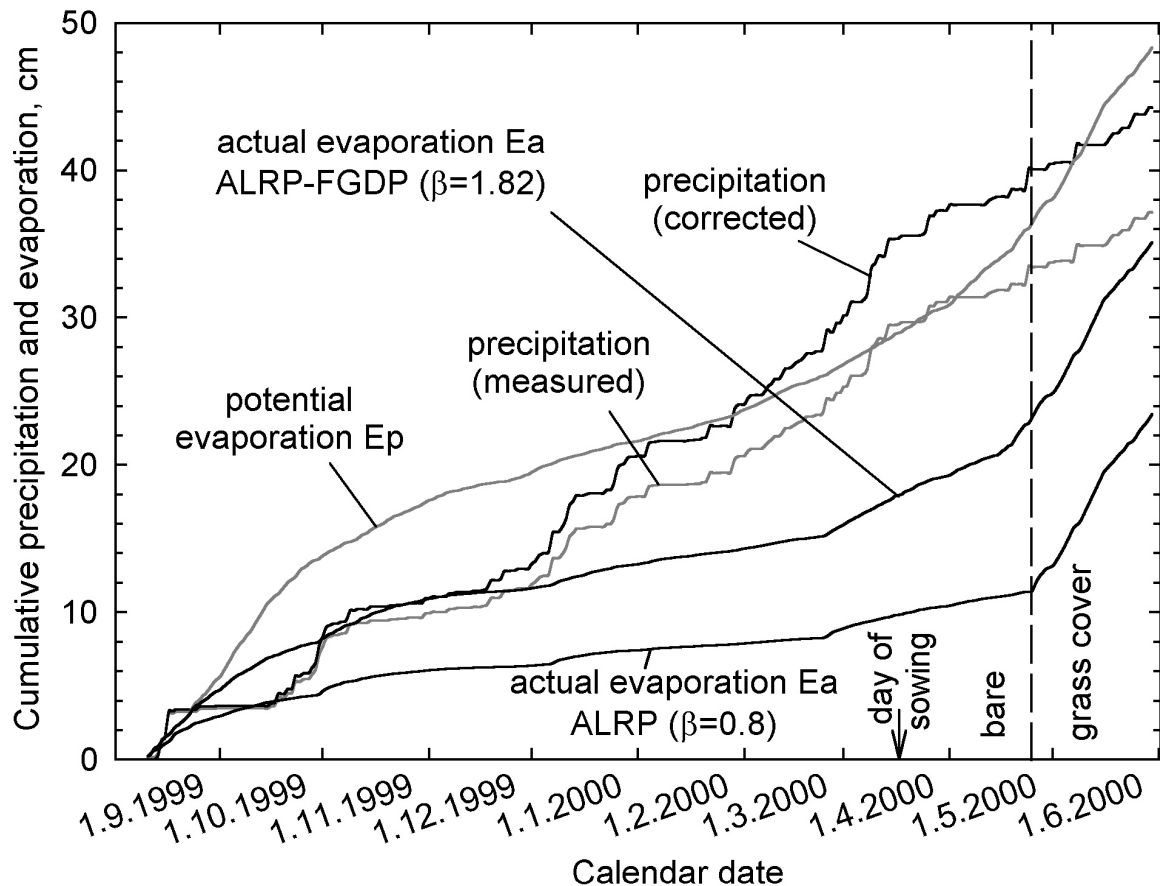
Fig. 4.3   *Atmospheric boundary conditions during the calibration period of the lysimeter experiment (11 Aug. 1999 to 31 May 2000, 294 d).*

Atmospheric boundary conditions (cumulative precipitation and evaporation) for the calibration period are shown in Fig. 4.3. Curves are plotted for measured and for corrected precipitation, as well as for potential and actual evaporation. Corrected precipitation and actual evaporation (black curves) were used in calibrating the water balance model. Gray curves are for additional information. Cumulative measured precipitation during the calibration period (294 d) was 371.4 mm. When this is extended computationally for the duration of 1 yr, 461.1 mm is obtained. This is only 70.5% of the 31-yr average annual precipitation (654 mm) as derived from the Hannover airport reference station data. Therefore, we rated conditions during the calibration period as comparatively dry. When correction percentages according to Richter (1995) were added to precipitation as measured at the lysimeter, a total of 442.5 mm was obtained for the calibration period, or 549.4 mm for 1 yr. Potential

evaporation, as calculated with Eq.[4.9], was 483.3 mm during the calibration period. The closest agreement between measured and calculated cumulative discharge during "forward" runs of the HYDRUS-1D model was obtained when actual evaporation from the bare lysimeter surfaces was calculated with Eq.[4.16], using values of 1.82 and 0.8 for β for ALRP-FGDP and ALRP, respectively. With these values, calculated actual evaporation at the end of the calibration period added up to 351.3 mm for ALRP-FGDP and 234.3 mm for ALRP. Computational extension for the duration of 1 yr resulted in 436.1 mm for ALRP-FGDP and 290.8 mm for ALRP. These values compare reasonably well with values that we derived for our lysimeters with a bookkeeper's approach in an earlier paper (Hermsmeyer et al., 2001b). From that approach, average annual evaporation was 425.4 mm for ALRP-FGDP and 337.5 mm for ALRP.

In Fig. 4.3, the day of sowing the lysimeters with ryegrass (16 Mar. 2000) is indicated. Four to five weeks after sowing (i.e., after a period of germination and early growth), the slope of the cumulative actual evaporation curve for both materials increased significantly. This indicates that actual evaporation for the remainder of the calibration period mainly resulted from root water uptake and transpiration, rather than from evaporation from a bare surface.

Figure 4.4 depicts a comparison between measured and calculated cumulative discharge from ALRP-FGDP and from ALRP during the calibration period. Measured discharge totaled 132.9 mm from ALRP-FGDP and 202.9 mm from ALRP. With respect to evaluating the efficiency of the materials as a soil-substitute in surface barrier construction, it is important to note that the amount of seepage collected from the mix was 70 mm less than that from ALRP. This makes ALRP-FGDP the better material for surface barrier construction. For both materials, we obtained a fairly close agreement between measured and calculated discharge when α was inversely estimated with Eq.[4.8] for the eight depths of each material. The calendar date of the first occurrence of discharge, the date when discharge ceased, and the outflow rates during the calibration period were all calculated with sufficient accuracy. For ALRP-FGDP, the regression coefficient (R^2) between calculated and measured data was 0.9878, and the mass balance error was 0.268%. For ALRP, R^2 was 0.9959, and the mass balance error was 0.276%. It is a characteristic feature of the weighted least squares approach of the objective function (Eq.[4.8]) that calculated values undulate around measured values, which were input data to Eq.[4.8].
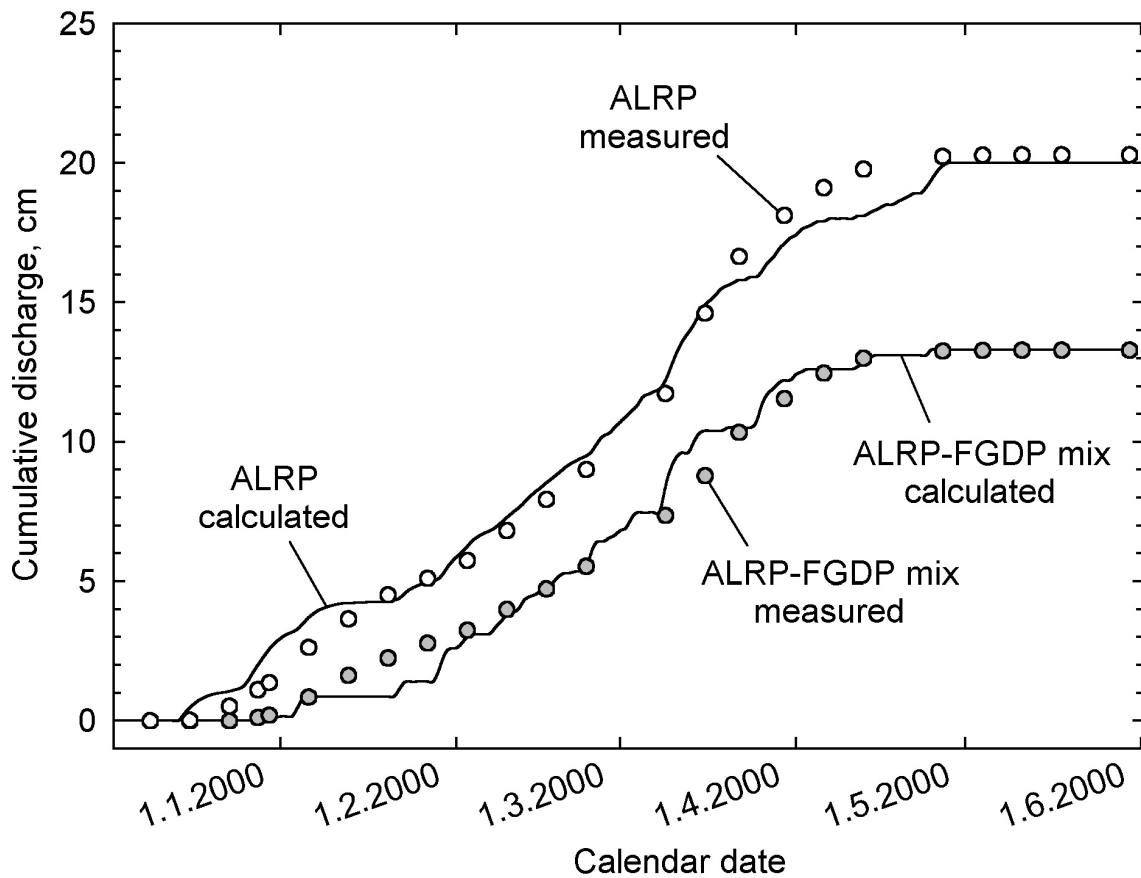
Fig. 4.4 *Measured and calculated values of cumulative discharge from ALRP-FGDP and from ALRP for the calibration period.*

In total, ALRP-FGDP lost more water by evaporation and discharge (484.2 mm) during the calibration period than ALRP (437.2 mm). The difference (47 mm), however, is small when expressed in terms of difference in water content of the entire soil profile. With respect to a profile length of 1.63 m, it accounts for only 2.8%. For comparison, measured values of water content at the end of the calibration period from Table 4.2 can be used. Average volumetric water content, weighted by the thickness of each layer as listed in Table 4.3, was 0.307 m^3 m^{-3} for ALRP-FGDP and 0.322 m^3 m^{-3} for ALRP.

Longterm atmospheric boundary conditions and model simulation results are shown in Fig. 4.5. Precipitation at the Hannover airport reference station totaled 24,319 mm in 11,627 d, or 763.6 mm per yr after correction percentages of Richter (1995) were added to the measured data. Potential evaporation as calculated with Eq.[4.9] added up to 18,730 mm, or 588 mm annually.
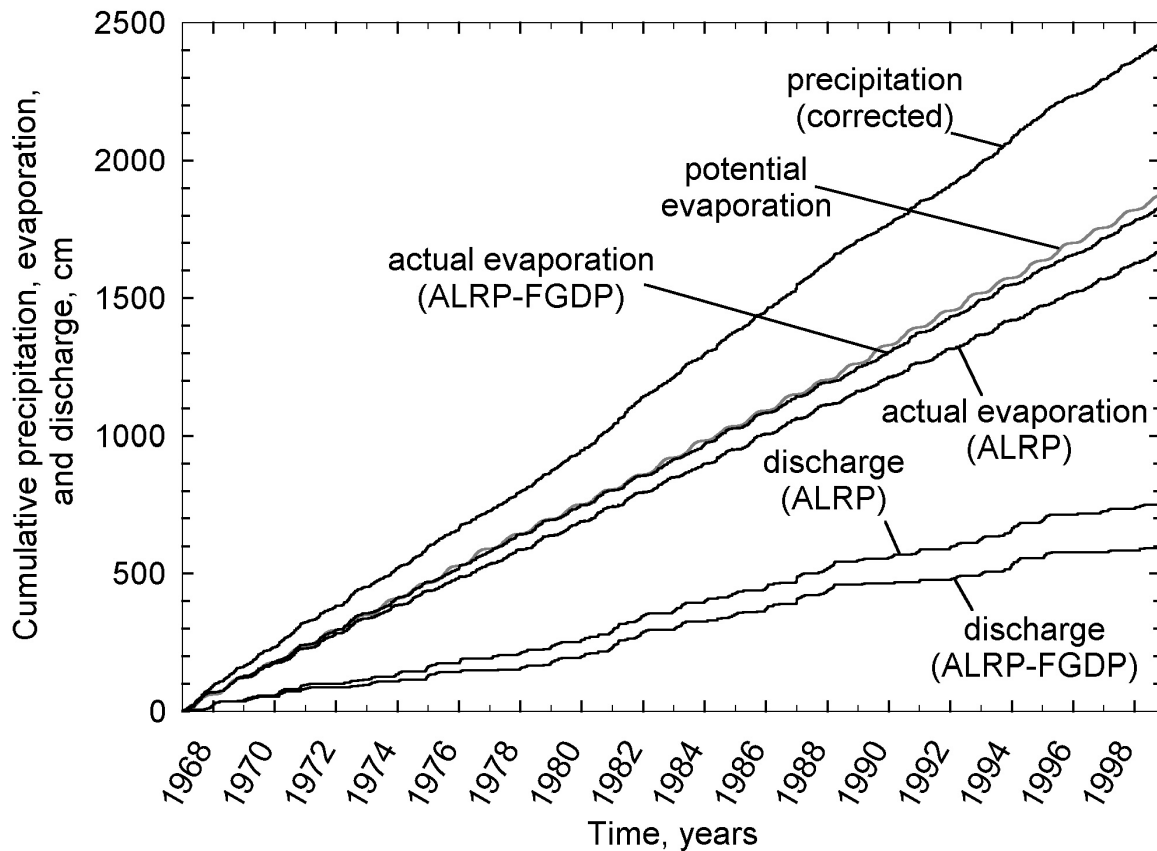
Fig. 4.5 *Atmospheric boundary conditions and cumulative discharge from ALRP-FGDP mix and from ALRP during the longterm simulation period.*

This is in close agreement with numbers given by Keller (1978), who derived values of average annual Penman-evaporation from 550 to 600 mm for our lysimeter site from weather records of the period 1951 to 1965. The seasonal variation in potential evaporation is reflected by the oscillation of the cumulative evaporation curve (Fig. 4.5). Because of high energy input, potential evaporation was considerably higher during summer than in winter.

Discharge calculated with Eq.[4.1], and with hydraulic parameters as listed in Table 4.3 (α from the HYDRUS-1D inverse approach), was 5,940 mm over 31 yr for ALRP-FGDP, or 186 mm annually. For ALRP, it was 7,540 mm, or 237 mm yearly. For ALRP-FGDP, discharge was 24.4% of longterm average annual (corrected) precipitation, for ALRP it was 31.0%.

During the period of calibration, the discharge collected from ALRP-FGDP was 65.5% of the discharge from ALRP. For the longterm simulation results, however, average annual discharge from the mix was 78.5% of that from ALRP. The difference can be attributed to the fact that lysimeter surfaces were bare during most of the calibration period, but were assumed to be covered with grass during the longterm simulation period. It thus appears that the impact of differences in hydraulic properties between materials on actual evaporation is less pronounced when evaporation is due mainly to plant root water uptake and transpiration rather than to evaporation from a bare surface (during longterm simulation, equal root distribution was assumed for both materials).

During the calibration period (11 Aug. 1999 to 31 May 2000), discharge occurred in the winter and ceased in spring. It is unlikely that more discharge would have been measured during the rest of the summer (i.e., from 1 Jun. to 10 Aug. 2000). It is therefore assumed that total discharge during the period of calibration (133 mm from ALRP-FGDP and 203 mm from ALRP) was equal to the discharge of the whole year. Surprisingly, longterm average annual discharge as calculated for the lysimeters covered with grass was higher than the discharge for the calibration year, although lysimeter surfaces were bare during most of the calibration period. This is explained by the fact that precipitation was about 30% lower during the calibration period than the longterm annual average.

It can be assumed that the difference in water content in the lysimeters between the first and the last day of the longterm simulation period was small as compared with total precipitation and evaporation during that period. Therefore, assuming that there was no runoff, daily values of actual evaporation can be calculated as the difference between precipitation and discharge. For ALRP-FGDP, actual evaporation thus estimated added up to 18,379 mm during 11,627 d, or 577 mm annually. Respective values for ALRP were 16,779 mm and 527 mm. When average annual values of actual evaporation are compared with potential evaporation, differences of 11 mm (ALRP-FGDP) and 61 mm (ALRP) are obtained. Again, these results can be compared with numbers given by Keller (1978). According to Keller, the average annual difference between potential (Penman-) evaporation and actual evaporation is about 50 mm for the site of our experiment, independent of the soil material.

Calculated longterm actual evaporation from ALRP-FGDP is close to potential (or maximum) evaporation (Fig. 4.5). Therefore, further reduction of seepage from an ALRP-FGDP surface barrier into the underlying mine waste, e.g. by replacing ALRP-FGDP with a material of higher field capacity, by

increasing the thickness of the surface barrier, or by applying plants with roots growing deeper than 0.4 to 0.5 m (the value we used in longterm simulation) seems hardly possible. Further reduction of water flow into the waste material could, however, be achieved by introducing a drainage layer into a sloping surface barrier to convey seepage water laterally, e.g. into a ditch.

Salt Concentration Effects

Unweathered ALRP and ALRP-FGDP have high salt (NaCl) contents of approximately 45% and 35%, respectively. But, in the theory we applied to describe water flow and evaporation, possible effects of high salinity are not accounted for. In the following discussion we explain why the Richards equation and the drying-stage concept of reducing potential (Penman-) evaporation are applicable to the conditions of our lysimeter experiment, in spite of high salinity.

Effects of Salt Concentration on Evaporation

Effects of high salt content in the soil matrix and in the soil solution on evaporation rates have been discussed in the literature. The decreasing effect of a salt crust on Ea under arid conditions has been studied both in the laboratory (Qayyum and Kemper, 1962) and in the field (Malek et al., 1990). It is assumed that a salt crust (i) physically separates the atmospheric boundary layer from the soil surface beneath and (ii) has a high resistance to water vapor transfer. As a result, the flow of moisture to the surface of the crust becomes significantly lower than the evaporative demand of the atmosphere.

Effects of salt concentration on evaporation in the case when no closed salt crust exists have also been reported (Qayyum and Kemper, 1962; Letey et al., 1969; Nassar and Horton, 1999). Results of such studies are controversial. Qayyum and Kemper (1962) found that mean daily loss of moisture from soil cores with low salt concentrations (0.4 wt.% NaCl mixed into the upper 0.1 m of 0.29-m-long columns) was 168% (2.7 mm) of that from columns with no salt treatment (1.9 mm) under equal atmospheric conditions. They attributed these results to concentration-gradient-induced diffusion, helping to move additional water to the surface. This prevented the surface from drying to depths as great as those observed with the salt-free control and thus supplied water to fulfill the evaporative demand of the atmosphere.

Opposite results of a decreased evaporation from saltwater systems compared with salt-free systems have also been reported. This is true for both open water surfaces (Turk, 1970; Salhorta et al., 1985) and laboratory soil columns (Nassar and Horton, 1999). Over an open saltwater surface, the saturation vapor pressure of the air decreases approximately proportionally to the increase of the density of the salt solution. Therefore, the saturation deficit of the air is lower over a saltwater surface as compared with a freshwater surface at equal temperature. As a net effect, the rate of actual evaporation from a saltwater system is lower than that from a freshwater system under equal weather conditions. Nassar and Horton (1999) studied cumulative evaporation from open soil cores filled with salinized and nonsalinized clay and clay-loam soils. Initial KCl concentrations were 1.11 and 0.92 mol kg^{-1}, and initial water content ranged from 0.181 to 0.271 m^3 m^{-3}. Under all conditions, evaporation was lower from salinized than from nonsalinized soils. The ratio of cumulative evaporation for salinized soil to solute-free soil increased from 0.78 to 0.89 for the clay soil, and from 0.9 to 0.95 for the clay-loam soil over a period of 14 d.

But when evaluating possible effects of salt concentrations on Ea in our study, it must be kept in mind that we operated lysimeters under humid field conditions. A closed salt crust at the soil surface was observed at no time during the calibration period. Typically, rates of Ea were highest on days with high values of Ep, after significant rainfall events, i.e. from a wet soil surface on warm, sunny, and windy days. Because of the high water content, the salt concentration of the near-surface soil water presumably was low during early evaporation stages under such conditions. As water evaporated, the salt concentration of the remaining solution gradually rose. Because of drying of the surface soil layer, the effect of a rising salt concentration on Ea may have increased, but the rate of Ea decreased as a result of depletion of water. Therefore, the error introduced when calculating daily values of Ea without taking salt concentrations into account should be small under humid field conditions. Also, with continued desalinization, near-surface salt concentrations decreased in the course of our experiment. Therefore, we did not modify the results of Eq.[16] to account for possible effects of salt concentrations on Ea.

Effects of Salt Concentration on Water Movement

High salinity may also affect water movement in variably saturated porous media. In the course of our experiment, near-surface layers of ALRP and ALRP-FGDP were desalinized by leaching. Low salt concentrations in the upper part of our lysimeters and high concentrations near the bottom existed simultaneously. Consequently, an osmotic pressure gradient may have built up.

The effect of osmotic pressure gradients on water movement in unsaturated soils has been discussed, e.g. by Letey (1968), Letey et al. (1969), and Bresler et al. (1982). To describe the one-dimensional volume of solution flux Q_v, Letey (1968) used the following equation:

$$Q_v = -K_S \frac{\partial P}{\partial z} + K_D \frac{\partial \pi}{\partial z} - K_q \frac{\partial T}{\partial z} \qquad [4.18]$$

where $\partial P/\partial z$, $\partial \pi/\partial z$, and $\partial T/\partial z$ denote the driving forces or gradients of solution flux resulting from water potential, or pressure P, osmotic pressure π, and temperature T, respectively. The symbols K_s, K_D, and K_q denote empirical coefficients describing material properties. Under uniform salt and temperature conditions, Eq.[4.18] reduces to the Darcy equation, and the coefficient K_s represents the hydraulic conductivity. It should be noted that Eq.[4.18] describes horizontal flow under steady-state conditions. For vertical flow, a gravitational component must be added to P.

For a system at uniform temperature, Letey (1968) introduced an osmotic efficiency coefficient σ and reduced Eq.[4.18] to

$$Q_v = K_S \left(-\frac{\partial P}{\partial z} + \sigma \frac{\partial \pi}{\partial z} \right) \qquad [4.19]$$

It is obvious that the coefficient σ is equal to K_D / K_s. According to Letey (1968), the theoretical range of σ is from 0 to 1. In case $K_D = 0$, σ will be equal to zero, i.e., salt concentration gradients will cause no water flow. When K_D is equal to K_s, σ will be equal to one and the osmotic pressure gradient is as effective in causing water to flow as the pressure gradient. The magnitude of σ depends upon the differential restriction of the solute relative to the solvent by a

membrane (Kemper and Evans, 1963). Complete restriction of the solute by a membrane would result in $\sigma = 1$. Kemper and Rollins (1966) studied the effect of average salt concentration, calcium as opposed to sodium, and chloride as opposed to sulfate, on the magnitude of σ for clays at different water contents. They found that σ was increased by decreasing the average solution concentration, saturating the clay with monovalent rather than divalent cations, using divalent rather than monovalent anions, and decreasing the water content of the clay. All of these factors are in agreement with the fact that σ is larger under conditions in which movement of the solute is restricted relative to that of the solvent.

It has been shown, however, that little water flows in response to an osmotic pressure gradient, especially at low suctions (Abd-El-Aziz and Taylor, 1965; Letey et al., 1969). At higher suctions, the amount of water moving in response to an osmotic pressure gradient is still low and becomes only relatively large when compared with the amount that moves due to a pressure gradient. Letey (1968) suggested that an approximate value of σ at soil water suctions of 2.54 to 10.19 m is about 0.03 and that σ can be assumed equal to zero at still lower suctions.

In the present study on the longterm performance of a surface barrier constructed from ALRP-FGDP mix or ALRP, we were interested in the absolute magnitude of water flow rather than the relative amounts of water flow caused by pressure and osmotic gradients. Therefore, it seemed appropriate to ignore salt concentration effects on water flow for the conditions in our lysimeter experiment.

4.5 Conclusions

The numerical model of water flow in variably saturated rigid porous media based on the Richards equation (Eq.[4.1]) adequately described cumulative lysimeter discharge from ALRP-FGDP and from ALRP during the calibration period. Predicted values of average annual potential evaporation and of actual evaporation from longterm simulations were similar to values given in the literature (Keller, 1978) for the site of our lysimeter experiment. Our discussion of the literature results on the effects of high salt concentrations on evaporation and on water flow through soil revealed that such effects are likely to be minor under humid conditions. Therefore, we conclude that application of the Richards equation (Eq.[4.1]) to water flow, of the Penman equation (Eq.[4.9]) to potential evaporation, and of the drying-stage method (Eq.[4.16])

to actual evaporation is a useful approach toward describing the water balance of lysimeters filled with initially highly saline ALRP and ALRP-FGDP – even though the applied models ignore possible effects of salt concentration.

Because discharge during the calibration period was considerably lower from ALRP-FGDP than from ALRP, we further conclude that ALRP-FGDP is the better material to be used as soil substitute in surface barrier construction. From longterm simulation results we calculated that actual evaporation from the mix annually is only 11 mm short of potential evaporation when the material is covered with grass and the root growth is dense to 40 or 50 cm below the surface. We therefore expect that the use of ALRP-FGDP in constructing a surface barrier over mine waste of the Sigmundshall potash mine will effectively reduce seepage water flow into the mine tailings. From a hydrological point of view, the use of ALRP-FGDP in surface barrier construction thus can be recommended. In view of the metallurgical origin of ALRP, however, it seems necessary to also evaluate other than hydrological parameters. For example, heavy metal concentrations and soil mechanical parameters of ALRP and ALRP-FGDP should be examined.

4.6 References

Abd-El-Aziz, M.H., and S.A. Taylor. 1965. Simultaneous flow of water and salt through unsaturated porous media. I. Rate equations. Soil Sci. Soc. Am. Proc. 29:141-143.

Ångstrom, A. 1924. Report to the International Commission for Solar Research on actinometric investigations of solar and atmospheric radiation. Quart. J. Roy. Met. Soc. 50:121-125.

Black, J.N., C.W. Bonython, and J.A. Prescott. 1954. Solar radiation and the duration of sunshine. Quart. J. Roy. Met. Soc. 80:231-235.

Black, T.A., W.R. Gardner, and G.W. Thurtell. 1969. The prediction of evaporation, drainage, and soil water storage for a bare soil. Soil Sci. Soc. Am. Proc. 33:655-660.

Blake, G.R., and K.H. Hartge. 1986. Bulk density. p. 363-376. *In* A. Klute (ed.) Methods of soil analysis. Part 1, 2nd ed. ASA and SSSA, Madison, WI.

Bresler, E., B.L. McNeal, and D.L. Carter. 1982. Saline and sodic soils. Principles-Dynamics-Modeling. Springer-Verlag, Berlin.

Deutscher Verband für Wasserwirtschaft und Kulturbau e.V. (DVWK) 1996. Determination of evaporation from land and water surfaces. Merkblätter zur Wasserwirtschaft 238. Kommissionsvertrieb Wirtschafts- und Verlagsgesellschaft Gas und Wasser mbH, Bonn, Germany (in German).

Feddes, R.A., P.J. Kowalik, and H. Zaradny. 1978. Simulation of field water use and crop yield. PUDOC, Wageningen, the Netherlands.

Gee, G.W., D.G. Felmy, J.C. Ritter, M.D. Campbell, J.L. Downs, M.J. Fayer, R.R. Kirkham, and S.O. Link. 1993. Field lysimeter test facility status report IV: fiscal year 1993. Prepared for the U.S. Department of Energy, contract DE-AC06-76RLO 1830. Pacific Nothwest Laboratory. Richland, WA.

Häckel, H. 1990. Meteorology. Eugen Ulmer Pub. Co. Stuttgart, Germany (in German).

Hermsmeyer, D., R. Diekmann, R.R. van der Ploeg, and R. Horton. 2001a. Physical properties of a soil substitute derived from an aluminum recycling by-product. Manuscript submitted for publication.

Hermsmeyer, D., J. Ilsemann, R.R. van der Ploeg, and R. Horton. 2001b. Lysimeter study of water flow and solute transport in a metallurgical waste: I. Construction, operation, and data acquisition. Manuscript submitted for publication.

Idso, S.B., R.J. Reginato, R.D. Jackson, B.A. Kimball, and F.S. Nakayama. 1974. The three stages of drying of a field soil. Soil Sci. Soc. Am. Proc. 38:831-836.

Jury, W.A., W.R. Gardner, and W.H. Gardner. 1991. Soil physics. 5th ed. John Wiley and Sons, New York.

Keller, R. (ed.) 1978. Hydrological atlas of the Federal Republic of Germany. Harald Boldt Pub. Co., Boppard, Germany (in German).

Kemper, W.D., and N.A. Evans. 1963. Movement of water as affected by free energy and pressure gradients. Soil Sci. Soc. Am. Proc. 27:485-490.

Kemper W.D., and J.B. Rollins. 1966. Osmotic efficiency coefficients across compacted clays. Soil Sci. Soc. Am. Proc. 30:529-534.

Kimball, H.H. 1927. Measurements of solar radiation intensity and determination of its depletion by the atmosphere. Month. Weath. Rev. 55:155-169.

Klute, A., and C. Dirksen. 1986. Hydraulic conductivity and diffusivity. p. 687-734. *In* A. Klute (ed.) Methods of soil analysis. Part 1. 2nd ed. ASA and SSSA, Madison, WI.

Koitzsch, R., M. Dzingel, and U. Wendling. 1990. The dependency of the radiation balance and soil heat flux on global radiation during daylight hours. Z. Meteorol. 40:205-208 (in German).

Letey, J. 1968. Movement of water through soil as influenced by osmotic pressure and temperature gradients. Hilgardia 39:405-418.

Letey, J., W.D. Kemper, and L. Noonan. 1969. The effect of osmotic pressure gradients on water movement in unsaturated soil. Soil Sci. Soc. Amer. Proc. 33:15-18.

Malek, E., G.E. Bingham, and G.D. McCurdy. 1990. Evapotranspiration from the margin and moist playa of a closed desert valley. J. Hydrol. 120:15-34.

Marquardt, D.W. 1963. An algorithm for least-squares estimation of nonlinear parameters. SIAM J. Appl. Math., 11:431-441.

Nassar, I.N., and R. Horton. 1999. Salinity and compaction effects on soil water evaporation and water and solute distributions. Soil Sci. Soc. Am. J. 63:752-758.

Palz, W., and J. Greif. 1996. European solar radiation atlas. Solar radiation on horizontal and inclined surfaces. 3rd ed. Springer Verlag, Berlin.

Penman, H.L. 1948. Natural evaporation from open water, bare soil and grass. Proc. Roy. Meteorol. Soc. A. 193:120-145.

Qayyum, M.A., and W.D. Kemper. 1962. Salt-concentration gradients in soils and their effects on moisture movement and evaporation. Soil Sci. 93:333-342.

Richter, D. 1995. Results of methodological studies to correct the systematic measurement error of the Hellmann rain gauge. Reports of the German Weather Bureau, No. 194. Deutscher Wetterdienst DWD, Offenbach, Germany (in German).

Ritchie, J.T. 1972. Model for predicting evaporation from a row crop with incomplete cover. Water Resour. Res. 8:1204-1213.

Salhorta, A.M., E.E. Adams, and D.R.F. Harleman. 1985. Effect of salinity and ionic composition on evaporation: Analysis of Dead Sea evaporation pans. Water Resour. Res. 21:1336-1344.

Schaap, M.G. 1999. Rosetta Version 1.0. U.S. Salinity Laboratory ARS-USDA. 450 W. Big Springs Road, Riverside, CA.

Schroeder, P.R., T.S. Dozier, P.A. Zappi, B.M. McEnroe, J.W. Sjostrom, and R.L. Peyton. 1994. The hydrologic evaluation of landfill performance (HELP) model: Engineering documentation for version 3. EPA/600/R-94/168b. U.S. Environmental Protection Agency. Office of Research and Development, Washington, D.C.

Shouse, P., W.A. Jury, L.H. Stolzy, and S. Dasberg. 1982. Field measurement and modeling of cowpea water use and yield under stressed and well-watered growth conditions. Hilgardia. 50:1-25.

Šimunek, J., M. Šejna, and M.Th. van Genuchten. 1998. The HYDRUS-1D software package for simulating the one-dimensional movement of water, heat, and multiple solutes in variably-saturated media. Version 2.0. U.S. Salinity Laboratory, Agricultural Research Service, U.S. Dept. of Agriculture, Riverside, CA.

Šimunek, J., M. Šejna, and M.Th. van Genuchten. 1999. The HYDRUS-2D software package for simulating the two-dimensional movement of water, heat, and multiple solutes in variably-saturated media. Version 2.0. U.S. Salinity Laboratory, Agricultural Research Service, U.S. Dept. of Agriculture, Riverside, CA.

Sonntag, D. 1994. Advancements in the field of hygrometry. Meteorol. Zeitschrift. N.F. 3:51-66.

Swift, L.W. 1976. Algorithm for solar radiation on mountain slopes. Water Resour. Res. 12:108-112.

Turk, L.J. 1970. Evaporation of brine: a field study on the Bonneville Salt Flats, Utah. Water Resour. Res. 6:1209-1215.

Unsaturated Soils Group. 1997. SoilCover Version 4.01. Department of Civil Engineering, University of Saskatchewan. Saskatoon, Canada.

van Genuchten, M.Th. 1980. A closed-form equation for predicting the hydraulic conductivity of unsaturated soils. Soil Sci. Soc. Am. J. 44:892-898.

Zaradny, H., and R.R. van der Ploeg. 1982. Calculation of the shortwave radiation flux from weather station data in evapotranspiration studies. Z. Pflanzenernaehr. Bodenk. 145:611-622.

5. Spatial and Temporal Variation of Solar Radiation and Potential Evaporation

5.1 Abstract

The spatial and temporal gradient of solar insolation is large across the surface of the Earth. Solar radiation data is needed in evaporation studies, but to monitor radiation with high spatial resolution is not feasible. This study was conducted to compute global radiation and potential evaporation across the surface of a potash mine tailings mound in northern Germany. Commercially available GIS computer software was extended to calculate global radiation from geographical location, slope steepness, orientation, cloud coverage, and visibility for every cell of a grid digital elevation model. Potential evaporation was estimated from the Priestley and Taylor equation. Radiation and temperature were measured in three positions around the mound and radiation was compared to computed data. The model adequately described *daily* values of global radiation in all three positions. Values of *hourly* global radiation were also well described when clouds covered 50% of the sky or less, but were often underestimated at more cloudy skies. Daily potential evaporation as calculated from radiation and temperature measured around the mound compared reasonably to evaporation from calculated radiation and air temperature measured at a reference station. Three-year average annual potential evaporation was calculated from daily values, and was mapped across the mound surface. Values ranged from 415 mm on north slopes to 745 mm on south slopes, and were 663 mm in unshaded horizontal positions. Three-year average evaporation was higher than the 30-yr average for the area, and so was temperature. Constructing large south slopes and small north slopes during future extensions of the mound may effectively enhance evaporation and reduce briny discharge.

5.2 Introduction

Solar radiation is the primary source of energy for environmental heating, evaporation and plant growth (Geiger, 1965; Gates, 1980; Dubayah and Rich, 1995). Because of its impact on evapotranspiration, solar radiation is a key component in the climatology of the Earth. Time of year, time of day, clouds, visibility, and topography (surface orientation and shadows cast by topographic features) are the major modulators of solar radiation at the surface (Gates, 1980), and often create large local gradients of insolation. To a large extent

evapotranspiration is driven by solar radiation, and is therefore also subject to such gradients. For most geographic locations, insolation measurements are not available. Simple areal interpolation of measurements taken at individual points, e.g. at weather stations, is not meaningful because many locations are affected by strong local variation. Accurate maps of insolation would require a dense monitoring network, should they solely be derived from measurements. This is not feasible because of high cost. In contrast, solar radiation models provide a cost-efficient means to understand the spatial and temporal variation of insolation and its impact on evapotranspiration and water balance.

Numerous studies have been conducted in ecology, agriculture, soil science, hydrology, architecture, design, urban planning, solar engineering, and other disciplines to assess components of solar radiation. Ångstrom (1924) provided an empirical equation to derive the daily surface shortwave radiation flux for a horizontal surface. Hutchinson et al. (1984), and Palz and Greif (1995) used the Ångstrom equation to derive solar radiation maps for Australia and Europe, respectively. Zaradny and van der Ploeg (1982) used the Ångstrom approach to provide shortwave radiation flux data for evapotranspiration studies. More spatial models of solar radiation have also been developed. Swift (1976) published a generalized algorithm providing the daily total of solar radiation for a point on any sloping surface at any latitude. However, this algorithm does not take into account shadows cast by topographic features surrounding the point of interest. Horton et al. (1984), in a study on soil temperature in a row crop with incomplete surface cover, developed an algorithm to track the shadow cast by plants of simplified (hexagonal) shape. Iqbal (1983), as well as Duffie and Beckman (1991) supplied textbooks to assess many problems of solar radiation, including solar radiation under cloudy skies. Brinsfield et al. (1984) also included cloud cover effects in their model to predict solar radiation on a horizontal surface. The German Association of Engineers (VDI, 1994) provided a compilation of equations to determine shortwave radiation from the orientation of the Earth relative to the Sun, the orientation of the point of interest on any slope, shadows cast by topographic features, cloud coverage, and visibility. Cloud coverage and visibility data are routinely recorded at many airfields.

Following the advance of new generation computers, models to compute solar radiation incident upon complex topographic surfaces have been developed. Resulting computer programs often are add-ons to geographic information systems (GIS) and require as user input a raster-based array (or grid) of surface elevation data (i.e., a digital elevation model, DEM). Dozier (1980) combined a clear-sky solar radiation model for direct and diffuse fluxes

with topographic calculations from digital terrain data to compute incident, reflected, and net radiation at any point on a snow surface in mountainous terrain. Dubayah (1994) developed a model to describe the spatial variability of solar radiation across the landscape based on an image processing system provided by Frew (1990). With the program SolarFlux (Rich et al., 1995), total direct radiation, duration of direct sunlight, total diffuse radiation, and a skyview factor for every cell in a grid, as well as hemispherical viewsheds of sky obstruction for specified surface locations can be calculated. SolarFlux calculations are based on surface orientation, solar angle, shadowing due to topographic features, and atmospheric attenuation. Other models, that essentially provide similar functionality, but may differ from the SolarFlux model in flexibility, convenience of data input, or the general (GIS) software environment of implementation, are the models TopoView (Fu and Rich, 1999), and SolarAnalyst (Fu and Rich, 2000). Venebrügge (1996) as well as Kumar et al. (1997) also presented models to compute solar radiation over a large area with use of commercially available GIS.

One hydrological application of models describing the heterogeneity of solar radiation across a landscape and potential evaporation resulting hereof is the water balance of engineered infiltration barriers over disposed waste or mine tailings. Solid waste materials are often piled up in mounds of complex topography, and are covered with surface barriers constructed from soil, or soil-like materials. To assess the amount of seepage from a surface barrier into underlying waste material, numerical hydrologic models are often used (Wilson et al., 1995; Hermsmeyer et al., 2001b). Potential evaporation is a parameter frequently needed in hydrologic models. For example in the model SoilCover (Unsaturated Soils Group, 1997), daily net radiant energy available at the surface is required (besides other parameters) as input data to calculate the daily soil evaporative flux. The HYDRUS-1D (Šimunek et al., 1998) and HYDRUS-2D (Šimunek et al., 1999) models require evaporation and transpiration data to be calculated previously to using these models in order to accomplish proper atmospheric coupling of the soil water balance (Hermsmeyer et al., 2001b).

A common approach for describing potential evaporation is the combined energy balance and aerodynamic concept, first proposed by Penman (1948). Priestley and Taylor (1972) published an empirically derived simplification of the Penman equation. With use of the Priestley and Taylor equation, potential evaporation can be estimated from energy balance (i.e., from radiation and temperature data) alone, and wind speed is not needed. When a grid of local radiation values (i.e. an insolation map) is used as input data to a GIS-embedded

algorithm to solve the Pristley and Taylor equation, a map of potential evaporation across the landscape can be derived.

In the present study, the spatial variation of potential evaporation from the surface of the tailings mound of the Sigmundshall potash mine near Hannover, Germany, is investigated. The mine and waste mound are operated by the K+S Company (Kali und Salz GmbH). The waste mound (at 9°21' latitude and 52°25' longitude) is currently about 160 m high (120 m above the surrounding terrain), has steep (about 35°) slopes facing all compass directions, and contains about 13.4 million m^3 of about 96% NaCl and 4% of mostly clay sized (< 0.002 mm) impurities (K+S, personal communication).

The purpose of this study was (i) to calculate maps of daily totals of hourly global radiation for a DEM of the Sigmundshall mine tailings mound from time of year, time of day, and data of cloud coverage and visibility (ii) to compare daily values of global radiation computed for individual grid cells of different orientation to data measured at corresponding locations with a tilted global radiation sensor, and (iii) to utilize the maps of daily solar radiation to derive maps of (Priestley and Taylor) potential evaporation. The approach provided by VDI (1994) was followed to calculate radiation. The radiation and evaporation model developed in the present study may be useful in other hydrological studies, or other applications of solar radiation in cases where cloud coverage, visibility, and temperature data are available.

5.3 Materials and Methods

Field Measurements

On the Sigmundshall potash mine tailings mound, we operated during three consecutive years in a different location each year, a CNR-1 net radiometer (Kipp & Zonen B.V., Delft, the Netherlands), as well as a thermocouple to record air temperature in a Young radiation screen. The radiometer was supplied with two CM3 pyranometers to record shortwave radiation (305 to 2800 nm) and with two CG3 pyrgeometers to record longwave or infrared radiation (5000 to 50000 nm). On the CNR-1, two sensors are faced upwards ('upper sensors', one CM3 and one CG3), and the other two sensors are faced downwards ('lower sensors'). In all three locations on the mound, we installed sensors in 2 m above the ground and tilted the radiometer to angles equal to local slope steepness in order to take measurements of radiation perpendicular to the mound surface. Readings were repeated once per minute,

and an automated data logger was set to store hourly average, minimum, and maximum values.

From 17 Jun. 1997 to 18 Jun. 1998, we took measurements over the south-southeast oriented slope of the mound. We operated the radiometer at an aspect of 160° (measured clockwise from north) tilted to a slope of 35° (south position). From 19 Jun. 1998 to 8 Jul. 1999, we took measurements over the north-northwest oriented slope, and operated the radiometer at an aspect of 350° and a slope of 34° (north position). To block direct beam solar radiation from the lower sensors, we mounted a radiation screen to the radiometer in the north position. In both the north and the south position, the surface of the tailings mound was bare because of high salt content. During the third year, i.e. from 11 Aug. 1999 to 30 May 2000, we operated the radiometer in a horizontal position over the surface of a lysimeter installation about 15 m to the south of the tailings mound. Lysimeters were filled with materials proposed as a soil substitute for the infiltration barrier over the Sigmundshall mine waste mound. Lysimeter surfaces were initially bare, but were sown with ryegrass (*Lolium perenne*, L.) on 16 Mar. 2000. Details about the lysimeter study were reported in two earlier papers (Hermsmeyer et al., 2001a and b).

Because of technical problems with data storage in the logger, and because of recalibration of the global radiation sensor, we were not able to collect data from 13 Aug. 1998 to 2 Oct. 1998 in the north position.

Reference Weather Station Data

Values of cloud cover (in eighths of sky obstruction), visibility (in m), and temperature are needed as input data to the radiation model used in the present study (see section below titled "Global Radiation"). In Germany, such data are routinely recorded on an hourly basis at many airfields and are available from the German Weather Bureau (Offenbach, Germany) upon request. For the present paper, hourly data from 17 Jun. 1997 to 30 May 2000 were used which were collected six km to the northeast of the Sigmundshall mine at the Wunstorf military airfield. The topography between the mine and airfield is little undulating, and we assumed general weather patterns to be identical at the airfield and the mine.

DEM and GIS Software Environment

Stereopairs of standard aerial color positive transparencies (0.23 x 0.23 m^2) were used in a softcopy or digital approach to derive a DEM with a grid spacing (ground resolution) of 5 x 5 m^2 of the tailings mound and surrounding terrain. Details about DEM generation from aerial photographs can be taken from textbooks on photogrammetry (e.g. Konecny and Lehmann, 1984, or Lillesand und Kiefer, 1994). Technical details on methods and computer software applied to derive the DEM used in the present study were reported in an earlier paper (Fischer and Hermsmeyer, 1999). In Figs. 5.1 and 5.2, the orthophoto and DEM of the Sigmundshall mine waste mound resulting from digital processing of the aerial photographs are shown. The longest distance in east-western and in north-southern direction covered by the base of the mound is about 850 and 500 m, respectively.

The DEM was imported to ArcView GIS software (ESRI, 1998a), including the SpatialAnalyst extension to provide for capabilities to process data sets in grid format. Slope orientation, or aspect, and slope steepness are needed for every cell of the DEM as input data to the solar radiation model. The SpatialAnalyst requests "Derive Aspect" and "Derive Slope" were used to calculate grids of such values. Aspect is identified as the downslope direction of the maximum rate of change in elevation from each DEM cell to its neighbors. Values of the aspect grid are the compass directions of aspect. Slope is identified as the maximum rate of change in elevation from each cell to its neighbors. The output slope grid was calculated as degree of slope. The "Derive Slope" request fits a plane to the DEM values of a 3 x 3 cell neighborhood around the processing or center cell. The slope for the center cell is calculated from the 3 x 3 cell neighborhood using the average maximum technique (Burrough, 1986). It should be noted that the slope steepness of vertical and downwardly oriented surfaces (with a slope of $\geq 90°$, as for example overhanging rocks) cannot be determined with this technique. Also, in standard aerial photographs, such surfaces are faced away from the camera and therefore remain invisible. However, overhanging surfaces did not occur on the Sigmundshall waste mound.
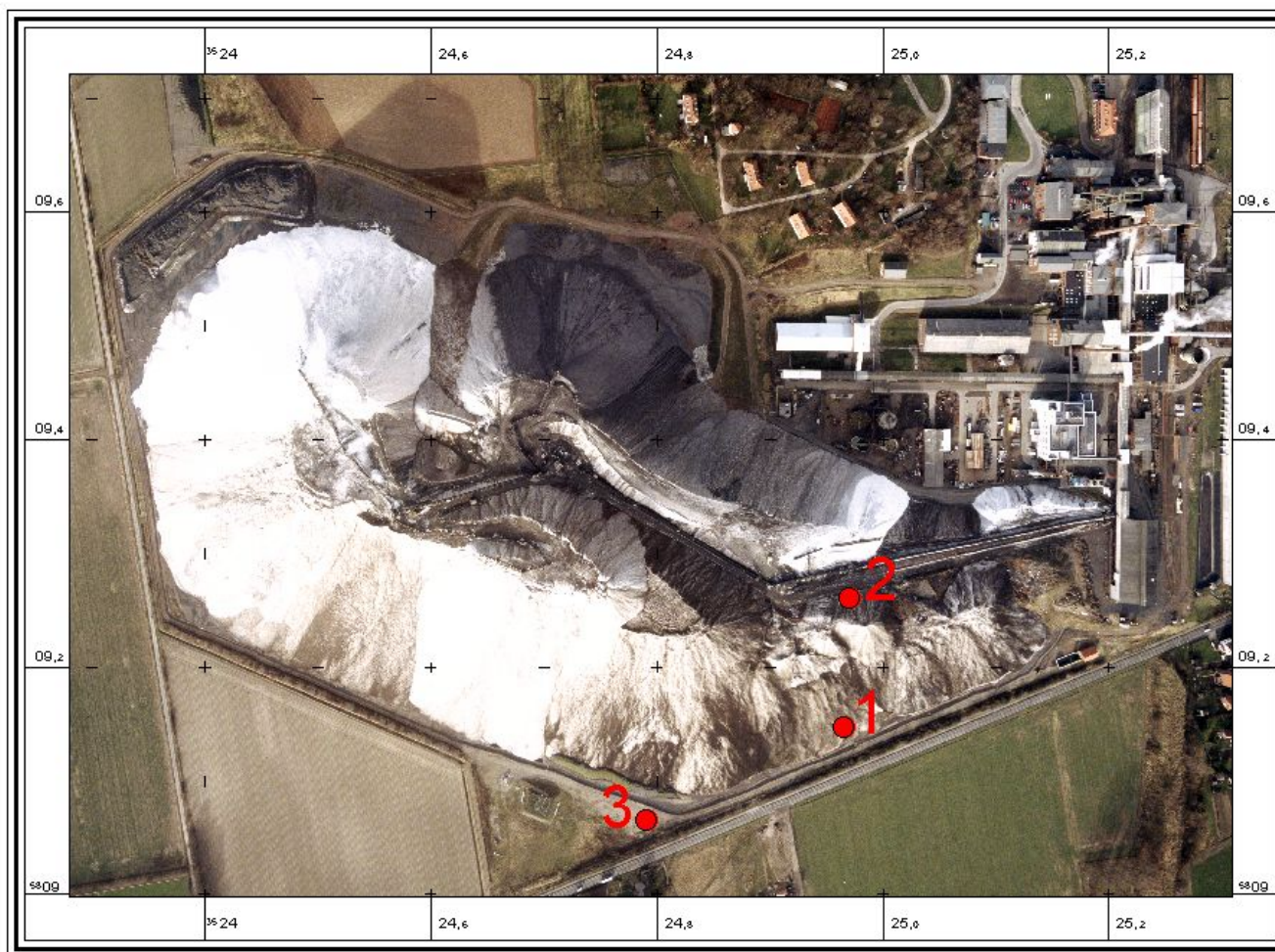
Fig. 5.1 *Orthophoto of the Sigmundshall mine waste mound. Red markers signify locations of radiation measurements on a south (1), north (2), and a horizontal slope (3). Distance between frame markers is 200 m, top is north.*

105
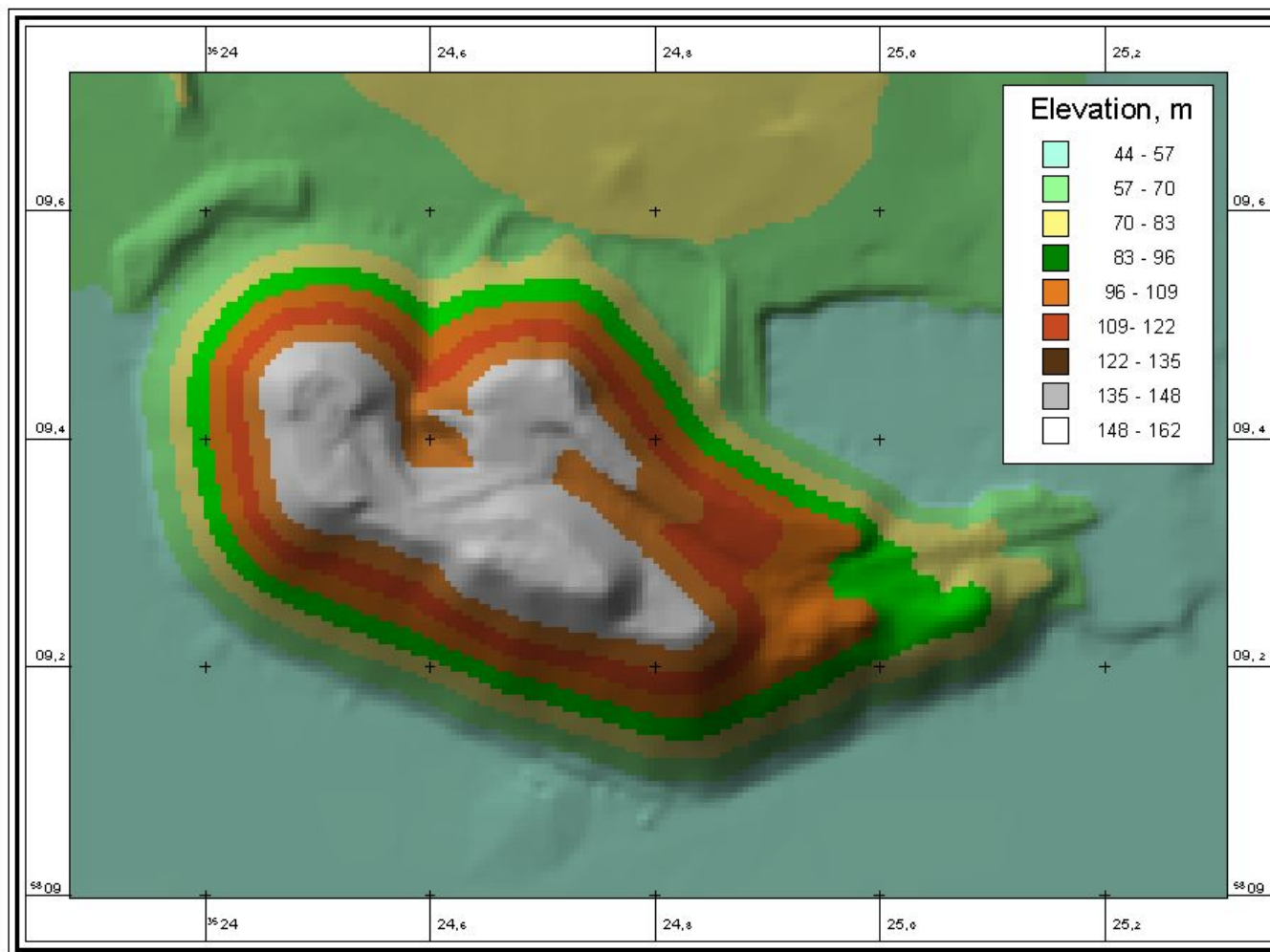
Fig. 5.2 *Digital elevation model (DEM) of the waste mound and surrounding terrain. Resolution: 5 x 5 m². Buildings and structures were excluded from DEM generation.*

106

Avenue object oriented programming language (ESRI, 1998b) was used to develop an extension to ArcView GIS to solve equations for direct, diffuse, global, and net shortwave radiation, as well as potential evaporation according to Priestley and Taylor (1972). The extension program reads hourly values of cloud coverage and visibility as measured at the reference weather station, and values of air temperature as measured around the Sigmundshall mound from a data base file. The model calculates evaporation and radiation components either for an individual point of user defined location and orientation, or for every cell of an input DEM within a user defined time span. Output from individual point calculations is tabulated in data base files. Values are readily comparable to measured values of global radiation. Output for a DEM is in grid format. In both the point and the grid mode, radiation results can be stored as hourly values (in W m^{-2}) and as daily integrals (in MJ m^{-2}). Output of potential evaporation across the landscape is in grid map format of daily totals (in mm). Details are described in the following sections.

Potential Evaporation

According to Penman (1948), values of daily potential evaporation (Ep, mm) can be calculated as the total of the evaporative demand of the atmosphere resulting from (i) the energy turnover at the surface in consideration, and (ii) wind speed and humidity of the atmosphere over that surface. In order to solve the Penman equation, values are needed of net radiation balance, soil heat flux, wind speed, air temperature, and humidity. In an effort to reduce the amount of input data required to estimate daily potential evaporation, Priestley and Taylor (1972) published the following, empirically derived simplification of the Penman equation:

$$\mathrm{Ep} = \alpha_{\mathrm{PT}} \ \frac{s}{s + \gamma_{\mathrm{P}}} \ \frac{Q - S}{L} \qquad\qquad [5.1]$$

In Eq.[5.1], α_{PT} is a constant which lumps the wind and humidity term of the Penman equation and has been proposed to equal 1.26 for agricultural crops (Priestley and Taylor, 1972). The quantity s (hPa K^{-1}) is the slope of the temperature-dependent saturation vapor pressure curve, which according to DVWK (1996) can be calculated as

$$s = \frac{\partial e_s}{\partial T} = e_s(T) \; \frac{4284}{(243.12 + T)^2} \qquad , \text{over water} \qquad [5.1a]$$

and as

$$s = \frac{\partial e_s}{\partial T} = e_s(T) \; \frac{6123}{(272.62 + T)^2} \qquad , \text{over ice} \qquad [5.1b]$$

where T is temperature (°C) and e_s is saturation vapor pressure (hPa). For the psychrometer constant γ_P, values of 0.655 and 0.576 hPa K^{-1} were used over water and ice, respectively (DVWK, 1996). The temperature dependent saturation vapor pressure e_s, was calculated as (see Sonntag, 1994)

$$e_s(T) = 6.11 \quad \exp\left(\frac{17.62 \, T}{243.12 + T}\right) \qquad , \text{over water} \qquad [5.1c]$$

and as

$$e_s(T) = 6.11 \quad \exp\left(\frac{22.46 \, T}{272.62 + T}\right) \qquad , \text{over ice} \qquad [5.1d]$$

For simplicity, a threshold air temperature value of 0 °C was used to separate periods when either Eqs.[5.1a] and [5.1c], with $\gamma_P = 0.655$ were used, or Eqs.[5.1b] and [5.1d], with $\gamma_P = 0.576$ hPa K^{-1}.

The expression $(Q - S) / L$ in Eq.[5.1] is part of the energy term of the Penman equation, with Q being the net radiation flux, S being the soil heat flux (both Q and S are in W m^{-2}), and L (in W m^{-2} mm^{-1} d) being the specific heat of evaporation of water. To calculate L from air temperatures above 0 °C, we used the expression (see DVWK, 1996)

$$L = (28.9 - 0.028 \, T) \qquad [5.1e]$$

For temperatures below 0 °C, we used a constant value of 32.8 W m^{-2} mm^{-1} d for L. Koitzsch et al. (1990) showed that for northern Germany the quantity $(Q - S)$ is approximately equal to 0.6 G, where G (in W m^{-2}) is the hourly average of the daily total of (shortwave) global radiation. Accordingly, we used the expression of Koitzsch et al. (1990) in solving Eq.[5.1]. Values of global radiation and temperature are required to estimate daily values of Ep from Eq.[5.1].

Global Radiation

The model to assess values of G used in the present study follows a set of equations as compiled by VDI (1994). The net radiation flux Q (in W m^{-2}) of a horizontal plane on the surface of the Earth is the sum of the shortwave and longwave radiation flux densities, Q_s, and Q_t:

$$Q = Q_s + Q_t \qquad\qquad [5.2]$$

or

$$Q = (G \downarrow - R \uparrow) + (A \downarrow - E \uparrow) \qquad\qquad [5.2a]$$

In Eq.[5.2a], R is the fraction of G reflected by the surface, A is the thermal radiation of the atmosphere (mainly from water vapor and clouds), and E is the thermal radiation of the surface. Arrows denote the direction of radiation components with respect to the surface. However, with $Q - S \approx 0.6$ G (Koitzsch et al., 1990), only G is required to estimate daily values of Ep. Other parameters of Eq.[5.2a] need not be assessed.

Global radiation, G, is the sum of direct (or beam) solar radiation, B, diffuse solar radiation from the sky, D, and reflected radiation from surrounding surfaces, R. Direct radiation onto a horizontal plane at the Earth's surface is the direct solar radiation received by a surface normal to the direction of irradiance, I, multiplied by the sine of the elevation angle of the Sun, γ, or by the cosine of the complement of that angle, which is the zenith angle of the Sun, ζ.

$$B = I \cdot \sin\gamma = I \cdot \cos\zeta \qquad\qquad [5.3]$$

In Eq.[5.3], the angle which the line of the Sun's rays at the Earth makes with the horizontal surface is γ, and the angle which the line of the Sun's rays at the Earth makes with the vertical drawn from nadir to zenith at the point of consideration, P, is ζ. The geometry is illustrated in Figs. 5.3 and 5.4.
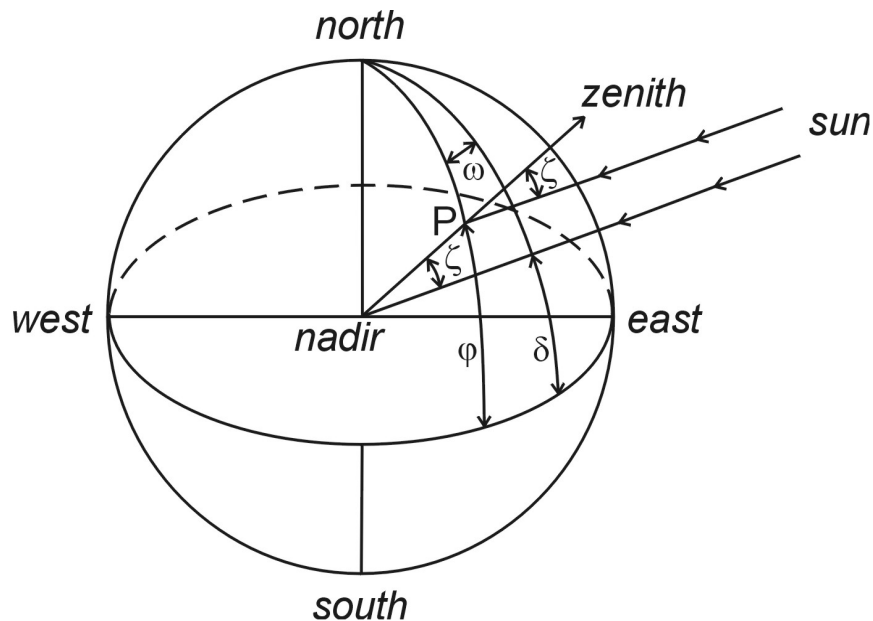
Fig. 5.3 *Geometrical relations of solar zenith angle ζ, latitude φ, solar declination δ, and hour angle ω. The observer is at P (redrawn from Gates, 1980).*

The quantity I is that fraction of the extraterrestrial solar radiation I_0 (the so-called "solar constant"), which reaches the Earth's surface after attenuation in the atmosphere. The solar constant is the amount of sunlight incident upon a surface perpendicular to the Sun's rays just outside the atmosphere. Atmospheric attenuation is mainly caused by scattering on air molecules, scattering on and absorption by particles and clouds, and absorption by gases (e.g. water vapor and ozone). To calculate I, the following equation is used (see VDI, 1994)

$$I = I_0 \cdot \exp\left(-T_L \cdot \delta_{RO} \cdot m \cdot p / p_0\right) \qquad [5.4]$$

where T_L signifies the so-called Linke turbidity factor, δ_{RO} signifies the vertical optical thickness of the clean and dry standard (or Rayleigh) atmosphere, m is

the relative optical air mass, and p/p_0 signifies a correction taking account of air pressure, i.e. of elevation.
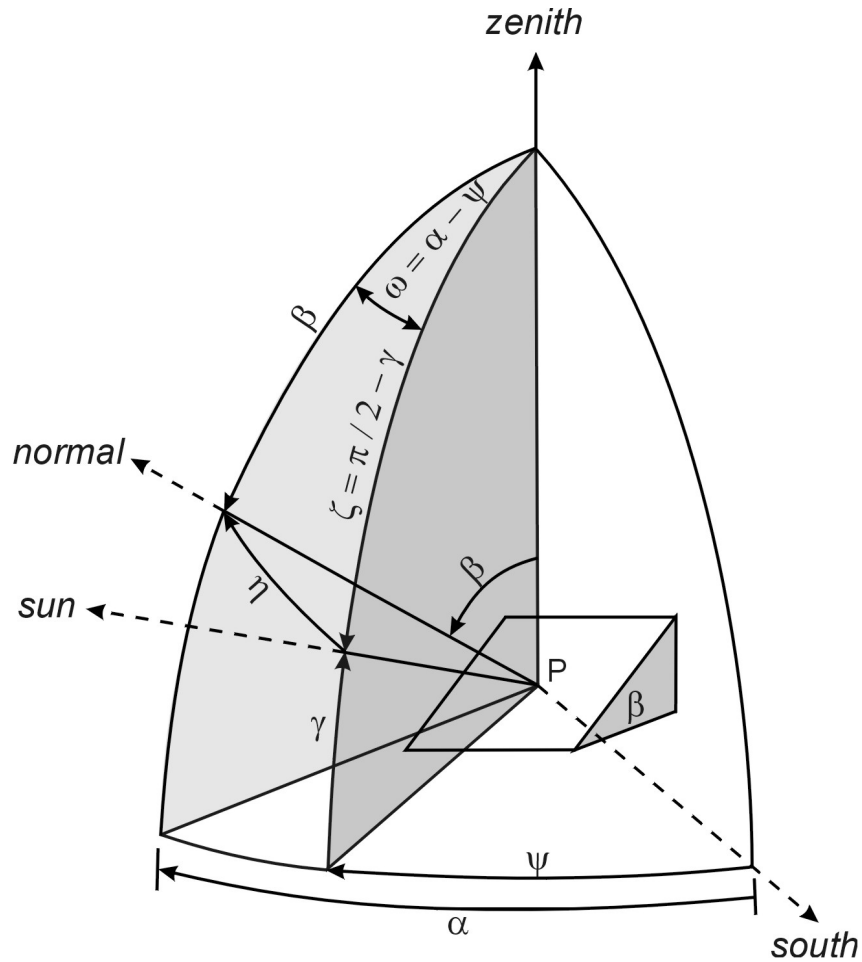
Fig. 5.4 *Geometrical relations of slope angle β, solar altitude γ, solar zenith angle ζ, solar azimuth ψ, azimuth of the surface normal α, hour angle ω, and the angle η between the direction towards the Sun and the normal of an inclined plane surface. The observer is at P (redrawn from VDI, 1994).*

The density of the radiation flux passing from the Sun out into space varies inversely with the square of the distance. The distance r of the Earth from the Sun varies with time of year and has a mean value of $\bar{r}$. The actual amount of solar radiation received at any point in the Earth's orbit, or "solar constant", I_0, varies with r, i.e. with time of year. In the present study an average value of $\bar{I_0} = 1367$ W m^{-2} is assumed. Instantaneous values of I_0 for discrete time intervals of 1 d for every day of the year are calculated as:

$$I_0 = \overline{I_0} \cdot \left(\overline{r}/r \right)^2 \qquad\qquad [5.5]$$

For the distance correction, $\left(\overline{r}/r \right)^2$, the following equations as defined in astronomy by means of trigonometry are used:

$$\left(\overline{r}/r \right)^2 = 1 + 0.03344 \cdot \cos x \qquad\qquad [5.5a]$$

and

$$x = 0.9856° \cdot J - 2.72° \qquad\qquad [5.5b]$$

where J is the number of the day in the year (1 to 365 or 366).

Individual processes of scattering and absorption in the atmosphere are not included in the present model. In an effort to assess overall atmospheric scattering and absorption, the Linke turbidity factor, T_L, is used instead to estimate the optical thickness of a turbid and moist atmosphere as a multiple of a clean and dry atmosphere. From visibility, V_M (in km), T_L was calculated as

$$T_L = 0.84 + 39 / V_M \qquad\qquad [5.6]$$

For cases when data of V_M are not available, functionality was integrated into the ArcView GIS extension software to alternatively use monthly values of T_L as provided by Kasten et al. (1984) for Germany (see Table 5.1).

The relative optical air mass, m, of Eq.[5.4] is the ratio of the air mass through which the solar radiation passes at the instantaneous solar altitude angle, γ, and the corresponding air mass when the Sun is in zenith ($\gamma = 90°$). According to Kasten and Young (1989), m can be calculated with an error of less than 0.5% as

$$m = 1 / \left[\sin \gamma + a \cdot (\gamma + b)^{-c} \right] \qquad\qquad [5.7]$$

where a = 0.50572, b = 6.07995°, and c = 1.6364. Negative solar altitude may occur in the case of an extension of the horizon, e.g. on high mountain peaks. However, only positive values of γ are treated in the present study.

Table 5.1 *Average monthly values of the Linke turbidity factor, T_L, for Germany, according to Kasten et al. (1984).*

Month	T_L	Month	T_L
Jan.	3.8	Jul.	6.3
Feb.	4.2	Aug.	6.1
Mar.	4.8	Sep.	5.5
Apr.	5.2	Oct.	4.3
May	5.4	Nov.	3.7
Jun.	6.4	Dec.	3.6

The vertical optical thickness of the Rayleigh atmosphere was calculated by use of the following approximation as provided by Kasten (1980):

$$\delta_{RO} = 1/(0.9 \cdot m + 9.4) \qquad , \text{ for } \gamma > 5° \qquad [5.8]$$

For values of $\gamma \leq 5°$, values of δ_{RO} as listed in Table 5.2 were used. For values of γ intermediate of those listed in Table 5.2, δ_{RO} was interpolated linearly.

The factor p/p_0 in Eq.[5.4] is a pressure correction to reduce the optical thickness of the standard atmosphere with an air pressure of 1013.25 hPa at sea level to the current atmospheric pressure, p. For the standard atmosphere, p/p_0 at the altitude z was estimated from the equation (VDI, 1994)

$$p/p_0 = \exp(-z/8434.5) \qquad [5.9]$$

If calculations are done for an individual point, user-input of z (in m) is required to solve Eq.[5.9]. If calculations are conducted for an elevation grid, the program automatically calculates and uses the average value of z from all grid cells of the input DEM.

Table 5.2 *Values of the vertical optical thickness, δ_{RO}, for angles of solar altitude, $\gamma \leq 5°$, according to Kasten et al. (1980).*

γ (°)	δ_{RO}
5	0.0548
4	0.0519
3	0.0491
2	0.0463
1	0.0435
0	0.0408

Direct solar radiation onto a plane of arbitrary orientation with no limitation of the horizon according to Lambert's cosine law is a function of the angle η between the surface normal (or perpendicular) and the direction towards the Sun:

$$I(\beta, \alpha) = I \cdot \cos \eta \qquad [5.10]$$

where the direction of the surface normal is determined from the azimuth of the surface normal, α, and from the angle of inclination of the surface with respect to the horizontal, or slope, β. The cosine of the angle η is derived from the following equation:

$$\cos \eta = \sin \gamma \cdot \cos \beta + \cos \gamma \cdot \sin\beta \cdot \cos (\alpha - \psi) \qquad [5.10a]$$

For illustration of the geometry, again see Figs. 5.3 and 5.4.

Note that in the present study, (i) azimuth (in the case of both α and ψ) is measured positively westward from south (= 0°) and negatively eastward, and (ii) only slopes of β < 90° are treated.

The position of the Sun is determined from solar azimuth, ψ, and from solar elevation, γ. From spherical trigonometry in astronomy it is known that

$$\sin\gamma = \sin\varphi\,\sin\delta + \cos\varphi\,\cos\delta\,\cos\omega \qquad [5.10b]$$

and

$$\cos\psi = (\sin\varphi\,\sin\gamma - \sin\delta)/(\cos\varphi\,\cos\gamma) \qquad [5.10c]$$

(VDI, 1994) where φ is the geographical latitude of the observation point, δ is the declination of the Sun, and ω is the hour angle of the Sun. Declination is the angle which the line of the Sun's rays at the Earth makes with the equatorial plane (see Fig. 5.3). As the Earth orbits around the Sun, the declination varies from - 23.5° at winter solstice on 22 Dec. to + 23.5° at summer solstice on 21 Jun. for the northern hemisphere. The maximum 24 h-change in declination (at vernal and autumnal equinox on 20 Mar. and 22 Sep., respectively) is less than 0.5°. Declination is assumed to be constant for 24 h in the model and is calculated anew for every day using the equation

$$\sin\delta = 0.3978\cdot\sin(x - 77.51° + 1.92°\cdot\sin x) \qquad [5.10d]$$

(VDI, 1994) and Eq.[5.5b] to determine values of x for every day of the year.

The hour angle of the Sun, ω, is the angle through which the Earth must turn to bring the meridian of an observer's point P directly under the Sun (see Fig. 5.3 or 5.4) and is a function of time of day. Counting from midday, ω changes 15° per hour. The hour angle is equal to zero at true noon (see discussion of true local time, or TLT, below), is positive in the afternoon, and is negative in the morning. The relation of ω to TLT (in h) is described by the following equation:

$$\omega = 15\,(\text{TLT} - 12) \qquad [5.11]$$

115

To find ψ and γ (i.e. the position of the Sun) TLT is needed, which is also called local apparent time, or true solar time. It is common in the meteorological network of many countries for hourly or instantaneous data (e.g. of cloud coverage and visibility) to be recorded against the local standard time (LST), rather than TLT, or daylight saving time. In the present study, such weather records were used. In order to compute the incidence angles ψ and γ, it is necessary to convert LST at instants for which meteorological data are recorded into TLT. To carry out the conversion, the geographical longitude of the standard meridian, L_s, for the local time zone is needed. In the extension program to ArcView, L_s needs to be provided via user input. International standard meridians are multiples of 15° east or west of Greenwich, England. Standard times are therefore hour multiples ahead of or behind the Greenwich mean time (GMT). TLT for a given LST can be written as

$$TLT = LST + 4\,(L_s - L_e) + Z \qquad\qquad [5.11a]$$

where $L_s = 15°$ in the case of the Sigmundshall mound, L_e is the local longitude of the observation point, Z is called the equation of time, and the corrections of LST are in minutes. Correction of TLT for Z is conducted because the solar day varies in length through the year. This, in turn, is caused by the fact that (i) the Earth sweeps out unequal areas on the ecliptic plane as it revolves around the Sun and (ii) the Earth's axis is tilted with respect to the ecliptic plane. The equation of time is the discrepancy of the length of the solar day measured relative to a perfectly uniform terrestrial motion. Astronomical formulae result in the following analytical expression for Z, which through the year varies between – 14 and + 15 minutes (VDI, 1994):

$$Z = -7.66 \cdot \sin x - 9.87 \cdot \sin (2\,x + 24.99° + 3.83° \cdot \sin x) \qquad [5.11b]$$

where values of x again are derived for every day of the year with use of Eq.[5.5b].

Direct solar radiation, $I(\beta,\alpha;N)$, is incident only upon those parts of the landscape with no obstacle between the Sun and the Earth's surface. When calculations are conducted for a DEM (rather than an individual point), hourly

values of solar azimuth, ψ, and of angular elevation of the Sun above the horizon, γ, are used as input parameters to the "hillshade" request available as part of ArcView's SpatialAnalyst extension. Hillshading determines the hypothetical illumination of the DEM surface under a cloudless sky at the relevant time (i.e. position of the Sun). The "hillshade" request creates a shaded relief grid for the input DEM, with the distance of the illumination source to the surface considered to be at infinity. The calculation considers the effects of both the local illumination angle and shadow. The analysis of shadows is done by considering the effects of the local horizon at each cell. Grid cells in shadow are assigned a value of 0. To determine the spatial variation of direct solar radiation across the mine waste mound, the hillshade grid was multiplied with the grid of I(β,α) as calculated from Eq.[5.10] for the same hour.

For global radiation without limitation of the horizon, G(0), the following parameterization as proposed by Kasten (1983) is used

$$G(0) = 0.84 \cdot I_0 \cdot \sin\gamma \cdot \exp\left[-0.027\left(p/p_0\right) T_L / \sin\gamma\right] \qquad [5.12]$$

In case of an overcast or partly cloudy sky, calculation of global radiation is conducted with use of the following equation:

$$G(N) = G(0) \cdot \left[1 - d\left(N/8\right)^e\right] \qquad [5.13]$$

where G(N) signifies global radiation in the case of a cloud coverage of the sky "dome" of N eighths of obstruction, and d and e are empirical constants which have been determined for Germany as d = 0.72 and e = 3.2 (VDI, 1994). In the extension to ArcView GIS, hourly values of N are required user input and are read from an input data base file.

Diffuse solar radiation from a cloudless sky onto a horizontal surface with no limitation of the horizon, D(0), is equal to the difference between G(0) and direct solar radiation, which is dependent on solar altitude, γ:

$$D(0) = G(0) - I \cdot \sin\gamma \qquad [5.14]$$

where I and G(0) are obtained from Eqs.[5.4] and [5.12], respectively. On an inclined surface, only a part of the diffuse solar radiation is received. Only for overcast conditions (N = 8) is the intensity of sky diffuse radiation approximately uniform over the sky dome (i.e. isotropic). In case of a cloudless sky, diffuse solar radiation is decidedly anisotropic, with maximum values coming from the direction of the Sun. Diffuse solar radiation is calculated as the sum of an anisotropic (or circumsolar) and an isotropic component, following a parameterization proposed by Hay and McKay (1985):

$$D(\beta, \alpha; 0) = D(0) \left[I \cdot \cos\eta / (I_0 \cdot \sin\gamma) + (1 - I/I_0) \cdot \cos^2(\beta/2) \right] \qquad [5.15]$$

The first term on the right hand side of Eq.[5.15] is the solar radiation $I(\beta, \alpha)$ on the inclined surface (see Eq.[5.10]), weighted with $D(0) / (I_0 \sin\gamma)$, thus representing the circumsolar radiation. The second term specifies the fraction of diffuse solar radiation from the remainder of the sky dome, which is assumed to be isotropic.

In the case of a cloudy sky (with N > 0) diffuse solar radiation on a *horizontal* surface is calculated analogously with Eq.[5.14] by

$$D(N) = G(N) - I(N) \cdot \sin\gamma \qquad [5.16]$$

where G(N) is obtained from Eq.[5.13], and I(N) is estimated from the following equation (VDI, 1994):

$$I(N) = (1 - N/8) \cdot I \qquad [5.17]$$

with I as obtained from Eq.[5.4].

The diffuse solar radiation received by an *inclined* surface depends on the instantaneous distribution of the cloud coverage over the sky dome. On average over time, diffuse solar radiation is approximated as being equal to the sum of a

component from the cloudless portion and a component from the overcast portion of the sky:

$$D(\beta, \alpha; N) = (1 - N/8) \cdot D(\beta, \alpha; 0) + (N/8) \cdot D(\beta, \alpha; 8) \qquad [5.18]$$

in which equation $D(\beta,\alpha;0)$ is obtained from Eq.[5.15] and $D(\beta,\alpha;8)$ is the diffuse solar radiation received by the surface in case of an overcast sky. This is assumed to be isotropic, and is approximated by the following equation (VDI, 1994):

$$D(\beta, \alpha; 8) = D(8) \cdot \cos^2(\beta/2) \qquad [5.19]$$

The term $D(8)$ is equal to $G(8)$, which is the global radiation from an overcast sky with $N = 8$. It follows from Eq.[5.13] that

$$D(8) = G(8) = G(0) \cdot (1 - d) \qquad [5.20]$$

A horizontal, *downwardly* oriented surface receives the portion R of the global radiation G which is reflected from the upwardly oriented surface below. This can be calculated as

$$R = \rho_s \cdot G \qquad [5.21]$$

where ρ_s is the shortwave albedo of the upwardly oriented surface. Downwardly oriented surfaces are not treated in the present model. However, an upwardly oriented surface, which is inclined at the angle β, receives a fraction of R reflected from surrounding surfaces. In the present model this fraction is calculated as

$$R(\beta, \alpha) = R \cdot \sin^2(\beta/2) \qquad [5.22]$$

where it is assumed that the Earth's surface reflects isotropically, and a value of $\rho_s = 0.25$ was used to solve Eq.[5.21].

Finally, the shortwave global radiation received by an arbitrarily oriented surface (with $\beta < 90°$) is calculated as the total of the direct, diffuse, and reflected shortwave radiation flux densities:

$$G(\beta, \alpha; N) = I(\beta, \alpha; N) + D(\beta, \alpha; N) + R(\beta, \alpha) \qquad [5.23]$$

where

$$I(\beta, \alpha; N) = (1 - N/8) \cdot I(\beta, \alpha) \qquad [5.23a]$$

with $I(\beta, \alpha)$ as obtained from Eq.[5.10],

$$D(\beta, \alpha; N) = (1 - N/8) \cdot D(\beta, \alpha; 0) + (N/8) \cdot D(\beta, \alpha; 8) \qquad [5.23b]$$

with $D(\beta, \alpha; 0)$ as obtained from Eq.[5.15], $D(\beta, \alpha; 8)$ as obtained from Eq.[5.19], and $R(\beta, \alpha)$ as obtained from Eq.[5.22].

Solar radiation as a source of energy for evaporation is available during daylight hours only. Measured values of air temperature at the Sigmundshall mound during hours when $\gamma > 0$ were averaged for every day. From the resulting daytime mean temperature, the term $s / (s + \gamma_P)$ and the specific heat of evaporation of water, L, were estimated by use of Eqs.[5.1a] to [5.1e]. Using these values and daily integrated values of global shortwave radiation, G, daily totals of potential evaporation were calculated from Eq.[5.1], with use of the simplification $Q - S \approx 0.6\,G$ (Koitzsch et. al., 1990).

For the slopes and aspects of different positions around the Sigmundshall mine tailings mound where we measured global radiation (see the section titled "Field Measurements") we calculated hourly and daily values of G with use of

Eq.[5.23], as well as daily values of Ep with use of Eq.[5.1]. Calculated values were compared to measurements to "ground-truth" Eqs.[5.23] and [5.1].

To depict the spatial variation of potential evaporation as depending on global radiation across the mound, we calculated maps of daily totals of Ep and totaled cell values from those maps over the duration of one year for the three consecutive years of our measurement campaign.

5.4 Results and Discussion

In Fig. 5.5, hourly values of global radiation as measured with the upper CM3 pyranometer in the south position (35° slope, 160° aspect) during eight consecutive days of fair weather (i.e. low cloud coverage and good visibility) are compared to results from Eq.[5.23]. For such conditions, global radiation mostly depends on geometrical constellations between the Sun and the Earth, the portion of direct radiation on global radiation is high, and model results are in good agreement with the measured data.

In Table 5.3, hourly values of global radiation during daytime hours (i.e., when the Sun was above the horizon) from the entire measurement campaign in three different positions around the waste mound are compared to results from Eq.[5.23]. Results of measured and calculated hourly global radiation were separated into nine classes defined by eighths of cloudiness from 0 (clear sky) to 8 (overcast sky) as reported from the Wunstorf airfield. In order to evaluate the performance of the global radiation model, a simple linear statistical model of the form $y = m \cdot x$ was fitted to the data in every class, and values of R^2 were calculated. The number of hours per class and the relative frequency are also listed. In total, data from 11503 daylight hours were evaluated. Because of gaps in the dataset as a result of sensor recalibration and data storage problems, the number of hours per year varies between years, but the relative frequency of hours per class of cloud coverage is similar in all three years.
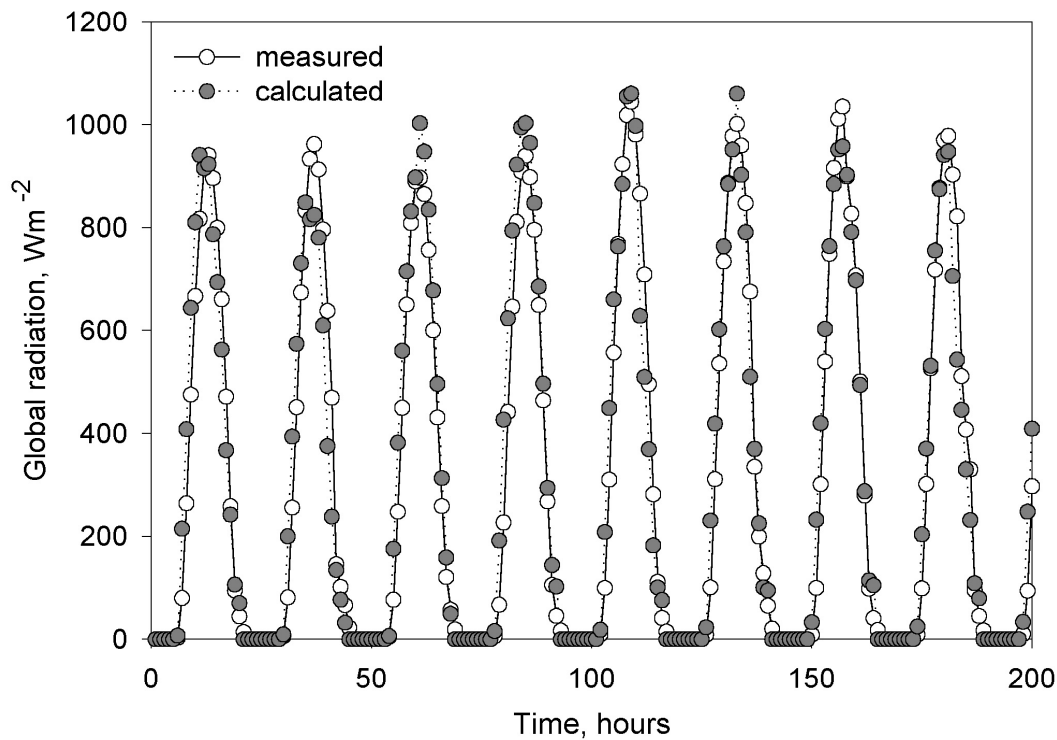
Fig. 5.5 *Global radiation on the south slope (34°/160°) from 10 to 17 May 1998.*

Table 5.3 *Performance of the global radiation model for different slopes and classes of cloud coverage (form 0/8 to 8/8 of sky obstruction).*

	South slope (34°/160°) (17.6.1997-18.6.1998)				North slope (35°/350°) (19.6.1998-8.7.1999) †				Horizontal (0°/0°) (11.8.1999-30.5.2000)			
Clouds	m ‡	R^2	No. of Hours	%	m ‡	R^2	No. of Hours	%	m ‡	R^2	No. of Hours	%
0/8	1.1195	0.947	71	1.7	1.1905	0.660	66	1.6	1.1074	0.924	107	3.3
1/8	0.9951	0.897	297	7.0	1.1523	0.763	154	3.8	1.0111	0.889	214	6.6
2/8	0.8871	0.875	223	5.3	1.0736	0.737	165	4.1	0.9343	0.857	148	4.5
3/8	0.8345	0.839	262	6.2	0.9052	0.618	234	5.8	0.8354	0.856	171	5.2
4/8	0.7626	0.716	233	5.5	0.8433	0.771	245	6.1	0.7965	0.732	133	4.1
5/8	0.6797	0.587	261	6.2	0.8097	0.664	335	8.3	0.7049	0.686	229	7.0
6/8	0.5917	0.299	382	9.1	0.7498	0.725	477	11.8	0.6387	0.572	384	11.8
7/8	0.5687	0.287	1478	35.1	0.7138	0.674	1437	35.7	0.6096	0.482	1168	35.8
8/8	0.6035	0.376	1006	23.9	0.8418	0.562	913	22.7	0.6540	0.355	710	21.8
Total			4213	100			4026	100			3264	100

† No data collected from 13 Aug. to 2 Oct. 1999.
‡ y = m · x, where x: hourly values of measured global radiation, and
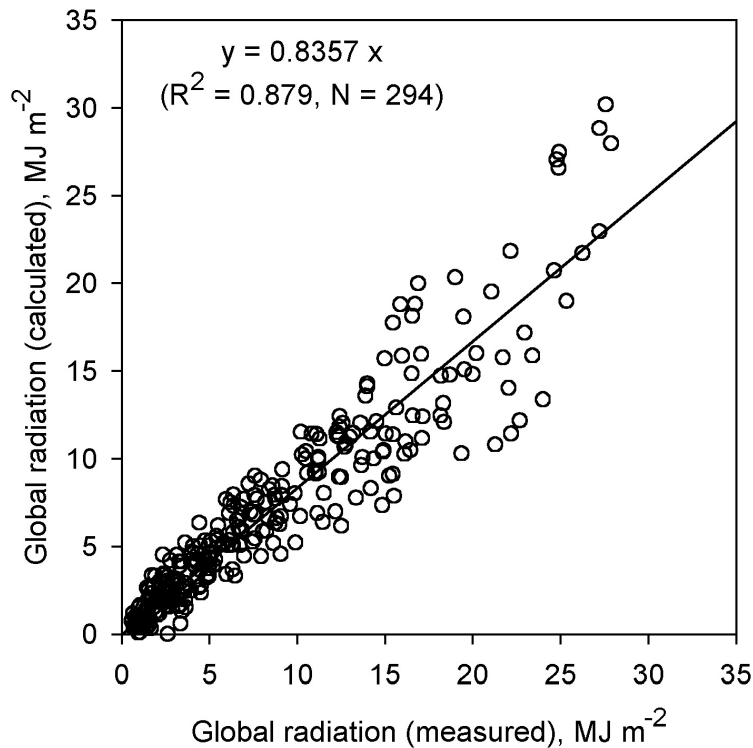   y: hourly values of calculated global radiation

Table 5.3 shows that Eq.[5.23] generally performs better for clear sky than for overcast conditions. For the south slope and the horizontal position, values of R^2 are high when clouds cover less than three eighths of the sky, but decrease to about 0.3 at more cloudy skies. Simultaneously, the slope of the linear model, m, which equals one in case of a perfect fit, decreases from values around 1.1 to 0.6. This indicates that Eq.[5.23] tends to underestimate global radiation measured during times when cloud coverage is large. This can presumably be explained with two reasons: (i) Cloud thickness and cloud altitude are not accounted for in the model. When large parts of the sky are cloudy, but clouds are thin and high, the pyranometer still may receive large amounts of radiation, while radiation calculated from Eq.[5.23] is low. (ii) This is also true in situations when cloud coverage is high, but wind speed at cloud altitude is low (i.e. clouds do not travel much within the duration of one hour). In such a case, the pyranometer may receive considerable direct radiation from the Sun through a gap between clouds during a considerable portion of one hour, and the model will underestimate measured radiation for that hour.

Independent of cloud coverage, the pyranometer in the north position (tilted by 34° to an aspect of 350°) did not receive direct radiation from the Sun, but only diffuse radiation and reflected radiation from surrounding surfaces during most hours of the measurement campaign. Calculations for the north position predominantly reflect D(β,α;N) and R(β,α) from Eqs.[5.18] and [5.22], respectively, rather than direct radiation from Eq.[5.23a]. Data from Table 5.3 shows that for the north position the variation of m and R^2 is less than for the horizontal or the south position. But, as in the other positions, there is a trend in calculated radiation data to underestimate global radiation measurements under overcast skies, i.e. m decreases slightly with increasing cloud coverage.

During one day, deviations between measured and calculated values of hourly global radiation resulting from problems of accurately describing the instantaneous distribution of clouds across the sky may average out. With many weather patterns clouds will travel considerable distances and will be reformed within one day. Therefore, with respect to calculating daily values of potential evaporation from Eq.[5.1], performance of the global radiation model on the basis of an hourly timestep may not be so important. We will evaluate the performance of Eq.[5.23] (and of Eq.[5.1]) based on a daily timestep next.

Figure 5.6 is shown as an example of daily values of global radiation in units of work (MJ m^{-2}). The figure compares radiation in the horizontal position measured on 294 d (11 Aug. 1999 to 30 May 2000) with calculated values for the same period. Again, we fitted a linear statistical model to the data. The slope

m of that model is somewhat smaller than one, i.e. the radiation model in general slightly underestimates the measured data, but the overall model performance appears reasonable.

Fig. 5.6 *Daily values of global radiation from 11 Aug. 1999 to 30 May 2000 (horizontal position).*

In Table 5.4, information to evaluate Eqs.[5.23] and [5.1] for the south, north, and the horizontal position is compiled. Values of Ep were calculated from Eq.[5.1] (i) with use of values of global radiation and air temperature as measured at the Sigmundshall mound (see section titled "Field Measurements" above), and (ii) with use of calculated values of $G(\beta,\alpha;N)$ from Eq.[5.23] and values of air temperature as measured at the Wunstorf airfield. In both cases, a value of 1.26 was used for the lumping factor α_{PT} of Eq.[5.1].

For all three positions, m varies between 0.8 to 0.9, and R^2 ranges from 0.81 to 0.92 (see Table 5.4). The fact that m and R^2 are higher for Ep than for $G(\beta,\alpha;N)$ in all positions may be caused by the fact that air temperature was taken into account as an additional independent variable when Ep was calculated.

Table 5.4 *Performance of the global radiation and evaporation models for calculating daily totals.*

Position	Quantity	Model	R^2	No. of Days
South (34°/160°)	$G(\beta,\alpha;N)$	y = 0.8283 x	0.809	367
(17.6.97-18.6.1998)	Ep	y = 0.8744 x	0.840	
North (35°/350°)	$G(\beta,\alpha;N)$	y = 0.8693 x	0.906	335
(19.6.1998-8.7.1999) †	Ep	y = 0.8989 x	0.919	
Horizontal (0°/0°)	$G(\beta,\alpha;N)$	y = 0.8357 x	0.879	294
(11.8.1999-30.5.2000)	Ep	y = 0.8919 x	0.894	
Total				996

† No data collected from 13 Aug. to 2 Oct. 1999.

Figure 5.7 is a map of global radiation across the waste mound, integrated over the duration of one day, 24 Sep. 1998. Figure 5.8 is a map of potential evaporation for that day. Maps were calculated with use of the extension program to ArcView GIS to solve Eqs.[5.23] and [5.1], respectively, for every cell of the grid DEM (Fig. 5.2). 24 Sep. 1998 was a partly cloudy day around autumnal equinox. The Sun was above the horizon for approximately 12 hr. Average air temperature during that time was 14.1 °C. Clouds covered 2 eighths of the sky in the morning and 6 eighths in the late afternoon. Visibility ranged from 1.2 km in the morning to 12.0 km in the afternoon. For such conditions, global radiation received by the surface of the mound is strongly dependent on slope orientation, and so is Ep. Global radiation ranged from about 3 to more than 13 MJ m^{-2} between north and south slopes (Fig. 5.7). Ep ranged from about 0.7 mm on parts of the north slope to 3.2 mm on the south slope (Fig. 5.8).

Figures 5.9 and 5.10 are evaporation maps for the mound for two days around winter solstice in consecutive years (25 Dec. 1997 and 24 Dec. 1998). The Sun was above the horizon from about 9 a.m. to about 4 p.m. only. 25 Dec. 1997 was a comparatively warm day (10.3 °C) with some sunshine during the middle of the day, while 24 Dec 1998 was cool (1.7 °C), overcast, and bleak. Evaporation ranged from 0.2 to 0.6 mm between slopes on 25 Dec. 1997. The effect of a long shadow of the mound on evaporation can be seen to the mound's north in Fig. 5.9. Evaporation was close to zero on 24 Dec. 1998, and slope orientation had no impact on Ep on that day. The color scheme in Fig. 5.10 strongly exaggerates Ep; it was selected to depict, besides Ep, the location of the mound. Also note that color schemes are similar in all evaporation maps shown, but that colors signify different ranges of Ep in different maps.
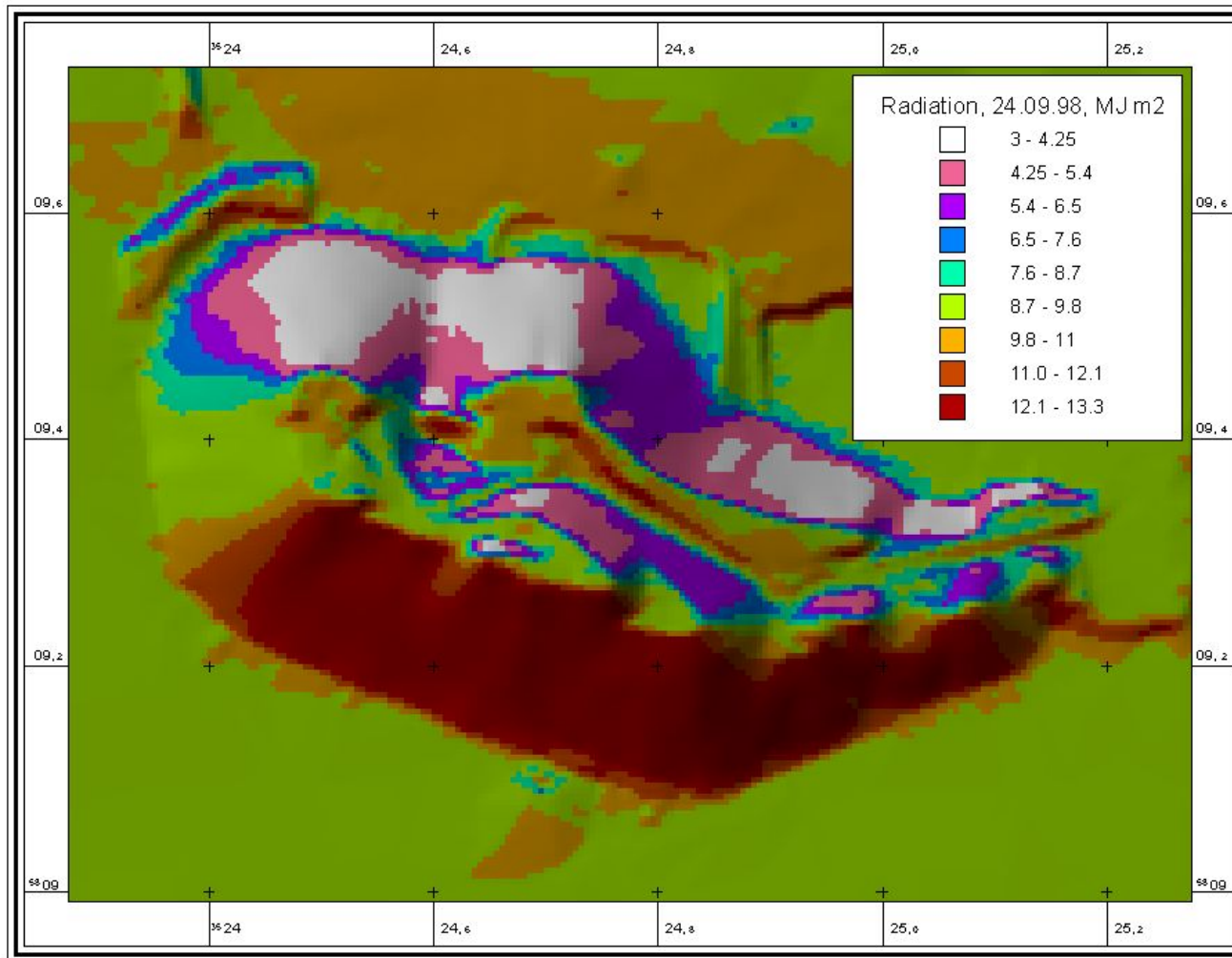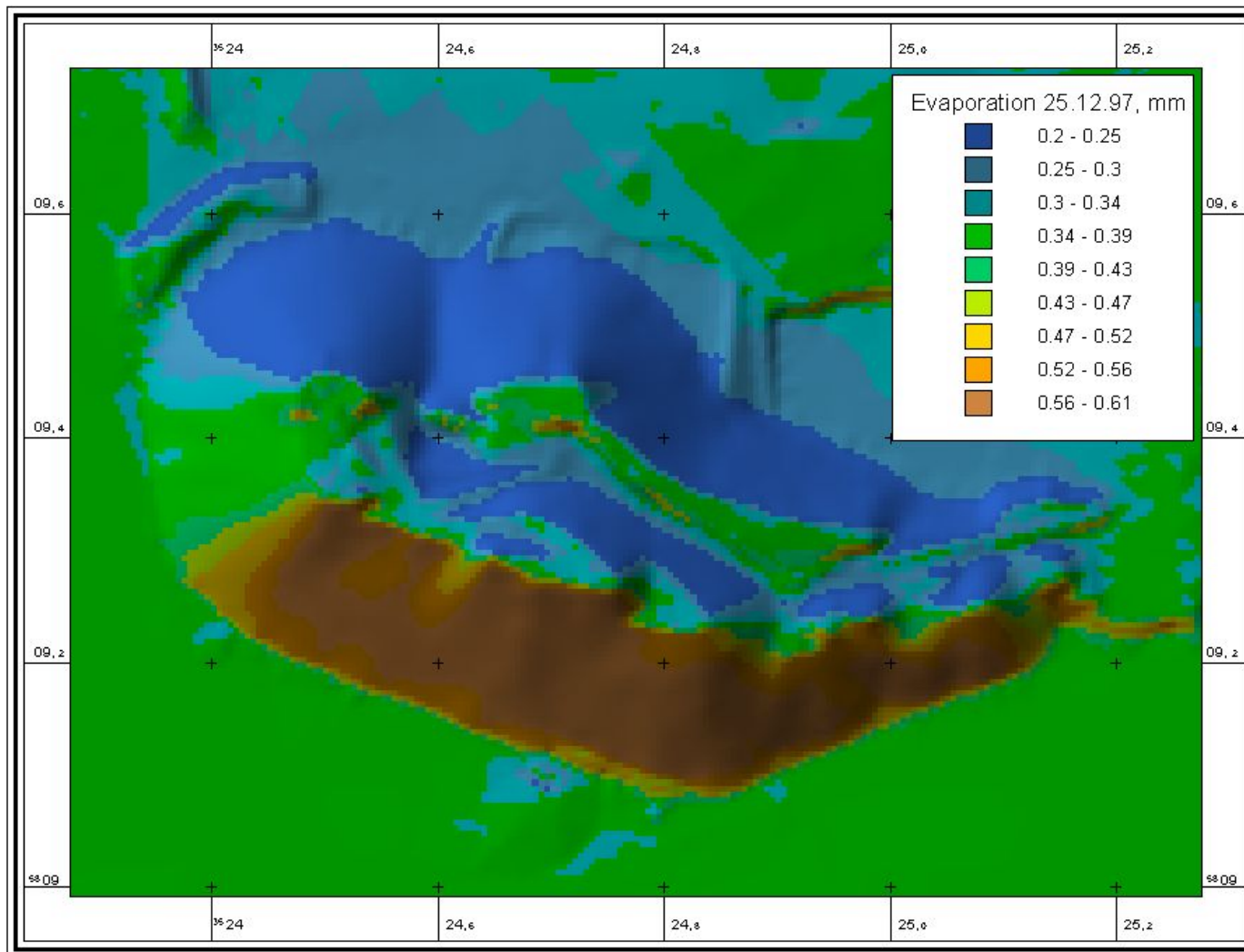
Fig. 5.7 *Daily values of global radiation for the Sigmundshall waste mound on 24 Sep. 1998, calculated from Eq.[5.23].*
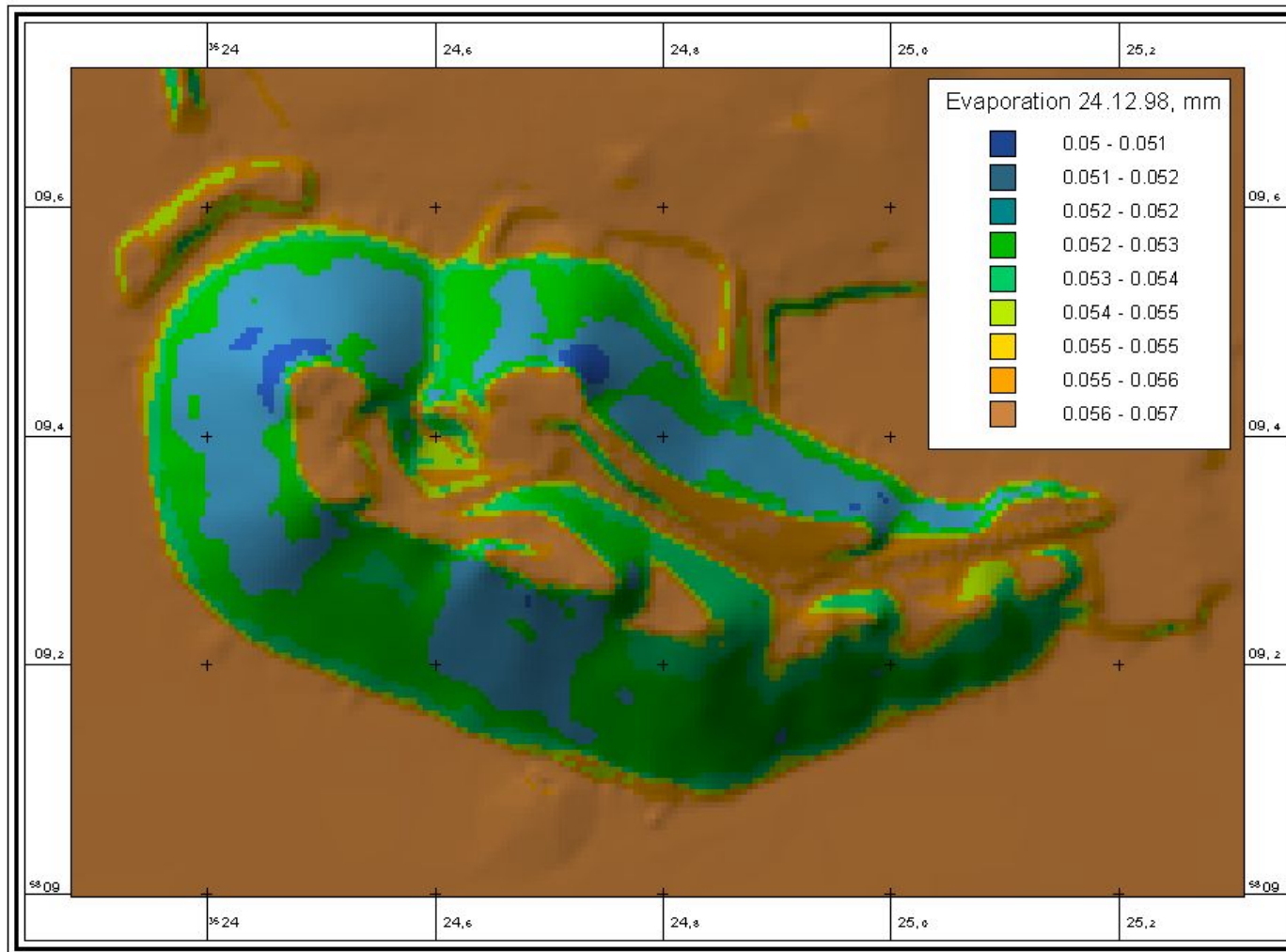
126
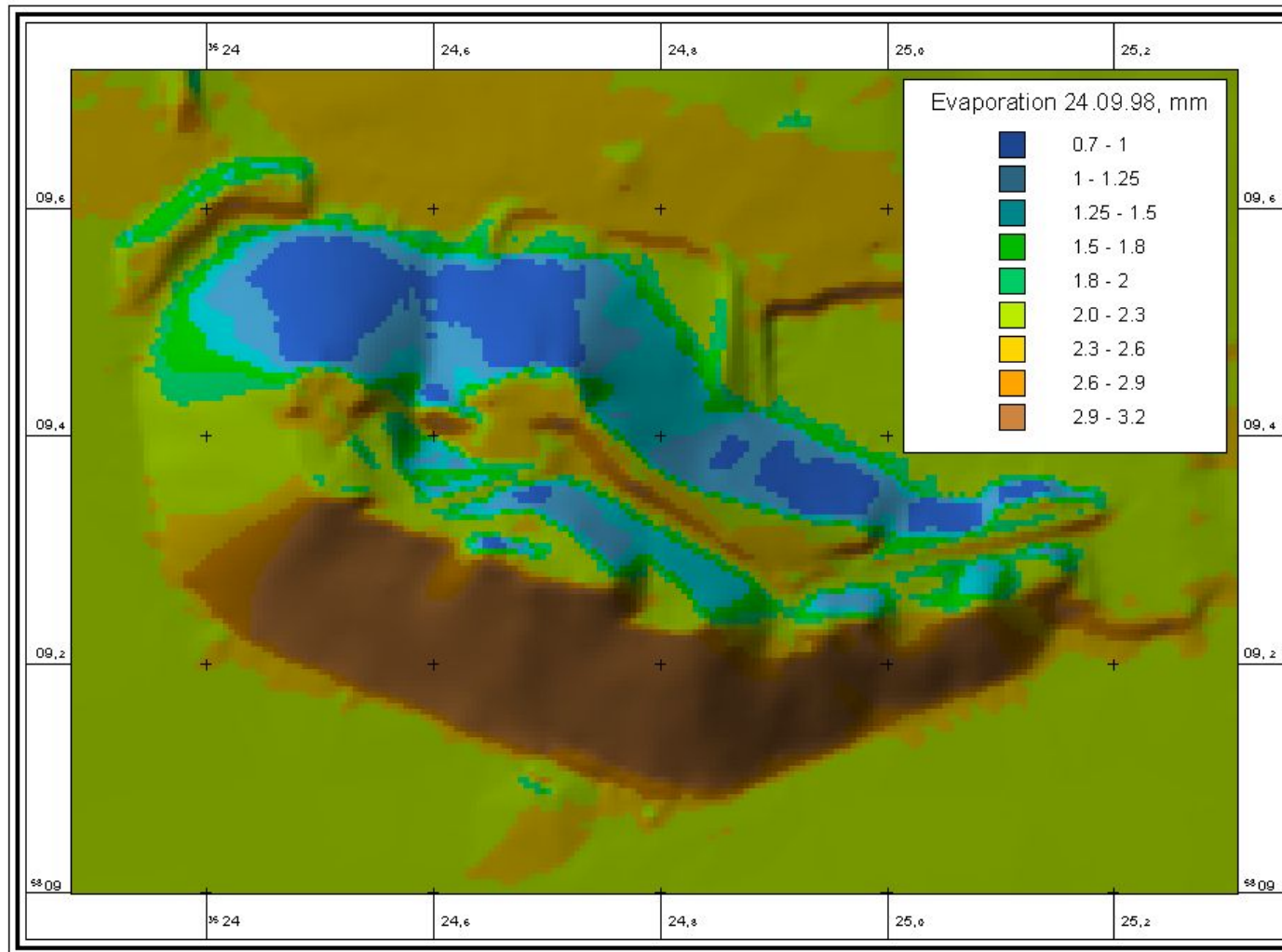
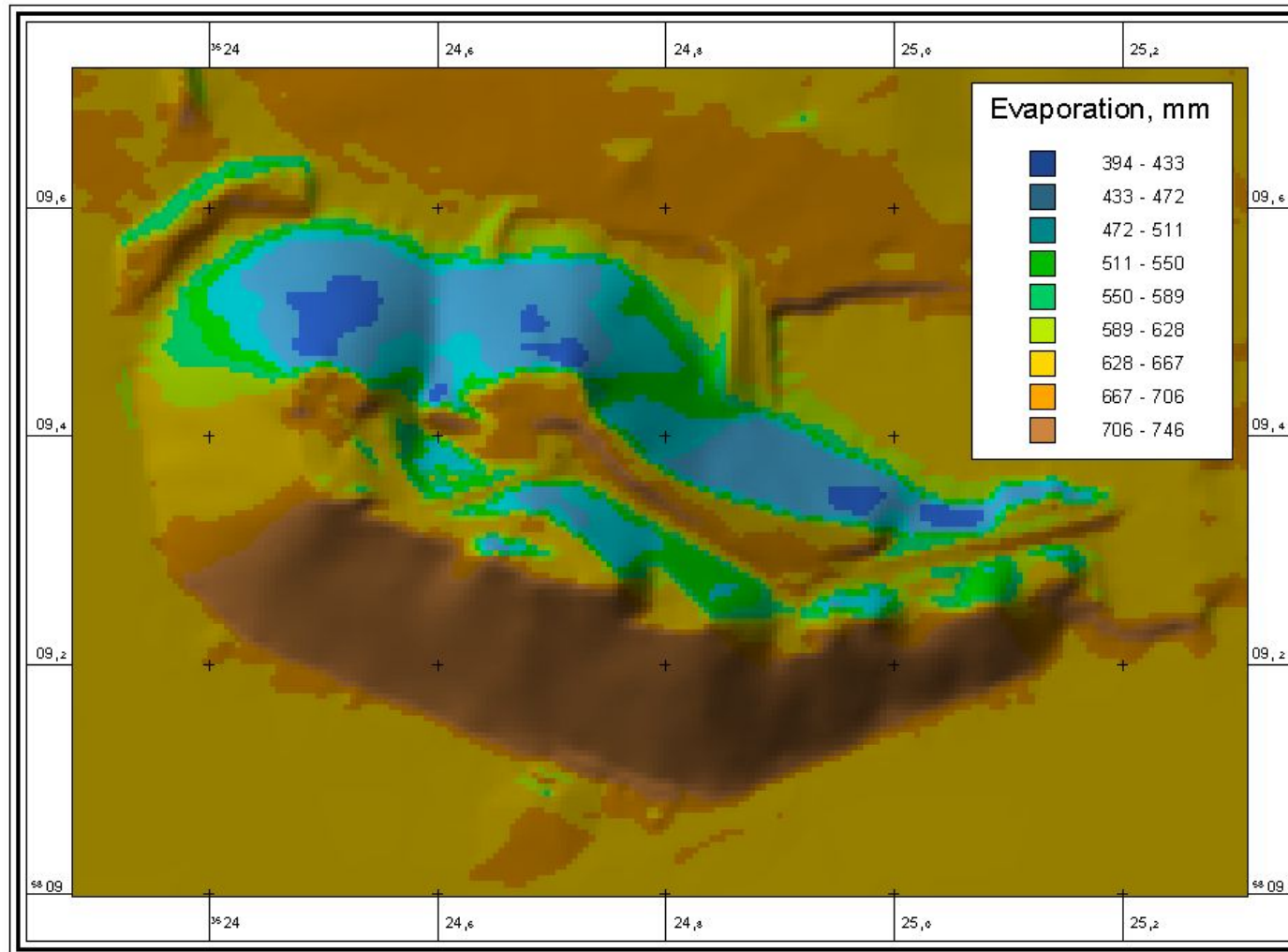***Fig. 5.8*** *Daily values of Ep for the Sigmundshall waste mound on 24 Sep. 1998, calculated from Eq.[5.1].*

Fig. 5.9 *Daily values of Ep for 25 Dec. 1997, calculated from Eq.[5.1].*

Fig. 5.10 *Daily values of Ep for 24 Dec. 1998, calculated from Eq.[5.1].*

Fig. 5.11 *Average annual Ep from the Sigmundshall waste mound, calculated from Eq.[5.1] for 17 Jun. 1997 to 18 Jun. 2000.*

130

Figure 5.11 is a map of average annual potential evaporation from 17 Jun. 1997 to 18 Jun. 2000, i.e. for the three years of our measurement campaign. For the mostly horizontal fields to the south of the waste mound (i.e. independent of the mound's shadow) average annual values of Ep around 663 mm were calculated. This is considerably higher than values given by Keller (1978), who derived values of annual Penman-evaporation from 550 to 600 mm for the area from weather records of the period 1951 to 1965. It is about 13% higher than the value of 588 mm that we calculated in a previous paper with the Penman-equation from weather records collected at the nearby Hannover airport (25 km from our site) from 1967 to 1996 (Hermsmeyer et al., 2001b).

Annual values of Ep varied considerably between the three years of our study. For horizontal positions south of the mound, Ep ranged from about 606 mm (or 3.1% more than the longterm average at Hannover) during the second year of our study to 722 mm (22.8% more than the longterm average) during the third year. During the first year, horizontal Ep was 661 mm, or 12.4% more than the longterm average.

Because $G(\beta,\alpha;N)$ as calculated from Eq.[5.23] for individual points rather underestimated the measured data (Fig. 5.6, Table 5.4), it is likely that higher than average Ep values resulted from higher than average air temperature. Besides radiation, temperature is the only input variable to Eq.[5.1].

Longterm average annual temperature at Hannover airport from 1967 to 1997 was 9.1°C, but temperatures at the nearby Wunstorf airfield (that we used for our calculations) were higher during all three years of our study. Average annual temperature was lowest in the second year (9.6°C, or 5.5% higher than the longterm average), highest in the third year (11.2°C, or 23.1% higher than average), and intermediate in the first year (10.5°C, or 15.4% higher than average at Hannover airport).

Ranking the years 1997 to 2000 with respect to either the deviation of calculated Ep or the deviation of measured air temperature compared to longterm average values of these quantities leads to identical results. Moreover, relative amounts of deviations of air temperature and Ep from the respective longterm average are similar. It appears likely that larger than longterm average air temperature caused larger than average longterm Ep during our measurement campaign.

Variation in average annual Ep between opposite slopes of the waste mound is considerably larger than variation from year to year in the same position. According to our model, the 1997 to 2000 average annual Ep ranged

from 415 mm on north slopes to 745 mm on south slopes (Fig. 5.11). In north positions, three-year average Ep was only 55.7% of the value calculated for south positions. Compared to a horizontal position (663 mm), Ep was 12.4% larger on south slopes, but 37.4% smaller on north slopes.

5.5 Conclusions

In the present study, a computer model was developed to calculate global radiation for individual points on the Earth's surface or across a landscape. The model is based on equations compiled by VDI (1994). Input parameters are geographic location, slope steepness, slope orientation, and hourly values of cloud coverage and visibility. Independent of slope orientation, the model adequately described daily values of global radiation measured in the field. Hourly values of global radiation were adequately described for predominantly clear skies, but were underestimated when clouds covered 50% of the sky or more.

The Priestley and Taylor (1972) equation is used to compute Ep from calculated values of radiation and measured values of air temperature. Potential evaporation at different slope aspects was adequately described by the model.

The model was applied to the DEM of a potash mine tailings mound to calculate a map of three-year average annual potential evaporation across the mound. Evaporation varied considerably between opposite (north and south) slopes. Three-year average evaporation in horizontal positions was higher than longterm average evaporation for the same area. This may be the result of temperature, which during our study also was higher than the longterm average.

The model appears useful in studying the effects of solar radiation and evaporation in a wide range of applications when measurements of visibility and cloud cover are available (e.g., from airfields). It may for example be studied how designing the mound's shape during future extensions to keep north facing slopes steep and short, but south facing slopes less steep and long can enhance evaporation and reduce the amount of briny discharge.

5.6 References

Ångstrom, A. 1924. Report to the International Commission for Solar Research on actinometric investigations of solar and atmospheric radiation. Quart. J. Roy. Met. Soc. 50:121-125.

Brinsfield, R., M. Yaramanoglu, and F. Wheaton. 1984. Ground level solar radiation prediction model including cloud cover effects. Solar Energy. 33:493-499.

Burrough, P.A., (1986). Principles of geographical information systems for land resources assessment. Oxford University Press, New York.

Dozier, J. 1980. A clear-sky spectral solar radiation model for snow-covered mountainous terrain. Water Resour. Res. 16:709-718.

Dubayah, R. 1994. Modeling a solar radiation topoclimatology for the Rio Grande river basin. Journal of Vegetation Science. 5:627-640.

Dubayah, R., and P.M. Rich. 1995. Topographic solar radiation models for GIS. International Journal for Geographic Information Systems. 9:405-413.

Duffie, J.A., and W.A. Beckman. 1991. Solar energy of thermal processes. John Wiley and Sons, New York, NY.

DVWK (Deutscher Verband für Wasserwirtschaft und Kulturbau e.V.) 1996. Determination of evaporation from land and water surfaces. Merkblätter zur Wasserwirtschaft 238. Kommissionsvertrieb Wirtschafts- und Verlagsgesellschaft Gas und Wasser mbH, Bonn, Germany (in German).

ESRI. Environmental Systems Research Institute. 1998a. ArcView GIS, Version 3.1 and online manuals. Redlands, CA.

ESRI. Environmental Systems Research Institute. 1998b. Avenue. Customization and application development for ArcView. Redlands, CA.

Fischer, C., and D. Hermsmeyer. 1999. Digital photogrammetry and GIS in tailings and mine waste management. *In* Tailings and Mine Waste '99. Proceedings of the Sixth International Conference on Tailings and Mine Waste '99. Fort Collins, CO. 24-27 Jan. 1999.

Frew, J. 1990. The image processing workbench. Doctoral Dissertation. University of California, Santa Barbara, CA.

Fu, P. and P.M. Rich. 1999. TopoView 1.1. User Manual. Helios Environmental Modeling Institute (HEMI). Kansas, U.S.A.

Fu, P., and P.M. Rich. 2000. A geometric solar radiation model and its applications in agriculture and forestry. *In* Proceedings of the Second International Conference on Geospatial Information in Agriculture and Forestry, Lake Buena Vista, 10-12 Jan. 2000.

Gates, D.M. 1980. Biophysical Ecology. Springer-Verlag, New York, NY.

Geiger, R.J. 1965. The climate near the ground. Harvard University Press. Cambridge, MA.

Hay, J.E., and D.C. McKay. 1985. Estimating solar irradiance on inclined surfaces: a review and assessment of methodologies. Int. J. Solar Energy. 3:203-240.

Hermsmeyer, D., J. Ilsemann, R.R. van der Ploeg, and R. Horton. 2001a. Lysimeter study of water flow and solute transport in a metallurgical waste: I. Construction, operation, and data acquisition. Manuscript submitted for publication.

Hermsmeyer, D., J. Ilsemann, J. Bachmann, R.R. van der Ploeg, and R. Horton. 2001b. Lysimeter study of water flow and solute transport in a metallurgical waste: II. Model calibration and application. Manuscript submitted for publication.

Horton, R., O. Aguirre-Luna, and P.J. Wierenga. 1984. Soil temperature in a row crop with incomplete surface cover. Soil Sci. Soc. Am. J., 48:1225-1232.

Hutchinson, M.F., T.H. Booth, J. P. McMahon, and H.A. Nix. 1984. Estimating monthly mean values of daily total solar radiation for Australia. Solar Energy. 32:277-290.

Iqbal, M. 1985. An introduction to solar radiation. Toronto, Canada. Academic Press.

Kasten, F. 1980. A simple parameterization of the pyrheliometric formula for determining the Linke turbidity factor. Meteorologische Rundsch. 33:124-127.

Kasten, F. 1983. Parameterization of global radiation from the degree of cloud coverage and turbidity factor. Ann. Meteorol. (N.F.) 20:49-50 (in German).

Kasten, F., K. Dehne, H.D. Behr, and U. Bergholter. 1984. The spatial and temporal distribution of diffuse and direct solar radiation in the Federal Republic of Germany. Forschungsbericht BMFT-FB-T84-125 (in German).

Kasten, F, and A.T. Young. 1989. Revised optical airmass tables and approximation formula. Appl. Optics. 28:4735-4738.

Keller, R. (ed.) 1978. Hydrological atlas of the Federal Republic of Germany. Harald Boldt Publ. Co., Boppard, Germany (in German).

Koitzsch, R., M. Dzingel, and U. Wendling. 1990. The effect of global radiation during daylight hours on radiation balance and soil heat flux (in German). Z. Meteorol. 40:205-208.

Konecny, G, and G. Lehmann. 1984. Photogrammetry. 4th edition. Berlin, Germany. DeGruyter (in German).

Kumar, L., A.K. Skidmore, and E. Knowles. 1997. Modeling topographic variation in solar radiation in a GIS environment. International Journal of Geographical Information Science. 11:475-497.

Lillesand, T.M., and R.W. Kiefer. 1994. Remote sensing and image interpretation. 3rd edition. John Wiley and Sons. New York.

Palz, W. and J. Greif. 1995. European solar radiation atlas. 3rd edition. Springer-Verlag. Berlin, Germany.

Penman, H.L. 1948. Natural evaporation from open water, bare soil and grass. Proc. Roy. Meteorol. Soc. A. 193:120-145.

Priestley, C.H.B., and R.J. Taylor. 1972. On the assessment of surface flux and evaporation using large-scale parameters. Month. Weath. Rev. 100:81-92.

Rich, P.M., W.A. Hetrick, and S.C. Seving. 1995. Modeling topographic influences on solar radiation: a manual for the SolarFlux model. Los Alamos National Laboratory. U.S. Department of Energy.

Šimunek, J., M. Šejna, and M.Th. van Genuchten. 1998. The HYDRUS-1D software package for simulating the one-dimensional movement of water, heat, and multiple solutes in variably-saturated media. Version 2.0. U.S. Salinity Laboratory, Agricultural Research Service, U.S. Department of Agriculture, Riverside, CA.

Šimunek, J., M. Šejna, and M.Th. van Genuchten. 1999. The HYDRUS-2D software package for simulating the two-dimensional movement of water, heat, and multiple solutes in variably-saturated media. Version 2.0. U.S. Salinity Laboratory, Agricultural Research Service, U.S. Department of Agriculture, Riverside, CA.

Sonntag, D. 1994. Advancements in the field of hygrometry. Meteorol. Zeitschrift. N.F. 3:51-66.

Swift, L.W., Jr. 1976. Algorithm for solar radiation on mountain slopes. Water Resour. Res. 12:108-112.

Unsaturated Soils Group. 1997. SoilCover Version 4.01. Department of Civil Engineering, University of Saskatchewan. Saskatoon, Canada.

VDI, Verein Deutscher Ingenieure (Association of German Engineers). 1994. Environmental Meteorology. Interactions between atmosphere and surfaces. Calculation of shortwave and longwave radiation. (in German and English). VDI Guideline. VDI-Richtlinie 3789, Part 2. Beuth Publ. Co. Berlin, Germany.

Venebrügge, G. 1996. Estimation of the shortwave, relief-dependent radiation in the Bornhöved Lake District using GIS (Arc/Info). EcoSys, Beiträge zur Ökosystemforschung. Vol. 12 (in German).

Wilson, G.W., S.L. Barbour, D. Swanson, and M. O'Kane. 1995. Instrumentation and modeling for saturated/unsaturated performance of soil covers for acid generating waste rock. Hydrgéologie. 4:99-108.

Zaradny, H. and R.R. van der Ploeg. 1982. Calculation of the shortwave radiation flux from weather station data in evapotranspiration studies. Z. Pflanzenernaehr. Bodenk. 145:611-622.

6. Schlussfolgerungen

Die vorliegende Arbeit behandelt die bodenhydrologischen Eigenschaften der Industrieabfälle ALRP und ALRP-FGDP mit Blick auf deren Eignung als Deckschichtmaterial für die Begrünung der Kali-Rückstandshalde Sigmundshall. Der Wasser- und Lufthaushalt von ALRP und ALRP-FGDP ähnelt dem feinkörniger, nicht plastischer Böden. Dies gilt insbesondere für die Wasserspannungskurven, die entsprechenden Kurven feinkörniger Böden mit vorwiegend engen Poren und mittlerer bis hoher nutzbarer Feldkapazität vergleichbar sind. Die Messdaten ließen sich mit dem für natürliche Böden häufig verwendeten Modell von van Genuchten (1980) beschreiben.

Überraschend hoch waren Porosität und Durchlässigkeitsbeiwert von ALRP und ALRP-FGDP. Die Dichte der Festsubstanz und die Lagerungsdichte entsprachen dem Mischungsverhältnis verschiedener Materialkomponenten.

Der Sickerwasserabfluss aus mit ALRP gefüllten Lysimetern vom 17.6.1997 bis 30.5.2000 betrug im Mittel 230 mm pro Jahr, oder 39% des mittleren jährlichen Niederschlags. Entsprechende Werte für ALRP-FGDP betrugen 143 mm oder 24% des Niederschlags. Auch nach vollständiger Aufsättigung beider Materialien war die Sickerung aus ALRP-FGDP deutlich geringer als aus ALRP. Ursache der unterschiedlichen Sickerung war daher nicht nur der unterschiedliche Anfangswassergehalt, sondern auch die bereits im unbewachsenen Zustand höhere Verdunstung aus den mit ALRP-FGDP gefüllten Lysimetern.

Im Lysimeterversuch waren beide Materialien nach etwa 28 Monaten bzw. 1361 mm Niederschlag mit Raygras (*Lolium perenne*, L.) begrünbar. Dies entsprach 281 mm (ALRP-FGDP) bzw. 444 mm (ALRP) Sickerung. In dieser Zeit hatte sich in beiden Materialien eine salzarme Schicht von etwa 0,3 m Mächtigkeit gebildet. Die mit dem Sickerwasser ausgewaschene Salzfracht betrug für ALRP etwa 159 kg und für ALRP-FGDP etwa 100 kg NaCl. Die elektrische Leitfähigkeit in Sauglösungen aus 0,6 m Tiefe war während des zweiten und dritten Winters des Lysimeterversuchs für ALRP-FGDP deutlich geringer als für ALRP. Es ist anzunehmen, dass Pflanzenwurzeln in der Mischung schneller in größere Tiefen vordringen können als in reinem ALRP. Damit sind für ALRP-FGDP bei Begrünung auch höhere Transpirationsraten zu erwarten als für ALRP. Die bereits im unbewachsenen Zustand festgestellten Unterschiede der Verdunstung von der Oberfläche der beiden Materialien werden sich im begrünten Zustand voraussichtlich noch verstärken.

Das kalibrierte numerische Wasserhaushaltsmodell beschrieb die während des dritten Versuchsjahres an den Lysimetern gemessenen Sickerwassermengen

sowie den zeitlichen Verlauf der Sickerung hinreichend genau. Die Simulation des Wasserhaushalts über 31 Jahre ergab für dicht bewachsenes ALRP-FGDP bei einer angenommenen Durchwurzelung bis in 0,5 m Tiefe bezogen auf eine ebene Lage eine mittlere jährliche tatsächliche Verdunstung von 577 mm. Dies sind nur 11 mm weniger als die für die Referenzstation Hannover-Langenhagen (Flughafen) mit dem Verfahren nach Penman (1948) ermittelte potenzielle Verdunstung.

Der langjährige mittlere Niederschlag an der Referenzstation, korrigiert um die von Richter (1995) angegebenen Faktoren, beträgt 764 mm. Die mittlere jährliche Abflussspende von der Basisabdichtung der Halde Sigmundshall (311 157 m^2) beträgt etwa 150 000 m^3 oder 482 mm. Geht kein Wasser durch die Basisabdichtung verloren, entspricht die Differenz einer mittleren tatsächlichen Verdunstung von 282 mm pro Jahr. Verdunsten statt dessen zukünftig von einer optimal begrünten ALRP-FGDP-Deckschicht 577 mm jährlich, so bleibt eine Abflussspende von 187 mm oder 58 186 m^3. Die bisherige Abflussspende würde um 61% vermindert. Ausgehend von weiterhin NaCl-gesättigter „Haldenlauge" würde die an die Leine abgegebene Salzfracht von derzeit 53 550 Tonnen auf 20 885 Tonnen pro Jahr verringert. Zukünftige Haldenerweiterungen sowie Unterschiede der Verdunstung zwischen Nord- und Südhang bleiben dabei unberücksichtigt.

Aus Sicht der Bodenhydrologie sind sowohl ALRP als auch ALRP-FDGP zum Aufbau einer Deckschicht mit dem Ziel der Verminderung der Sickerung in den Haldenkörper geeignet. Nach Auswaschung der leicht löslichen Bestandteile ist der Wasser- und Lufthaushalt beider Materialien für die Durchwurzelung vorteilhaft. Der Vergleich von ALRP-FGDP und ALRP zeigt jedoch, (i) dass eine Deckschicht aus ALRP-FGDP die Sickerung in den NaCl-Körper der Halde bereits vor der Begrünung stärker reduziert, (ii) dass die Auswaschungszeit für leicht lösliche Salze aus ALRP-FGDP kürzer bzw. die zur Auswaschung notwendige Niederschlagsmenge geringer ist, und (iii) dass eine schnellere Durchwurzelung von ALRP-FGDP zu erwarten ist. Zum Aufbau einer Deckschicht ist deshalb ALRP-FGDP unvermischtem ALRP vorzuziehen.

Der Einfluss der Topografie des Haldenkörpers wurde mithilfe eines auf der Basis eines geografischen Informationssystems entwickelten Modells für die Globalstrahlung und die Verdunstung ermittelt. Das berechnete dreijährige Mittel der potenziellen Jahresverdunstung war für den Südhang der Halde (745 mm) um 12% höher, für den Nordhang (415 mm) hingegen um 37% geringer als für einen ebenen Standort (663 mm). Bei der zukünftigen Haldenerweiterung kann im Sinne der Erhöhung der Verdunstung (Reduzierung der

Abflussspende) möglicherweise auf ein Profil des Haldenkörpers mit langem, flachem Südhang und kurzem, steilem Nordhang hingearbeitet werden.

Vor einer abschließenden Bewertung der Eignung von ALRP-FGDP als Deckschichtmaterial erscheinen insbesondere chemische Untersuchungen notwendig. Mit Blick auf die metallurgische Herkunft von ALRP sowie auf einige Angaben zu Schwermetallgehalten vergleichbarer Materialien (Manfredi et al., 1997) ist zu erwarten, dass chemische eher als physikalische Eigenschaften der Verwendung von ALRP-FGDP als Deckschichtmaterial im Wege stehen.

7. Literatur

In der folgenden Literaturliste sind nur die in den Kapiteln 1 (Einführung) und 6 (Schlussfolgerungen) zitierten Titel gelistet. Literaturlisten zu den Kapiteln 2 bis 5 befinden sich am Ende des jeweiligen Kapitels.

ESRI. Environmental Systems Research Institute. 1998. ArcView GIS, Version 3.1 and online manuals. Redlands, CA.

Hryn, J.N., E.J. Daniels, T.B. Gurganus, and K.M. Thomaswick. 1995. Products from salt cake residue-oxide. p. 905-916. *In* P.B. Queneau and R.D. Peterson (eds.) Third International Symposium on Recycling of Metals and Engineered Materials. TMS, Warrendale, PA.

Jody, B.J., E.J. Daniels, P.V. Bonsignore, and D.E. Karvelas. 1992. Recycling of aluminum salt cake. Journal of Resour. Management and Technol. 20:39-49.

Karvelas, D.E., E.J. Daniels, B.J. Jody, and P.V. Bonsignore. 1991. An economic and technical assessment of black-dross- and salt-cake-recycling systems for application in the secondary aluminum industry. Energy Systems Division, Argonne National Laboratory. Argonne, IL.

Manfredi, O., W. Wuth, and I. Bohlinger. 1997. Characterizing the physical and chemical properties of aluminum dross. Journal of the Minerals, Metals, and Materials Society 49(2):48-51.

Penman, H.L. 1948. Natural evaporation from open water, bare soil and grass. Proc. Roy. Meteorol. Soc. A. 193:120-145.

Priestley, C.H.B., and R.J. Taylor. 1972. On the assessment of surface flux and evaporation using large-scale parameters. Month. Weath. Rev. 100:81-92.

Richter, D. 1995. Ergebnisse methodischer Untersuchungen zur Korrektur des systematischen Messfehlers des Hellmann-Niederschlagsmessers. Berichte des Deutschen Wetterdienstes, Nr. 194. Deutscher Wetterdienst DWD, Offenbach.

Šimunek, J., M. Šejna, and M.Th. van Genuchten. 1998. The HYDRUS-1D software package for simulating the one-dimensional movement of water, heat, and multiple solutes in variably-saturated media. Version 2.0. U.S. Salinity Laboratory, Agricultural Research Service, U.S. Department of Agriculture, Riverside, CA.

Statistisches Bundesamt. 1997. Statistisches Jahrbuch für die Bundesrepublik Deutschland. Metzler-Poeschel Verlag, Stuttgart.

van Genuchten, M.Th. 1980. A closed-form equation for predicting the hydraulic conductivity of unsaturated soils. Soil Sci. Soc. Am. J. 44:892-898.

VDI, Verein Deutscher Ingenieure. 1994. Umweltmeteorologie. Wechselwirkungen zwischen Atmosphäre und Oberflächen. Berechnung der kurz- und der langwelligen Strahlung. VDI-Richtlinie 3789, Blatt 2. Beuth Verlag. Berlin.

Weast, R. 1987. Handbook of chemistry and physics. 67th ed. CRC Press, Boca Raton, FL.

Lebenslauf

Dirk Hermsmeyer, geboren am 25.12.1964 in Bünde/Westfalen.

Schule

1971 - 1975   Grundschule Löhne Obernbeck

1975 - 1984   Städtisches Gymnasium Löhne / Westfalen

Zivildienst

07.'84 - 06.'87   Ziviler Ersatzdienst an der Schule für Körperbehinderte,
                   Landschaftsverband Westfalen-Lippe, Bad Oeynhausen

Berufsausbildung

09.'85 - 06.'87   Ausbildung zum Gärtner

07.'87 - 09.'88   Berufstätigkeit als Gärtner

Studium

10.'88 - 06.'94   Univ. Hannover, Fachbereich Geowissenschaften (Institut für
                   Geografie), Nebenfächer: Bodenkunde und Hydrologie

                   Berufspraktika:
                   Umweltbundesamt, Berlin, Fachgebiet Bodenschutz;
                   National Park Service, Milford, Pennsylvania, USA;
                   Iowa State University, Dept. of Agronomy, Ames, Iowa, USA

                   Diplomarbeit: Denitrifikationsleistungen verschiedener Böden
                   eines landwirtschaftlich genutzten Trinkwassereinzugsgebiets
                   bei Viersen am Niederrhein.

Berufstätigkeit

05.'95 - 11.'95   Bundesanstalt für Geowissenschaften und Rohstoffe (BGR),
                   Hannover

01.'96 - 11.'00   Wissenschaftlicher Mitarbeiter, Institut für Bodenkunde der
                   Universität Hannover, Fachbereich Bodenphysik

seit 06.'94   Tätigkeit als Geograf in verschiedenen Planungsbüros